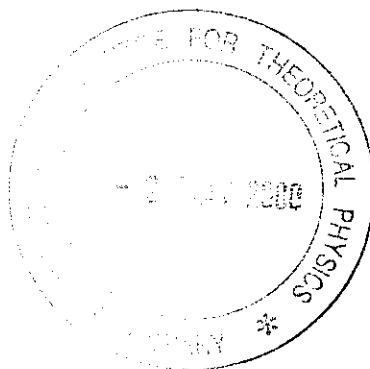Joint INFM - the Abdus Salam ICTP School on
"Magnetic Properties of Condensed Matter Investigated by Neutron
Scattering and Synchrotron Radiation Techniques"

1 - 11 February 2000

Polarimetric Neutron Scattering for Magnetic Structure Determination and Beyond

F. TASSET
INSTITUT LAUE-LANGEVIN
156X,
F-38042 Grenoble Cedex, France

Joint ICTP-INFM School
*Magnetic Properties of Condensed Matter Investigated by Neutron Scattering
and Synchrotron Radiation Techniques*

1-11 February, 2000
Trieste, Italy

Polarimetric Neutron Scattering
for magnetic structure determination
and beyond

F. Tasset

Institut Laue-Langevin, 156x, F38042 Grenoble Cedex, France

Contents

1- Introduction:

Ever since the pioneering experiment of Shull and Smart on MnO[1] the spin configuration of the magnetically ordered condensed state has traditionally been determined using unpolarized neutron diffraction intensities. Often the sample studied is polycrystalline and although the technique works remarkably well for collinear spin structures, it often fails for a more complicated spin configuration, for example, non collinear, incommensurate helimagnetic structure. For such structures even a neutron diffraction investigation on good-quality single crystals may not yield a unique solution. For high-symmetry crystal structures the existence of several magnetic domains adds further uncertainty. Even traditional polarized neutron diffraction methods with one-dimensional polarization analysis on single crystals may fail to give a unique spin configuration. [2]

In that context , the second part of this lecture aims at introducing a powerful novel technique, Spherical Neutron Polarimetry {SNP}, which is often able to determine unambiguously the spin configuration of incommensurate modulated magnetic structures and commensurate antiferromagnetic structures like triangular ones. It was also used very recently for high precision measurement of antiferro-magnetic form factor. All that rely on our ability to measure the transverse components of the final polarisation vector using Cryopad, a zero-field neutron polarimeter developed at ILL [3, 4]. Cryopad-II is presently used for more difficult but highly interesting inelastic measurements of mixed magnetic –nuclear pair correlation functions in low dimension magnetic systems [5].

1.1-Various examples of ordered magnetic Structures

ferromagnetic   antiferromagnetic   ferrimagnetic

(1.1.a)   (1.1.b)   (1.1.c)

triangular   canted

(1.1.d)   (1.1.e)   umbrella
                                          (1.1.f)

Tm	Er,Tm	Er	Ho,Er	Tb,Dy,Ho	Gd,Tb,Dy
(a)	(b)	(c)	(d)	(e)	(f)

(1.1.g)
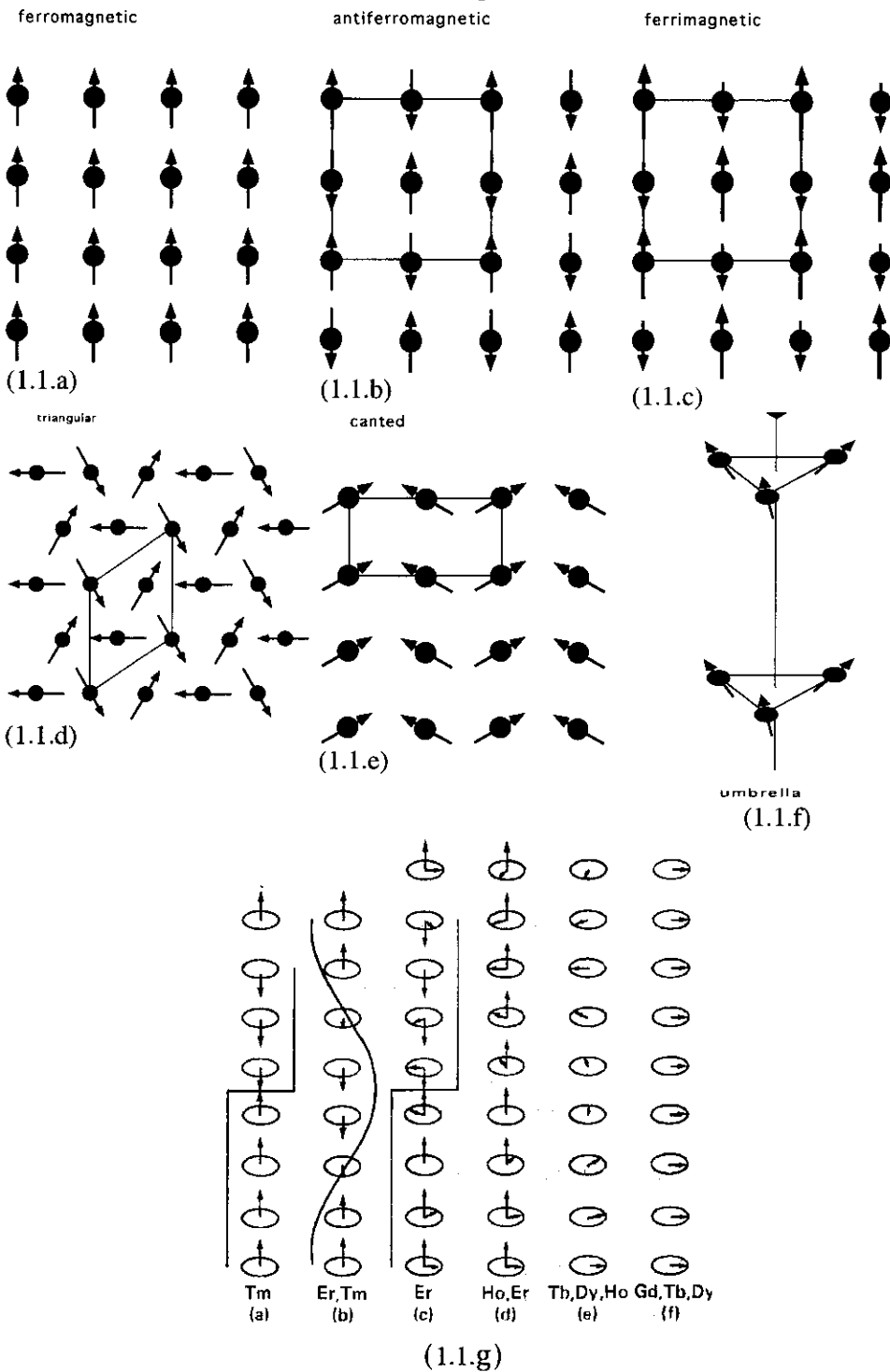
Fig.1(a-g) :Various examples of ordered magnetic structures

5

1.2- The crystalline Bravais lattice:

The invariant nuclear crystal lattice translations are given using the direct Bravais lattice:

$$\vec{l} = n_1\vec{a} + n_2\vec{b} + n_3\vec{c} \tag{1.1}$$

n_1, n_2, n_3 being integer numbers.

The position coordinates for an arbitrary atom in the unit cell reads

$$\vec{R}_{lj} = \vec{l} + \vec{r}_j \tag{1.2}$$

with
$$\vec{r}_j = x_j\vec{a} + y_j\vec{b} + z_j\vec{c} \tag{1.3}$$

x, y, z being less than unity.
A dual vectorial space is defined which is called reciprocal space

$$\vec{a}^* = \frac{2\pi}{v_0}\vec{b} \wedge \vec{c} \tag{1.4}$$

$$\vec{b}^* = \frac{2\pi}{v_0}\vec{c} \wedge \vec{a} \tag{1.5}$$

$$\vec{c}^* = \frac{2\pi}{v_0}\vec{a} \wedge \vec{b} \tag{1.6}$$

in which vectors are defined which connect the origin to a given node in reciprocal space

$$\vec{\tau} = h\vec{a}^* + k\vec{b}^* + l\vec{c}^* \tag{1.7}$$

when h, k, l are integer numbers
or a point in the 1st Brillouin zone

$$\vec{k} = k_1\vec{a}^* + k_2\vec{b}^* + k_3\vec{c}^* \tag{1.8}$$

when k_1, k_2, k_3 are less than unity.

1.3- Mathematical Crystallography

The mathematical operations which are necessary when describing the magnetic structures, their stability, and the corresponding neutron cross-sections are summarized in the following tables:

Table 1: Periodic density in direct space:

Direct Space	Reciprocal Space
For a periodic crystal $$\rho(\vec{r} + \vec{l}) = \rho(\vec{r}) \qquad (1.9)$$	The Fourier transform of $\rho(\vec{r})$ is discrete, it has non zero coefficients only at reciprocal lattice nodes $$F(\vec{k}) = \int \rho(\vec{r})e^{\vec{k}\vec{r}}d^3\vec{r} \qquad (1.10)$$

Table 2: Arbitrary distribution at nodes of reciprocal space:

Reciprocal Space	Direct Space
For an arbitrary distribution of amplitudes $F(\vec{k})$ at nodes in reciprocal space	the inverse Fourier transform $$\rho(\vec{r}) = \sum_k F(\vec{k})e^{-i\vec{k}\vec{r}} \qquad (1.11)$$ gives a continuous and periodic function in direct space $$\rho(\vec{r} + \vec{l}) = \rho(\vec{r}) \qquad (1.12)$$

It is therefore possible to demonstrate the following theorem:
The reciprocal lattice of the reciprocal lattice is the direct lattice.

Table 3: From direct lattice nodes to reciprocal lattice:

Direct lattice	Reciprocal Space
For an arbitrary amplitudes distribution at real lattice nodes $m(\vec{l})$ The inverse Fourier transform of $$m(\vec{l}) = \int \rho(\vec{k})e^{-i\vec{k}\vec{l}}d^3\vec{k} \qquad (1.13)$$	The Fourier transform $$\rho(\vec{k}) = \sum_l m(\vec{l})e^{i\vec{k}\vec{l}} \qquad (1.14)$$ is a periodic and continuous function in reciprocal space $$\rho(\vec{k} + \vec{K}) = \rho(\vec{k}) \qquad (1.15)$$

Generalization: Instead of dealing with a scalar distribution m, we begin with a vector distribution $\vec{m}$. In addition we consider the case of several interpenetrating Bravais lattices identified with index j

Table 4: Vectorial generalization

$$\vec{m}_j(\vec{l}) = \int \vec{\rho}_j(\vec{k})e^{-i\vec{k}\vec{l}}d^3\vec{k} \qquad (1.16)$$	$$\vec{\rho}_j(\vec{k}) = \sum_l \vec{m}_j(\vec{l})e^{-i\vec{k}\vec{l}} \qquad (1.17)$$
Integration is in the first Brillouin zone only	

In this way we can decompose an arbitrary distribution of magnetic moments $\vec{m}_j$ in a crystal.

1.4- The stability of magnetic structures

The interactions between the magnetic moments are described using the following Hamiltonian:

$$H = -\sum_{\substack{l,l' \\ j,j'}} J_{ll'j'} \vec{m}'_{lj} \vec{m}_{l'j'} \tag{1.18}$$

When we cool the sample, the magnetic moments $\vec{m}_{lj}$ get eventually ordered;

The solutions $\vec{m}_{lj}$ must leave the Hamiltonian invariant by lattice translations.

The general solution is:

$$\vec{m}_{lj} = \int \vec{\rho}_j(\vec{k}) e^{-i\vec{k}\vec{l}} d^3\vec{k} \tag{1.19}$$

where $\vec{k}$ is restricted to the first Brillouin zone.

Due to minimization in the magnetic energy for the system,

1) one $\vec{k}$ vector is more favorable than others, the system will choose this ground state:

$$\vec{m}_{l,j} = \vec{m}_j^{\vec{k}} e^{-\vec{k}\vec{l}} \tag{20}$$

in case there is several vectors $\vec{k}$ equivalent by symmetry it can choose to rest in a multi $\vec{k}$ configuration

$$\vec{m}_{l,j} = \sum_{star of \ \vec{k}} \vec{m}_j^{\vec{k}} e^{-i\vec{k}\vec{l}}, \tag{1.21}$$

2) may be one $\vec{k}$ vector and its harmonics are favorable

$$\vec{m}_{l,j} = \sum_{harmonics} \vec{m}_j^{\vec{k}} e^{-i\vec{k}\vec{l}} \tag{1.22}$$

and in case we have a star of equivalent $\vec{k}$ vectors we can have the crossed harmonics which are sometimes called intermodulations.

1.5- Direct space representation

For sake of simplification we are going to suppose that we have a single atom per unit cell. This means that we have only one lattice, j=1.

$$\vec{m}_l = \sum_{\vec{k}} \vec{m}^{\vec{k}} e^{-i\vec{k}\vec{l}} \tag{1.23}$$

$$\vec{k}\vec{l} = 2\pi(n_1 k_1 + n_2 k_2 + n_3 k_3) \tag{1.24}$$

We must distinguish 2 cases, $\vec{k}\vec{l}$ *is a multiple of* π , $\vec{k}\vec{l}$ *is not a multiple of* π

We must note that $\vec{m}_l$ is *real*. If $\vec{k}\vec{l}$ is *not a multiple of* π then for all $\vec{k}$ we have to associate $-\vec{k}$ which is not equivalent through lattice translation. Knowing that

$$\vec{m}^{-\vec{k}} = (\vec{m}^{\vec{k}})^* \tag{1.25}$$

then

$$m_{x,l} = \hat{x}.\sum_k (\vec{m}^k e^{-i\vec{k}\vec{l}} + (\vec{m}^k)^* e^{i\vec{k}\vec{l}}) = 2|\vec{m}^{\vec{k}}| \cos(kl + \varphi) \tag{1.26}$$
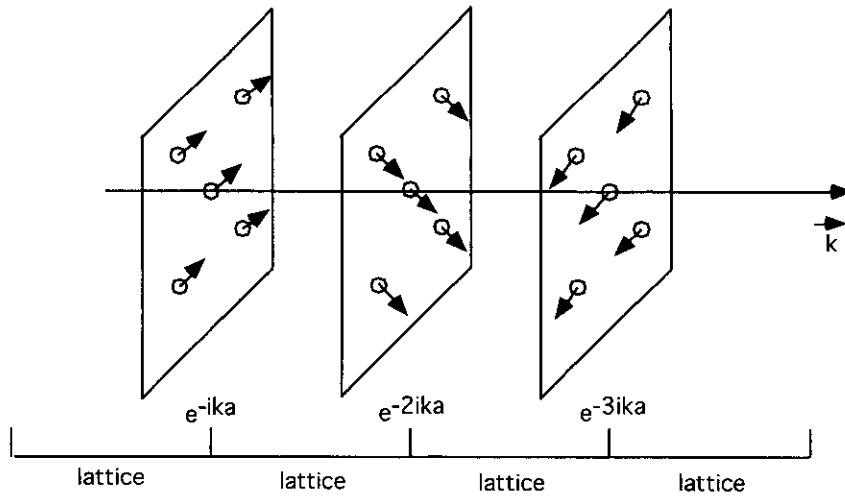
magnetic moments contained in planes perpendicular to kare parrallel

Fig. 2 : magnetic moments contained in planes perpendicular to k are parallel

1.6- Looking for the propagation vector

Magnetic reflections are generally observed by comparison of powder diagrams obtained above and below the magnetic ordering temperature. They tell us about the length of $\vec{Q} = \vec{\tau} \pm \vec{k}$

The intuitive identification can be made when the modulus of k is small (long wavelength modulation) and the powder diagram is not too crowded with peaks (highly symmetrical space group). The satellites appear as being attached to a reciprocal lattice vector and we shall speak, for example, of the satellites at the origin which give intense lines at small scattering angles.

In that circumstance it is possible to use a simple graphical technique as illustrated in the following figure. The circles drawn having a radius

$$H_i = \frac{4\pi \sin \theta_i}{\lambda}$$

(1.27)
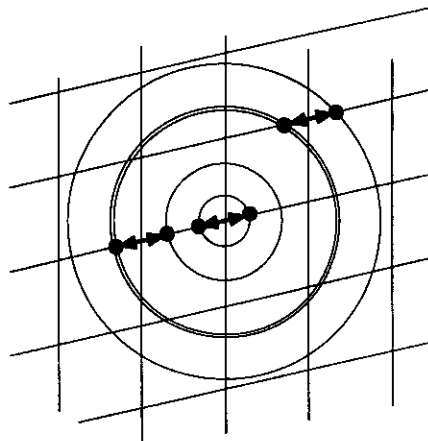
Fig. 3 : Looking for the propagation vector

The most effective method is to enter in a computer programme a list of measured lengths Q as well as the reciprocal lattice description for a systematic search of all the k vectors which are satisfactory. The Brillouin zone is sliced into a fine grid of $\vec{k}_i$ and for each $\vec{\tau}$ we calculate all the $\vec{Q} = \vec{\tau} \pm \vec{k}_i$. Then a comparison is made of $\left|\vec{Q}_{cal}\right|$ and $H_i \pm \Delta H_i$
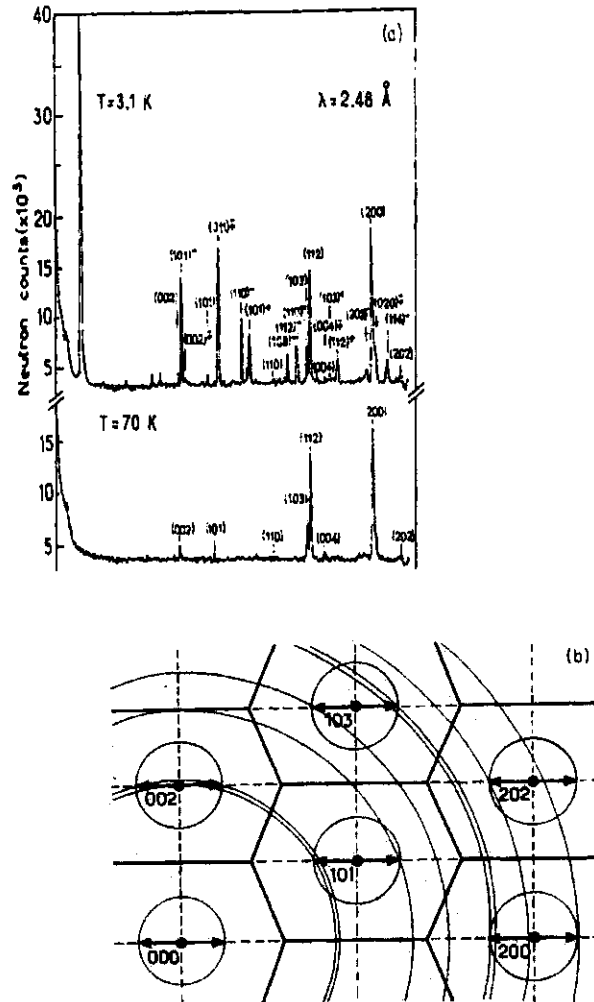
Fig. 4 : Propagation vector for TbRu$_2$Si$_2$

As an example, TbRu$_2$Si$_2$ crystallizes in a quadratic structure with I4/mmm space group. Neutron Powder diagrams a) have been recorded at 2 temperatures on both sides of the transition T$_N$=55K The reciprocal lattice and the related Brillouin zones are shown in b). We can see that the magnetic order correspond to k=<0.232,0,0>

10

2- Essential Neutron scattering

When a neutron meets a magnetic atom it experiences two scattering potentials:
1) a nuclear scattering which reveals the existence and nature of the nucleus
2) a magnetic scattering, arising principally from unpaired electrons.

2.1 Coherent Nuclear scattering

The nuclear scattering interaction operator for atom j reads:

$$a_{Nj} = b_j + A_j \vec{\sigma}.\vec{I}_j \tag{2.1}$$

$\vec{I}_j$ is the nuclear spin vector operator. At room temperature the nuclear spin angular momentum is randomly oriented and the mean, coherent part, which is of interest here averages to zero. We shall therefore assume in the following $a_{nj} = b_j$ which we will call the scattering length or Fermi length. It is often expressed in 10^{-12} cm.

The coherent nuclear cross-section for all the atoms in the crystal is

$$\left(\frac{d\sigma}{d\Omega}\right)_N = \left|\sum_{lj} b_j e^{i\vec{Q}\vec{R}_{lj}}\right|^2 = N\frac{(2\pi)^3}{v_0}\sum_{\tau}|F_N|^2 \delta(\vec{Q}-\vec{\tau}) \tag{2.2}$$

With

$$F_N(\vec{Q}) = \sum_j b_j e^{i\vec{Q}\vec{r}_j} e^{-W_j} \tag{2.3}$$

N.B. it is important to realize that $A_j \vec{\sigma}.\vec{I}_j$ is not the magnetic interaction we are interested in, it is the spin dependent part of the strong nuclear force which is responsible for the neutron-nuclear interaction.

2.2 Magnetic scattering amplitude:

$$a_{Mj} = p\vec{\sigma}.\vec{M}_{j\perp}(\vec{Q}) \tag{2.4}$$

$$p = \frac{\gamma e^2}{2m_e c^2} = \frac{\gamma r_0}{2} = 0.2696 \quad 10^{-16} cm \tag{2.5}$$

$\vec{M}(\vec{Q})$ is the Fourier component of the magnetization density $\vec{M}(\vec{r})$ at scattering vector $\vec{Q}$ and $\vec{M}_\perp(\vec{Q})$ is the projection of $\vec{M}(\vec{Q})$ on the plane perpendicular to the scattering vector $\vec{Q}$
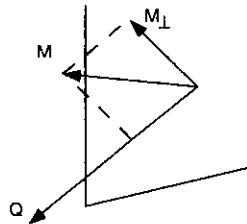
Fig. 5: The projection due to dipolar interaction (Fourier space)

It can be shown that

$$\vec{M}_\perp = \hat{Q} \wedge (\vec{M} \wedge \hat{Q}) = \vec{M} - \hat{Q}(\vec{M}.\hat{Q}) \tag{2.6}$$

$$\hat{Q} = unit\ vector = \frac{\vec{Q}}{|\vec{Q}|}$$

With $\qquad\qquad$ (2.7)

$$\vec{M}_j(\vec{Q}) = \vec{m}_j f(\vec{Q}) \tag{2.8}$$

and

2.3 The two main scattering cross sections for neutrons
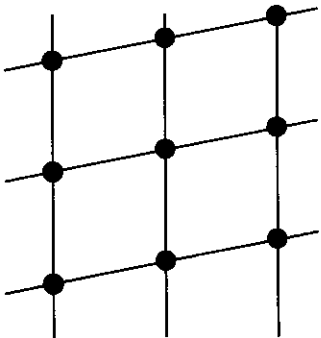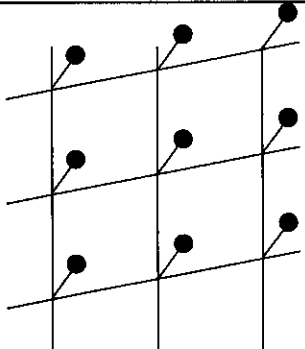
nuclear	magnetic
$$\left(\frac{d\sigma}{d\Omega}\right)_N = \left\|\sum_{lj} b_j e^{i\vec{Q}\vec{R}_{lj}}\right\|^2 \quad (2.9)$$	$$\left(\frac{d\sigma}{d\Omega}\right)_M = \left\|\sum_{lj} a_{Mlj} e^{i\vec{Q}\vec{R}_{lj}}\right\|^2 \quad (2.10)$$
	$$a_{Mlj}(Q) = pf(Q)\vec{\sigma}.\vec{m}_{lj\perp} \quad (2.11)$$
	$$\vec{m}_{lj} = \sum_k \vec{m}_j^k e^{-i\vec{k}\vec{l}} \quad (2.12)$$
$$\left(\frac{d\sigma}{d\Omega}\right)_N = N\frac{(2\pi)^3}{v_0}\sum_\tau |F_N|^2 \delta(\vec{Q}-\vec{\tau})$$ (2.13)	$$\left(\frac{d\sigma}{d\Omega}\right)_M = \frac{(2\pi)^3}{v_0} N \sum_k \sum_\tau |\vec{F}_{M\perp}(\vec{Q})|^2 \delta(\vec{Q}-\vec{k}-\vec{\tau})$$ (2.14)
$$F_N(\vec{Q}) = \sum_j b_j e^{i\vec{Q}\vec{r}_j} e^{-W_j} \quad (2.15)$$	$$\vec{F}_M(\vec{Q}) = p\sum_j f_j(Q)\vec{m}_j^k e^{i\vec{Q}\vec{r}_j} e^{-W_j} \quad (2.16)$$
	$$\vec{F}_{M\perp} = \hat{Q} \wedge (\vec{F}_M \wedge \hat{Q}) = \vec{F}_M - \hat{Q}(\vec{F}_M.\hat{Q}) \quad (2.17)$$
	$$|\vec{F}_{M\perp}|^2 = \vec{F}_M.\vec{F}_M^* - (\hat{Q}.\vec{F}_M)(\hat{Q}.\vec{F}_M^*) \quad (2.18)$$
$\vec{Q} = \vec{\tau}$	$\vec{Q} = \vec{\tau} + \vec{k}$

Table 5: Scattering cross sections and graphs

2.4 Various kind of magnetic cross-sections
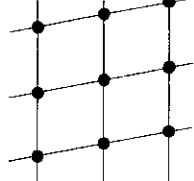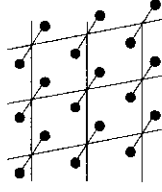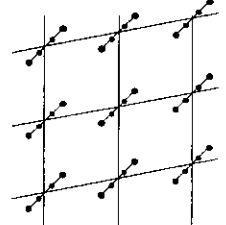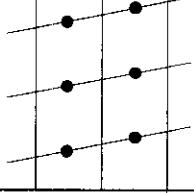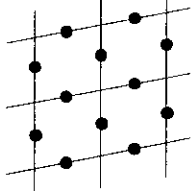
$\vec{k} = 0$ ferromagnetism (ferri-antiferro) $$\left(\frac{d\sigma}{d\Omega}\right)_M = \sum_\tau \left|\vec{F}_{M\perp}(\vec{Q})\right|^2 \delta\left(\vec{Q} - \vec{\tau}\right) \quad (2.19)$$	
$\vec{k} = k_x \vec{a}^* + k_y \vec{b}^* + k_z \vec{c}^*$ sinusoidal modulation or helix. To each $\vec{k}$ is associated $-\vec{k}$ $\vec{k} \Rightarrow \vec{Q} = \vec{\tau} + \vec{k}$ $-\vec{k} \Rightarrow \vec{Q} = \vec{\tau} - \vec{k}$	
$\vec{k}$ with harmonics	
$\vec{k} = \frac{1}{2}\vec{a}^*$	
multi-k	

Table 6: Cross sections and graphs in reciprocal space

2.5 Instrumentation

2.5.1- Two axis diffractometer for powder neutron scattering
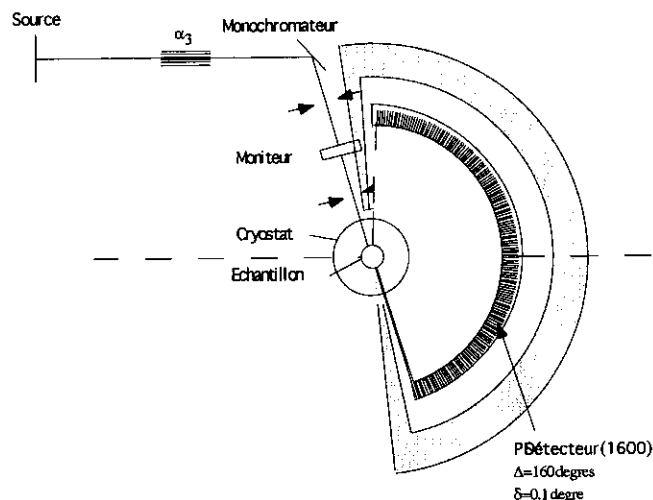
Le Diffractomètre à poudre D20 de l'ILL
(d'après P.Convert)

Fig. 6: The high flux large position sensitive detector powder diffractometer D20 at ILL
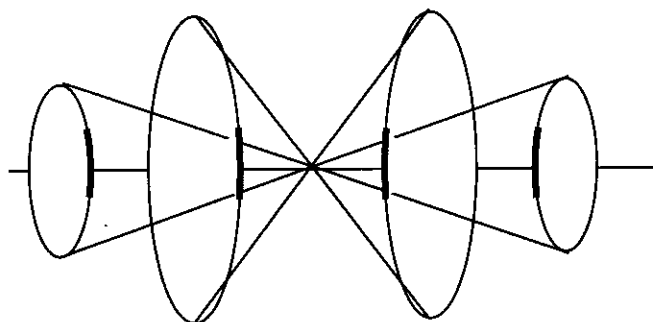
Fig. 7: Debye Scherrer cones (side view)

$$I_{int} = \Delta(2\theta)\sum_i J(2\theta_i) = \int \frac{d\sigma}{d\Omega}d\Omega = \frac{N}{v_0}\frac{\lambda^3}{8\pi \sin\theta \sin2\theta}\frac{l}{r}\sum |F^2|A$$

$$(2.20)$$

the Lorentz factor is $\dfrac{1}{\sin\theta \sin2\theta}$

resulting from the product of the probability for a crystallite to be oriented in the

appropriate direction $\sin(\frac{\pi}{2} - \theta) = \cos\theta$

times the portion of the cone intercepted by the detector. $\dfrac{l}{r\sin\theta}$ (the detector being

at distance r, correspond to a section $\rho = r\sin\theta$)

2.5.2- Single crystal diffractometer

2.5.2.1- 1st method, the classical 4 circles one:

by using a 4 circles diffractometer, the reciprocal vector $\bar{\tau}$ is made to cross the Ewald sphere in the horizontal plane. The scattering plane is horizontal and the detector set in the appropriate Bragg angle. Recently small position satellites have been introduced.
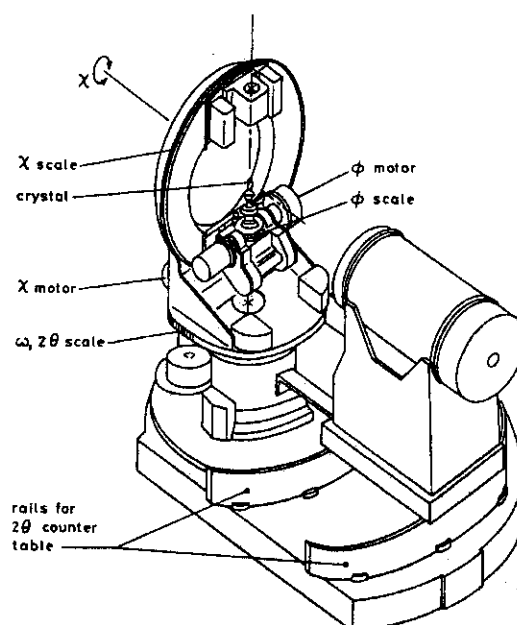
Usual names for the 4 circles	
ω	crystal
χ	crystal
φ	crystal
γ or 2θ	detector

Fig. 8: Four Circles Diffractometer
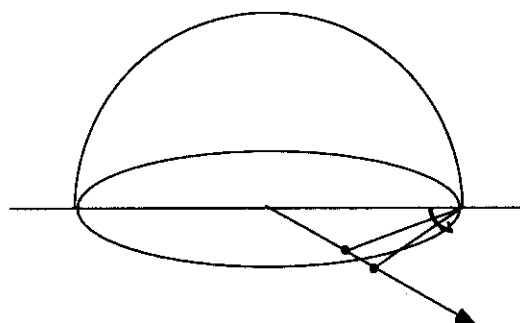
Fig. 9: Integrated intensities are measured in the horizontal plane by rotating the crystal. The reciprocal lattice node goes through the Ewald Sphere.

15

By rotating the crystal with the angle ω, one makes $\vec{\tau}$ to cross the Ewald sphere
A neutron reflection is obtained which is being integrated in the detector.
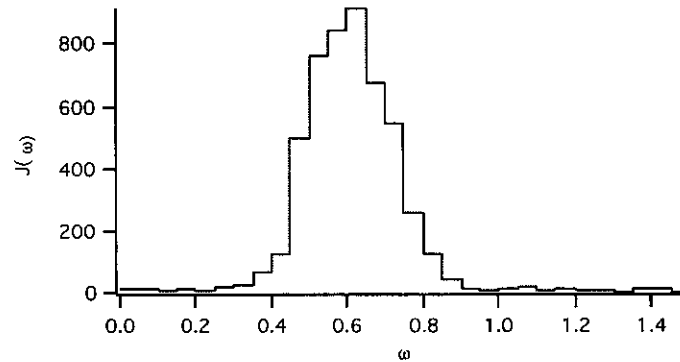
Fig. 10: Histogram of the number of neutron detected during the step rotation (i.e a
neutron scan)

$$I_{int} = \Delta(\omega)\sum_i J(\omega_i) = \int \frac{d\sigma}{d\Omega}d\Omega = \frac{N}{v_0}\frac{\lambda^3}{\sin 2\theta}|F^2|A$$

(2.21)

the Lorentz factor is $\dfrac{1}{\sin 2\theta}$

2.5.2.2- The normal beam method with tilting detector

Alternative Geometry with a tilting detector which is better suited when using large cryostats
like superconducting magnets (see D3 description section 4.2)
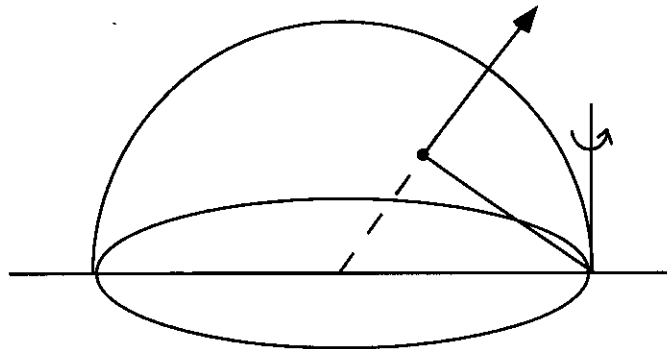
The 3 normal beam angles	
ω	crystal
γ	detector
ν	detector lift

Fig. 11: Integrated intensities are measured outside the horizontal plane by rotating
the crystal on a vertical axis . Here the reciprocal lattice node goes through the
Ewald Sphere in the north hemisphere and the detector has to be lifted to collect the
scattered neutrons.

By rotating the crystal around the vertical axis with angle ω, $\vec{\tau}$ crosses the Ewald sphere. Except for the horizontal reciprocal "zero-layer" the Bragg reflection is not in the horizontal plane. The detector is tilted in order to collect the scattered neutrons.

$$I_{int} = \Delta(\omega)\sum_i J(\omega_i) = \int \frac{d\sigma}{d\Omega}d\Omega = \frac{N}{v_0}\frac{\lambda^3}{\sin\gamma\sin\upsilon}|F^2|A$$

(2.22)

in that case the Lorentz factor is $\dfrac{1}{\sin\gamma\sin\upsilon}$

2.5.3 Investigating the magnetic moments, size and direction

Due to the dipolar nature of the magnetic neutron interaction, the scattering amplitude has 3 components transforming as a vector. We shall call it the magnetic interaction vector $\vec{M} = p\vec{F}_{M\perp}$.
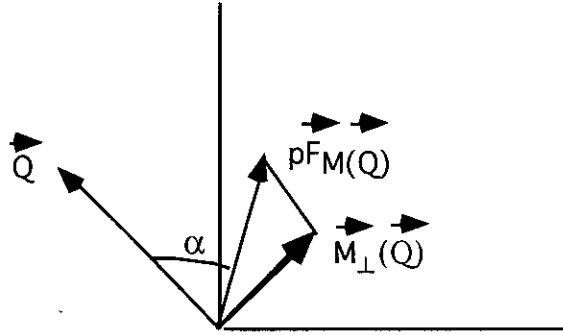
Fig. 12: The magnetic interaction vector

We note that

$$|\vec{m}\perp| = m\sin\alpha$$

(2.23)

and that

$$\vec{F}_{ML}(\vec{Q}) = \sum_j p_j f_j(\vec{Q})\, \vec{m}_{j\perp}^k e^{i\vec{Q}\vec{r}_j}$$

(2.24)

It is interesting to note that for a magnetic reflection on a collinear magnetic structure such as $\vec{m} \,//\vec{Q}$, $\alpha = 0$, the magnetic interaction vector is zero due to all $\vec{m}_{j\perp}^k$ being zero. Reciprocally knowing the magnetic interaction vector for a single reflection

17

does not tell anything about the component along $\bar{Q}$ of the magnetic Fourier structure factor (only 2 out of 3 components are seen by the neutron).
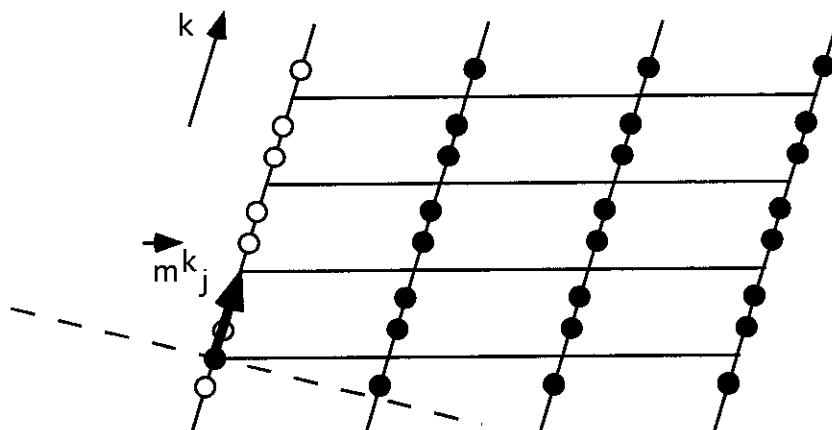
Fig. 13: Cancellation of magnetic scattering can result from the dipolar interaction

Possible indetermination of the Magnetic moments directions.

Suppose that the structure is collinear and that we are looking at the direction of magnetic moments on the basis of intensities in a powder diagram.

$$\left|\vec{F}_{M\perp}(Q)\right| = \sin\alpha \left|\sum_j \pm p_j f_j(Q)\left|m_j^k\right|e^{i\vec{Q}\vec{r}_j}\right|$$

(2.25)

The intensity at a given peak results from all reflections having the same Q length since they arrive in the detector at the same angle 2ϑ. All those reflections may or may not have the same structure factor

$$\left|\sum_j \pm p_j f_j(Q)\left|m_j^k\right|e^{i\vec{Q}\vec{r}_j}\right|$$

(2.26)

but they have different $\sin\alpha$ (I.e. different magnetic interaction vectors). Therefore

$$I \propto \sum_{Qnonequivalent} z_Q\left\langle\sin^2\alpha\right\rangle\left|\sum_j \pm p_j f_j(Q)\left|m_j^k\right|e^{i\vec{Q}\vec{r}_j}\right|^2$$

(2.27)

Shirane has shown that, for cubic symmetry, $\left\langle\sin^2\alpha\right\rangle = 2/3$ independent of the moment direction and for uniaxial symmetry the intensity depends on θ but not on φ.
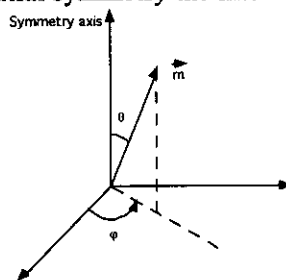
Fig. 14: Definition of the polar angles relative to a symmetry axis

2.5.4 Magnetic domains

2.5.4.1- K Domains

When ordering magnetically, the system choose the K vector which minimize the energy. But several K might be equivalent due to the symmetry of the crystal. One part of the crystal will choose k_1 and other parts k_2, k_3, etc. The famous example of MnO with its 4 ternary cubic directions is shown here:
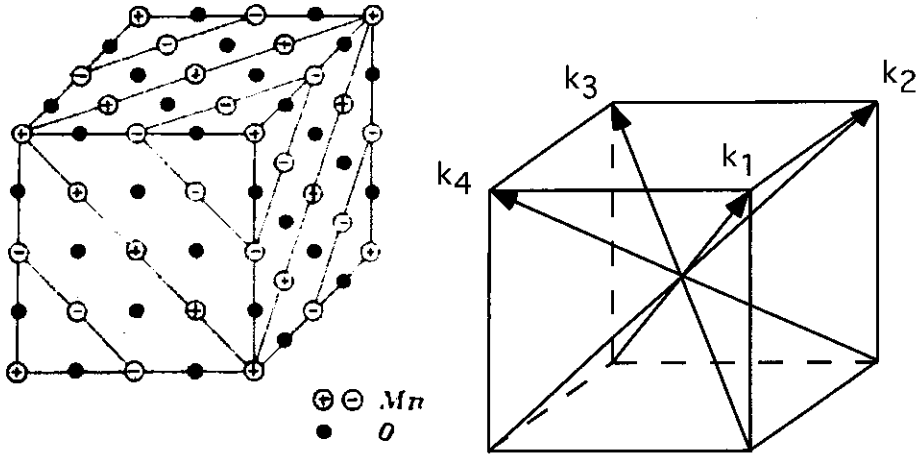
Fig. 15: The 4 k domains in MnO

$$\vec{k}_1 = (\frac{1}{2},\frac{1}{2},\frac{1}{2}) \ ; \ \vec{k}_2 = (\frac{\bar{1}}{2},\frac{1}{2},\frac{1}{2}) \ ; \ \vec{k}_3 = (\frac{1}{2},\frac{\bar{1}}{2},\frac{1}{2}) \ ; \ \vec{k}_4 = (\frac{1}{2},\frac{1}{2},\frac{\bar{1}}{2})$$

(2.28).

Those different directions can be distinct in reciprocal space or be superposed as a result of lattice translations as in the following example

$$\vec{k}_1 = (\frac{1}{2}, 0, 0$$

$$\vec{k}_2 = (0, \frac{1}{2}, 0)$$

(2.29)
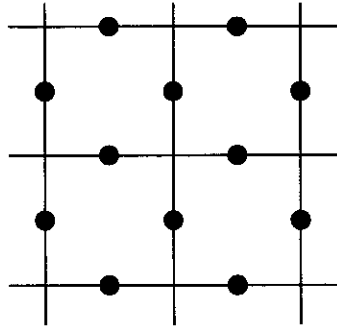
Fig. 16: Superposition of 2 k due to lattice translations

2.5.4.2- S domains

It exists an other kind of magnetic domains: those due to the various directions equivalent by symmetry of the crystallographic site on which the magnetic moment orders itself. Such domains are called S domains (S for Spin).

Within one K domain, one may find that the magnetic moments $\vec{m}_j^k$ have only one possible direction or, may be, several equivalent directions relatively to a, b, c axis and the direction k.

It can be shown that, due to the existence of S domains, the conclusion of Shirane relative to the limitations in investigating the magnetic moments directions based on neutron intensities remains on a single crystal as long as the proportions of S domains are equal. In order to remove the ambiguity, it is necessary to unbalance the domains. This can be done by applying an external uniaxial constraint or a magnetic or electric field.

2.5.5- Mutual orientation of the magnetic moments

We have seen the effect
-of the propagation vector
-of the magnetic moments direction
We are left with the relative orientation of the magnetic moments when there is more than one magnetic atom in the unit cell:

$$I \propto \left|\vec{F}_{M\perp}\right|^2 = \vec{F}_M \vec{F}_M{}^* - (\hat{Q}\vec{F}_M)(\hat{Q}\vec{F}_M{}^*) \tag{2.30}$$

$$\vec{F}_M(\vec{Q}) = p\sum_j f_j(\vec{Q})\,\vec{m}_j^k e^{i\vec{Q}\vec{r}_j} \tag{2.31}$$

It must be stressed here that we have to add the amplitudes from several atoms in the unit cell,

- First, for a given crystallographic site, the various positions which are related with symmetry elements·such as
    Rotations
    Inversions
    Rotation +fractionally translation
- Second, for the various crystallographic sites.

3- Magnetic interactions

Although, in direct space the interactions must be added on all atoms in the crystal

$$H = -\sum_{lj}\sum_{l'j'} J_{lj'j'}\,\vec{m}_{lj}\,\vec{m}_{l'j'} \tag{3.1}$$

in reciprocal space

$$H = -\sum_{\vec{k}}\sum_{jj'} J_{jj'}(\vec{k})\,\vec{m}_j^k\,\vec{m}_{j'}^{-k} \tag{3.2}$$

it is enough to add Fourier components of the interactions for atoms inside the unit cell.
As a matter of fact

$$\vec{m}_{lj} = \sum_k \vec{m}_j^k e^{-i\vec{k}\vec{l}} \quad \text{and} \quad \vec{m}_{l'j'} = \sum_{k'} \vec{m}_{j'}^{k'} e^{-i\vec{k}'\vec{l}'} \tag{3.3}$$

then

$$H = -\sum_{ll'}\sum_{jj'} J_{ll'jj'} \sum_{kk'} \vec{m}_j^k e^{-i\vec{k}\vec{l}} \vec{m}_{j'}^{k'} e^{-i\vec{k}'\vec{l}'}$$

(3.4)

Introducing

$$e^{-i\vec{k}\vec{l}'} e^{i\vec{k}\vec{l}'} = 1$$

then

$$H = -\sum_{ll'}\sum_{jj'}\sum_{kk'} \vec{m}_j^k \vec{m}_{j'}^{k'} e^{-i\vec{l}'(\vec{k}+\vec{k}')} J_{ll'j'} e^{-i\vec{k}(\vec{l}-\vec{l}')}$$

(3.5)

defining

$$J_{jj'}(k) = \sum_l J_{ll'jj'} e^{-i\vec{k}(\vec{l}-\vec{l}')}$$

(3.6)

we note that this Fourier transform is independent on l'
Then

$$H = -\sum_{jj'}\sum_{kk'} \vec{m}_j^k \vec{m}_{j'}^{k'} J_{jj'}(\vec{k}) \sum_{l'} e^{-i\vec{l}'(\vec{k}+\vec{k}')}$$

(3.7)

$$\sum_{l'} e^{-i\vec{l}'(\vec{k}+\vec{k}')} = \delta(\vec{k}+\vec{k}'-\vec{\tau})$$

(3.8)

and in the first Brillouin zone $\vec{\tau} = 0$ and therefore $\vec{k}' = -\vec{k}$.
We find the expression we were looking for:

$$H = -\sum_{k}\sum_{jj'} J_{jj'}(\vec{k}) \vec{m}_j^k \vec{m}_{j'}^{-k}$$

(3.9)

3.1- The classification of Magnetic structures

Let us take the general case in which the $\vec{k}$ vector is a non symmetric point in the Brillouin zone. We say that the structure is incommensurate because $\vec{k}\,\vec{l}$ is not a multiple of 2π.
Example: the sinusoidal structure:

$$\vec{m}_{lj} = \vec{m}_j^k e^{-i\vec{k}\vec{l}} + \vec{m}_j^{-k} e^{i\vec{k}\vec{l}} = \vec{u}_j \cos(\vec{k}\vec{l} + \varphi_j)$$

(3.10)

The length of the magnetic moments will change from one cell to the next

$$\vec{m}_j^k = \frac{\vec{u}_j}{2} e^{i\varphi_j}$$

(3.11)

$$\vec{F}_M(Q) = p\sum_j f_j(Q) \frac{\vec{u}_j}{2} e^{i(\vec{Q}\cdot\vec{r}_j + \varphi_j)}$$

(3.12)
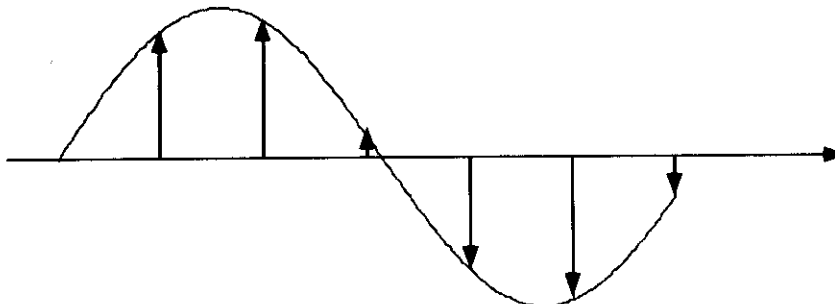
Fig. 17: The sinusoidal magnetic structure

The Fourier coefficient is real. We can present a commensurate structure as a discontinuity for a more general modulated structure.

3.1.4-The mono-k and multi-k structures

For the sake of simplification we now consider structures with a single atom per cell and also that $\vec{m}^k \, / \, /\vec{k}$.

We have

$$\vec{m}_l = \sum_k \vec{m}^k e^{-\vec{k}l} \tag{3.29}$$

$\vec{k} \, / -\vec{k}$ are already automatically associated.

In addition we will suppose that there is several equivalent $\vec{k}$ vectors: $\vec{k}_1, \vec{k}_2, \vec{k}_3$

3.1.4.1- Table: magnetic modes and the associated Hamiltonian

1st domain	$\vec{m}_l = \vec{m}^{k_1} e^{-i\vec{k}_1 l}$ (3.30)	$H_1 = -J(k) \vec{m}^{k_1} \vec{m}^{-k_1}$ (3.31)
2nd domain	$\vec{m}_l = \vec{m}^{k_2} e^{-i\vec{k}_2 l}$ (3.32)	$H_2 = -J(k) \vec{m}^{k_2} \vec{m}^{-k_2}$ (3.33)
multi-k	$\vec{m}_l = \vec{M}^{k_1} e^{-i\vec{k}_1 l} + \vec{M}^{k_2} e^{-i\vec{k}_2 l}$ (3.34)	$H = -J(k)\left[\vec{M}^{k_1} \vec{M}^{-k_1} + \vec{M}^{k_2} \vec{M}^{-k_2} \right]$ (3.35)

Table 8: magnetic modes

$H = H_1 = H_2$ if $M^{k_1} = \dfrac{1}{\sqrt{2}} m^{k_1}$ (double k); $M^{k_1} = \dfrac{1}{\sqrt{3}} m^{k_1}$ (triple k)

Being given the following magnetic Hamiltonian:

$$H = -J\sum_{k_i} m^{k_i} m^{-k_i} + A_4 \sum_{k_i} \left(m^{k_i} \right)^4 + A_4' \sum_{k_i k_{i'}} \left(m^{k_i} \right)^2 \left(m^{k_{i'}} \right)^2$$

$$+ A_6 \sum_{k_i} \left(m^{k_i} \right)^6 + A_6' \sum_{k_i k_{i'}} \left(m^{k_i} \right)^4 \left(m^{k_{i'}} \right)^2 + A_6'' \sum \cdots \tag{3.36}$$

it can be shown that a limitation in the order n of terms included in the Hamiltonian results in

- n= 2 no difference in energy for a single-k structure with domains and a multi-k structure
- n= 4 the structure can switch from single-k to triple-k
- n= 6 the structure can switch from single-k to double k or triple-k (rare earths)

3.1.5- The Multi-k structures

In general

$$\vec{m}_l = \vec{m}^{k_1} e^{-i\vec{k}_1 \vec{l}} + \vec{m}^{k_2} e^{-i\vec{k}_2 \vec{l}}$$

(3.37)

but $\vec{m}_l$ is real, for all $\vec{k}_1 / -\vec{k}_1$ and $\vec{k}_2 / -\vec{k}_2$

$$\vec{m}_l = \vec{m}^{k_1} \cos(\vec{k}_1 \vec{l} + \varphi_1) + \vec{m}^{k_2} \cos(\vec{k}_2 \vec{l} + \varphi_2)$$

(3.38)

if we make the assumption that $\vec{m}^k // \vec{k}$
we will have the following structures

Single-k structure:
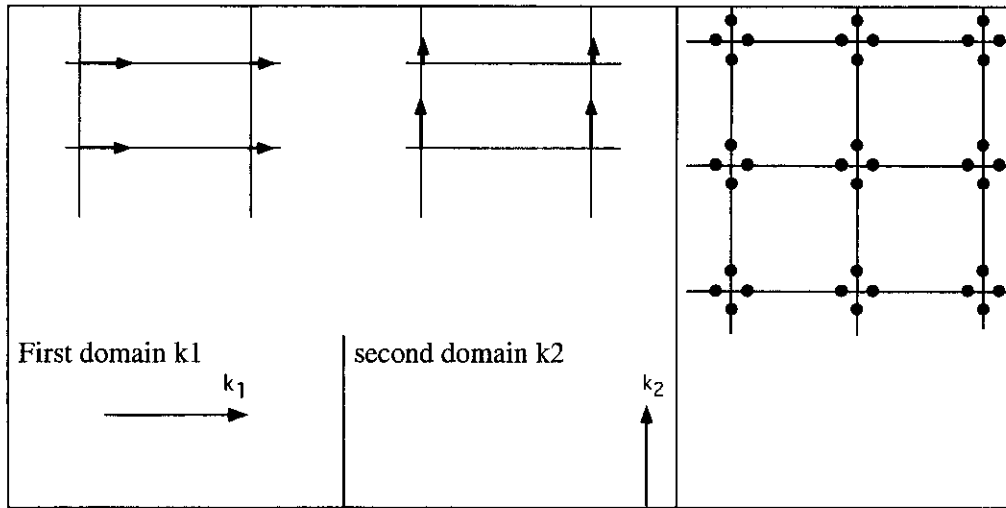
Table 9: Graphs for Single-k structure and cross sections

Double-k structure:

There is only one domain:	Beware this differs from a single propagation vector $\vec{k}_1 + \vec{k}_2$	
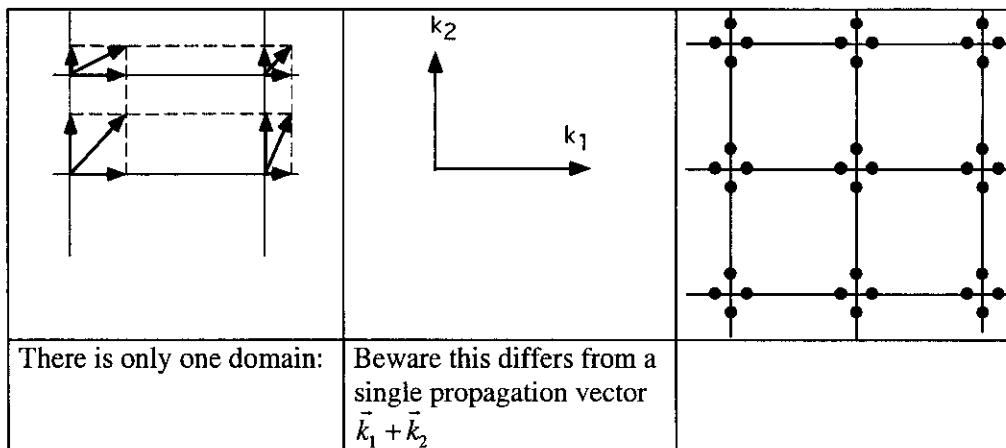
Table 10: Graphs for Double-k structure and cross sections. Note: The same image with the same intensities is obtained in reciprocal space for the single-k structure as soon as the domain distribution is balanced.
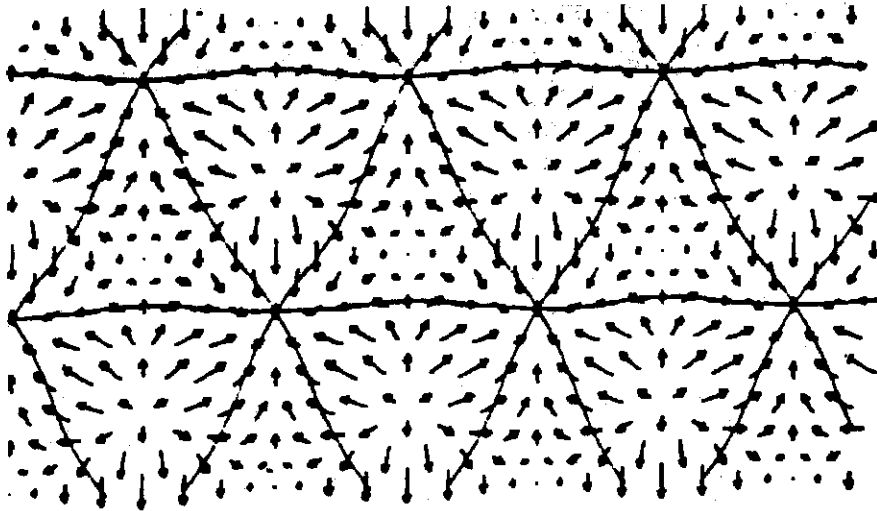
Fig. 19: *Example for a triple k structure:*

3.2 How to remove ambiguities for multi-k structures:

3.2.1- Applying a constraint on the multi-k
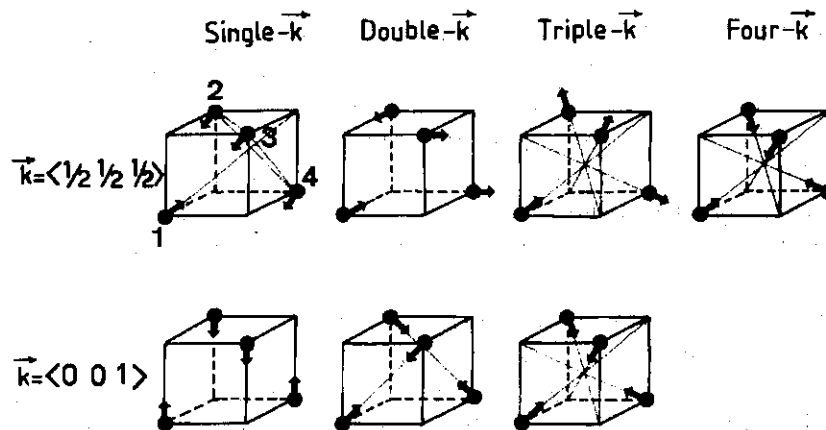
Fig. 20: multi-k structures

Example of the most symmetrical multi-k structures associated with the propagation vector k= <1/2,1/2,1/2> and k=<0, 0, 1> for a face centered cubic (FCC) lattice. Ions 1,2,3,4 are sitting at the center of the faces.

On the following example it can be seen that the intensities associated with the various reflections become different when an external perturbation is applied.
UAs: Applying a uniaxial constraint distorts the lattice in such a way that the domain k for which the modulation propagates parallel is favored. We conclude that the structure is single-k. We can think that it was so before applying the constraint.

26

USb: The same uniaxial constraint distorts the lattice without changing the intensities.
The structure remains triple-k with a single domain.

4- Polarised neutron scattering

4.1 Theory : Atomic magnetization density maps and the spin dependence in the neutron cross section

Let us call $\vec{F}_N(\vec{Q})\,[cm]$ the nuclear structure factor and $\vec{F}_M(\vec{Q})\,[\mu_B]$ the vectorial magnetic structure factor, $\vec{Q}$ being the scattering vector. In a magnetic crystal, the magnetic moment of the neutron interacts with the periodic field of the magnetic electrons resulting in a magnetic scattering amplitude. Due to the dipolar nature of this coupling only the component of $\vec{F}_M(\vec{Q})$

which is perpendicular to $\vec{Q}$ is effective.

$$\vec{F}_{M\perp}(Q) = \hat{Q} \wedge (\vec{F}_M(\hat{Q}) \wedge \hat{Q}) \tag{4.1}$$

It can be shown that the corresponding neutron scattering amplitude operator, expressed in the spin space of the neutron, reads:

$$a_M(\vec{Q}) = p\vec{F}_{M\perp}(\vec{Q})\cdot\vec{\sigma} \tag{4.2}$$

The vector operator $\vec{\sigma}$ has 3 components which are the Pauli matrices and

$$p = 0.269510^{-12}[cm/\mu_B] \tag{4.3}$$

is the scattering length corresponding to one Bohr magneton.
It is then useful to define the magnetic interaction vector:

$$\vec{M}(\vec{Q}) = p\vec{F}_{M\perp}(\vec{Q}) \tag{4.5}$$

Figure 21: The magnetic interaction vector

The spin dependent cross section reads:

$$\frac{\partial\sigma}{\partial\omega} = NN^* + \vec{P}_i(\vec{M}N^* + \vec{M}^*N) + \vec{M}\cdot\vec{M}^* + i\vec{P}_i(\vec{M}^* \wedge \vec{M}) \tag{4.6}$$

$$\text{with } N = N(\vec{Q}) \text{ et } \vec{M} = \vec{M}(\vec{Q}) \tag{4.7}$$

For simplification we shall suppose that the crystal is ferromagnetic or paramagnetic with a vertical applied field and that we are measuring horizontal plane reflections.

We also make the hypothesis that the polarisation is ± 1, that is parallel (+) or opposite(-) to the applied magnetic field. Then:

$$\frac{\partial \sigma}{\partial \Omega} = NN^* + MN^* + M^*N + MM^* \tag{4.8}$$

$$\text{with } M = p\left|\vec{F}_M(\vec{Q})\right| = pF_M \tag{4.9}$$

If, in addition, the crystal has a center of symmetry $N = N^*$, $M = M^*$ and we are left with the very simple expression for the flipping ratio:

$$R = \frac{\sigma^+}{\sigma^-} = \left(\frac{N+M}{N-M}\right)^2, \tag{4.10}$$

From the experimental values of $R(\vec{Q})$, the preceding quadratic equation provides two solutions for the ratio M/N. The crystal structure having been measured by other neutron techniques, the values of N are known and it is normally easy to select the appropriate M.

In the presence of magnetic-nuclear interference terms , these measurements provide us with very sensitive information on the amplitude of magnetic interactions terms.

4.2 Instrumentation: A recent version for a high-magnetic-field single-crystal diffractometer equipped with polarized neutrons: the D3 at ILL.

D3 is a single-crystal diffractometer with polarized incident neutron beam. In practice, the instrument is set at a Bragg peak of an already-known crystalline structure. Then by simply reversing the beam polarisation, D3 performs a highly sensitive measurement of the spin-dependent nuclear-magnetic-interference amplitude term which is present in the Bragg scattering of polarized neutrons from a small single-crystal specimen magnetized in a field [6].No special attention being paid to the scattered polarisation, the data consists in a collection of pure ratios and we may call it a 0D or Scalar approach.

Helium gaz
pumping group

Sample rotation

Liquid nitrogen
dewar

Cryomagnet

Lifting detector

Beam Stop

Cryoflipper

Hot neutron
beam H₄

Lyre

Rotating
plate

Polarising
monochromator

Harmonic filters,
secondary shutters
and monitor

Chariot

Motorised slits

Rotating platform
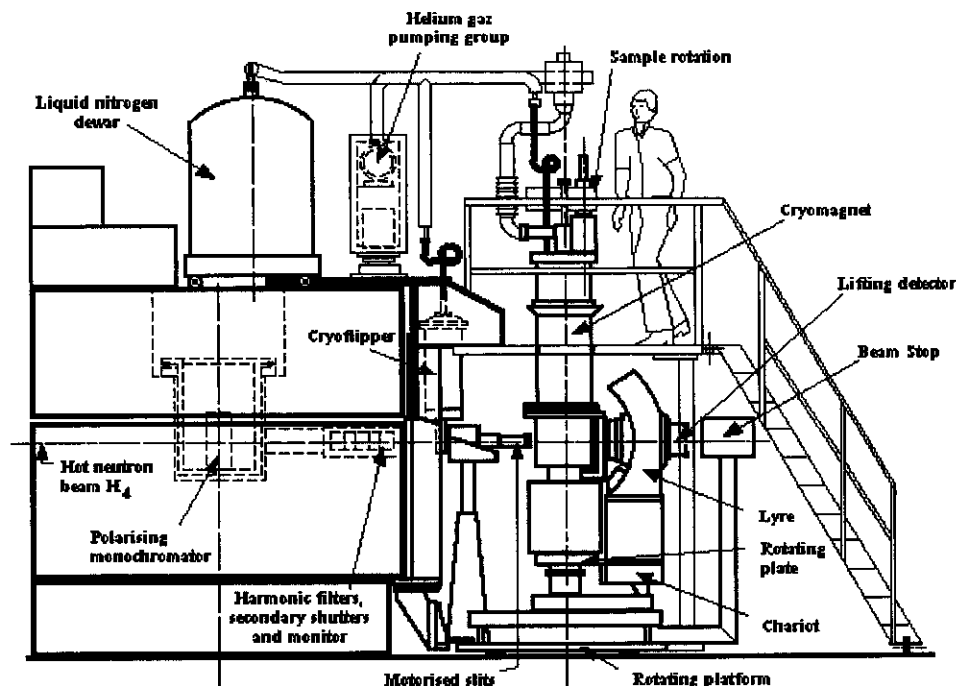
Fig 22:   The polarized neutron diffractometer D3   (http://www.ill.fr/YellowBook/D3/)

(a) *The hot neutron beam.* Being installed at H4, D3 can use neutrons from the hot source with wavelengths as short as 0.4Å. It is, therefore, possible to measure magnetic structure factors up to $\sin\vartheta/\lambda = 2$ Å^{-1}, a value corresponding to a direct-space resolution which is better than any details nature provides in the smallest magnetic ions.

(b) *The polarizing primary spectrometer.* D3 uses readily exchangeable CoFe and Cu2MnAl monochromator cassettes. Wavelength change is an on-line operation, including the insertion of the appropriate resonant harmonic filter. This is particularly useful when extinction or multiple scattering are present. The range of calibration is from 0.42 to 0.84 Å. The highest neutron flux is 0.5 10^6 cm^{-2} s^{-1}. The beam polarisation is good and depends slightly on the wavelength, the monochromator and the in-pile collimation used: it is 90% at its lowest and reaches 99% at its best. Polarisation reversal is made with a "Cryoflipper".

(c) *The magnetic normal beam diffractometer.* The secondary axis is set on a "ILL-Tanzboden" floor, mechanically attached to the monochromator exit port (Fig. 7). Normal-beam geometry with a lifting detector is used and therefore, the large cryomagnet is kept vertical. The detector support arm and the sample adjustment table being non magnetic, cryomagnets with large stray fields can be used. A pneumatic half-shutter system in front of the 5 cm diameter single 3He detector facilitates the determination of the exact orientation matrix for the crystal.

(d) *High-field, low temperature sample environment.* Most measurements carried out on D3b require the sample to be at low temperature and in an intense magnetic field, therefore a 4.6 Tesla Oxford Instrument cryomagnet is dedicated to the instrument. A precision temperature controller and a cryomagnet controller are interfaced to the instrument computer which can set variables in the range (1.5-4.62 Tesla, 1.5-273.0

Kelvin). An airtight chamber attached to the top of the cryostat makes it possible to insert dangerous (alpha emitter) or air-sensitive samples without any contact with the atmosphere.

(e) *Data acquisition. The* instrument is extensively automated. Positioning, measurement, data storage and transfer are under control of a dedicated computer. The software acquisition system provides the user with many simple commands ranging from elementary actions (such as "*SMF 4.62" to set the nominal field, "*WAV .843" to select the wavelength followed by "*SBH Er" to insert the appropriate Erbium filter) up to sophisticated data-collection sequences. Input-stream files containing such orders can be prepared in advance. Output files resulting from the measurements are stored on a file server. They can readily be analyzed by a powerful system of programs making use of the CCSL [7]. This provide quick reduction, sorting and averaging of the various data sets already collected. Resulting magnetic structure factors are then Fourier-transformed for direct visualization of the atomic magnetization density maps and then used to refine models for the magnetic electrons.

4.3 Ferro, Ferri and Paramagnetic Spin density determination

The various means to exploit these Fourier coefficients M(k) will not be developed here, as a recent comprehensive discussion is given by J Schweizer in his course "Form Factors and Magnetization densities" [8]

5 – Polarisation analysis in the scattered beam

5.1 Principle of Neutron Polarimetry
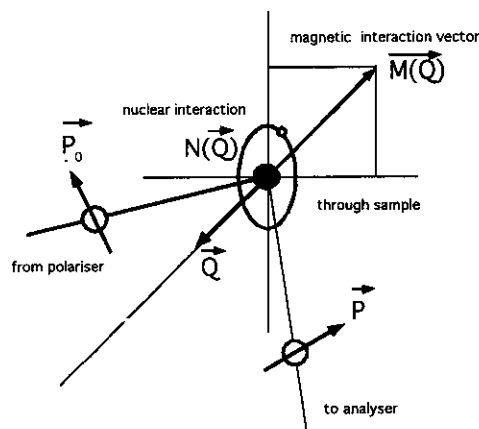
Fig. 23: Neutron Polarimetry: The incident polarised beam is scattered at wave vector Q . The incident polarisation vector is oriented in a particular direction. Due to the magnetic interaction it reorient itself in a way which tells us about the Q Fourier components of the magnetic and nuclear potential experienced in the sample.

5.2 Theory of Elastic Neutron Polarimetry

As early as 1963 the complete theory for elastic neutron nuclear-magnetic theory including polarisation was published by M. Blume [9]. Two master equation were

used, the first one describing the neutron scattering cross section and the second one its polarisation vector as a function of the incident polarisation and the 2 main interactions described in the preceding section. Using the same notations as in 2.2, the general formulae for the polarisation vector $\vec{P}$ of Bragg scattered neutrons with incident polarisation $\vec{P}_0$ becomes:

$$\sigma_t = NN^* + \vec{P}_0(\vec{M}N^* + \vec{M}^*N) + \vec{M}\cdot\vec{M}^* + i\vec{P}_0(\vec{M}^* \times \vec{M}) \tag{5.1}$$

$$\vec{P}\sigma_t = \vec{P}_0 NN^* + \vec{M}N^* + \vec{M}^*N - i(\vec{P}_0 \times \vec{M}N^* - \vec{P}_0 \times \vec{M}^*N)$$
$$+ \vec{M}(\vec{P}_0.\vec{M}^*) + \vec{M}^*(\vec{P}_0.\vec{M}) - \vec{P}_0(\vec{M}.\vec{M}^*) - i(\vec{M}^* \times \vec{M}) \tag{5.2}$$

These two master formulae can be sliced and sorted out into 4 parts with well identified physical origins which are presented in the table below:

The cross section

$$\sigma_t = \left(NN^*\right) + \left(\vec{M}.\vec{M}^*\right) + \left(i\vec{P}_0.(\vec{M}^* \times \vec{M})\right) + \left(\vec{P}_0.\left(\vec{M}N^* + \vec{M}^*N\right)\right) \tag{5.3}$$

The scattered polarisation

$$\vec{P}\sigma_t = \left(\vec{P}_0 NN^*\right) + \left(-\vec{P}_0(\vec{M}.\vec{M}^*) + \vec{M}(\vec{P}_0.\vec{M}^*) + \vec{M}^*(\vec{P}_0.\vec{M})\right) + \left(-i\left(\vec{M}^* \times \vec{M}\right)\right)$$
$$+ \left(N\vec{M}^* + N^*\vec{M} + i\left(N\vec{M}^* - N^*\vec{M}\right) \times \vec{P}_0\right) \tag{5.4}$$

Equations for Nuclear &Magnetic&Interference Neutron Polarimetry

$$\sigma_t = \sigma_n + \sigma_m + \sigma_c + \sigma_i \qquad (5.5)$$

$$\vec{P}\sigma_t = \overrightarrow{(P\sigma)}_n + \overrightarrow{(P\sigma)}_m + \overrightarrow{(P\sigma)}_c + \overrightarrow{(P\sigma)}_i \qquad (5.6)$$

(index) /mode	elastic contribution	comment
(n) nuclear	$\sigma_n = N\,N^*$ (5.7) $\overrightarrow{(P\sigma)}_n = \vec{P}_0\,\sigma_n$ (5.8)	Intensity as modulus square of the structure factor Incident Polarisation is conserved
(m) magnetic normal part	$\sigma_m = \vec{M}.\vec{M}^*$ (5.9) $\overrightarrow{(P\sigma)}_m = -\vec{P}_0\,\sigma_m\{1-2(\hat{P}_0\cdot\hat{M})\hat{M}\}$ (5.10)	Intensity as modulus square of the Magnetic Interaction Vector (MIV) Incident Polarisation is flipped except for its component along the MIV
(c) magnetic chiral part	$\sigma_c = i\left(\vec{M}^* \times \vec{M}\right)\cdot\vec{P}_0$ (5.11) $\overrightarrow{(P\sigma)}_c = -i\left(\vec{M}^* \times \vec{M}\right)$ (5.12)	Intensity depends on incident Polarisation. $\vec{M} \times \vec{M}^* \neq 0$ creates Polarisation along the scattering vector
(i) nuclear-mag. interference	$\sigma_i = \left(N\vec{M}^* + N\vec{M}\right).\vec{P}_0$ (5.13) $\overrightarrow{(P\sigma)}_i = N\vec{M}^* + N^*\vec{M}$ $+ i\left[\left(N\vec{M}^* - N^*\vec{M}\right)\times\vec{P}_0\right]$ (5.14)	Intensity depends on incident polarisation when N&M are in phase Polarisation is created along $\vec{M}$ when N&M are in phase. Incident polarisation is rotated on a cone around $\vec{M}$ when N&M are in quadrature.

Table 11: The 4 main parts in Elastic Polarimetric Neutron Scattering:
At a position $\vec{Q}$ in reciprocal space, the neutron scattering amplitude operator is

$F(\vec{Q}) = N(\vec{Q}) + \vec{M}(\vec{Q})\cdot\vec{\sigma}$ \qquad (5.15)

$N(\vec{Q}) = -n^{-\frac{1}{2}}\sum_n b_n e^{i\vec{Q}.\vec{R}_n}$ *is the Nuclear structure factor* \qquad (5.16)

$\vec{M}(\vec{Q}) = p\vec{F}_{M\perp}(\vec{Q})$ *is the Magnetic interaction vector* \qquad (5.17)

$p = 0.269510^{-12}[cm/\mu_B]$ \qquad (5.18)

$\vec{F}_{M\perp}(\vec{Q}) = p\sum_m f_m(\vec{Q})\left[\vec{m}_m - (\hat{Q}.\vec{m}_m)\hat{Q}\right]e^{i\vec{Q}.\vec{r}_m}e^{-W_m}$ \qquad (5.19)

The 3 components of $\vec{\sigma}$ are the Pauli Matrices (vector operator), $\vec{r}_m$ is the position of the magnetic atom m, $\vec{m}_m$ the local magnetic moment in Bohr magnetons μ_B and $f_m(\vec{Q})$ the magnetic form factor normalized to 1 at $Q = 0$.

32

5.2.1 How the 3 components of scattered polarisation can detect the absolute magnetic configurations

If we assume that the imaginary and real part of the complex magnetic interaction vector $\vec{M}$ are parallel (i.e. $\vec{M} = M.\hat{M}$) the last term disappears. An interesting representation for the polarisation directions [10] is given in a set of coordinates

where the polar axis is parallel to $\vec{M}$.

Fig 24 Rotation of the neutron polarisation vector $\vec{P}$ relative to the direction of the magnetic interaction vector $\vec{M}$. γ is a complex number which expresses the length and the phase of the magnetic interaction vector $\vec{M}$ relatively to the nuclear structure factor N. Special directions (i) are discussed in the text.

Then, using the standard set of polar coordinates and assuming $P_i = 1$:

$$\vec{P}_i[1,\theta_i,\varphi_i], \quad \vec{P}_f[1,\theta_f,\varphi_f], \quad \text{and} \quad \delta\varphi = \varphi_f - \varphi_i \tag{5.20}$$

$$\delta\varphi = \cos^{-1}\left[\frac{NN^* - MM^*}{\sqrt{(NN^* + MM^*)^2 - (NM^* + N^*M)^2}}\right] \tag{5.21}$$

$$\cos\theta_f = \frac{(NN^* + MM^*)\cos\theta_i + NM^* + N^*M}{NN^* + MM^* + (NM^* + N^*M)\cos\theta_i} \tag{5.22}$$

At this stage it is useful to introduce the complex ratio

$$\Gamma = \frac{M}{N}$$

(5.23)

When M and N are in phase, Γ is a real number. When in quadrature it is purely imaginary.

We note the following remarks: (number in parenthesis refer to those in Fig 6)

-θ and φ are completely decoupled when Γ is real or pure imaginary.

-The "precession" angle $\delta\varphi$ by which the $(\vec{M}, \vec{P})$ plane rotates around $\vec{M}$ is independent of the initial φ.

In addition:

-If Γ is real $\delta\varphi$ is zero. The polarisation remains in the initial $(\vec{M}, \vec{P})$ plane. It does not precess but tilts toward $\vec{M}$ when Γ increases. Starting from the direction (1) (initial direction) for $\Gamma = 0$ (pure nuclear) it passes (2) when Γ increases and becomes collinear to $\pm\vec{M}$, (3), when $\Gamma = \pm 1$. For $\Gamma = \pm\infty$ (pure magnetic case) it is flipped over on the symmetrical direction (6) (as if it has precessed by π around $\vec{M}$).

-If Γ is pure imaginary then $\theta_i = \theta_f$, the component of polarisation parallel to $\vec{M}$ remains unchanged. We can say that the polarisation "precesses" purely around $\vec{M}$ by the amount $\delta\varphi$ with no change in the nutation angle θ. $\delta\varphi$ varies from $-\pi$ for $\Gamma = -i\infty$ (6) to π for $\Gamma = i\infty$ (6) passing by $\pi/2$ (5) when $|\Gamma| = 1$. The sign of $\delta\varphi$ is the same as Γ, the polarisation rotates positively around $\vec{M}$ when Γ is positive.

-Note the consistency in the 4 different paths towards the pure magnetic case ($\Gamma = \pm\infty$; $\Gamma = \pm i\infty$). All paths go to the same point using 4 different routes on the sphere),

-In the general case where Γ is complex the situation is complicate: The "real" and "imaginary" source of polarisation are not simply additive because of mixed terms coming from the spin dependent cross-sections. Nevertheless the final polarisation remains in distinct "quadrants of the spherical calotte", with the well defined frontiers and special points discussed above. Those "geometrical" constraints often provide useful first hints on the direction, length and phase of the magnetic interaction vector. The complete analysis of the actual measurements [11] requires, of course, computer calculations [7] based on the complete formalism and taking into account the symmetry of the problem (Different magnetic domains give different Qs, resulting in different final polarizations which are not additive because they are weighted by different cross-sections [10].

5.2.2 Restricted theory for the longitudinal component: LPA

Historically, the first arrangement made to look at the scattered neutron polarisation (outside the direct beam) was made at Oak-Ridge. The direction of the incident polarisation vector $\vec{P}_0$ was fixed adiabatically with a strong magnetic guide-field at the sample position. This particular axis, although not specially vertical was called z and chosen as the quantification axis for describing the spin state (+, -) of the neutron (see appendix). In such a guide-field the only component of scattered polarisation $\vec{P}$ which is conserved for subsequent analysis is P_z, the "longitudinal component". Moon Riste and Koehler [12] actually thought that it was impossible to work without a guide field and focussed their attention on it. In a simplified theory they produced a subset of 4 spin state indexed cross-sections which became famous:

$$\sigma_{zz}^{++} = \left| \left(b + pS_{\perp}^{z} \right) \right|^{2} \tag{5.24}$$

$$\sigma_{zz}^{--} = \left| \left(b - pS_{\perp}^{z} \right) \right|^{2} \tag{5.25}$$

$$\sigma_{zz}^{+-} = \left| \left(p \cdot (S_{\perp}^{x} + iS_{\perp}^{y}) \right) \right|^{2} \tag{5.26}$$

$$\sigma_{zz}^{-+} = \left| \left(p \cdot (S_{\perp}^{x} - iS_{\perp}^{y}) \right) \right|^{2} \tag{5.27}$$

We have added as a subscript to the partial σ's the 2 axis of quantification zz (pre and post scattering) which were implicit in MRK mind but unfortunately forgiven in their notations. Using the zero-field cryopad arrangement we have now access to 12 independent cross sections ($\sigma_{zz}^{++}, \sigma_{zz}^{--}, \sigma_{zz}^{+-}, \sigma_{zz}^{-+}, \sigma_{zx}^{++}, \sigma_{zx}^{--}, \sigma_{zx}^{+-}, \sigma_{zx}^{-+}, \sigma_{zy}^{++}, \sigma_{zy}^{--}, \sigma_{zy}^{+-}, \sigma_{zy}^{-+}$) which are more conveniently expressed in the formalism published earlier by Blume based on the universal concept of polarisation vector, i.e asymmetries in the cross-sections. (beware that in SNP z is always vertical)

Meanwhile, and for 20 years, LPA (unfortunately called Polarisation Analysis by the authors) was the first technique available at finite $\bar{Q}$. Experimentalist got used to the original formalism, forgetting the assumption made, up to the point where it was wrongly called "Full Polarisation Analysis" by over enthusiastic promoters!

The measurement of such Spin-Flipped SF (+-; -+) and non-spin-flipped NSF (++, --) processes along the guide field direction z being the only one possible when "In-field studies" are to be made, it is now common practice to use this simplified theory which is everywhere in the books. because it is not measuring the transverse components of final polarisation.

We recommend to use "Longitudinal Polarisation Analysis" {LPA} to describe this technique and to be very cautious with too strong an interpretation of the results: because LPA technique is unable to detect the transverse component of polarisation we should now prefer SNP in all antiferromagnetic studies where the application of a magnetic field is not strictly required

For example, it is strongly believed that LPA can separate the nuclear (b) from the magnetic (p) terms in the interaction: by putting the z quantization axis (magnetic guide-field) along the scattering vector one can geometrically cancel the non-spin flip magnetic interaction $\mathbf{p} \cdot \mathbf{S}_{\perp}^{z}$. Then all nuclear terms are unflipped and all magnetic terms flipped along z. This technique is true and easy but not sensitive! Knowing the low statistics which are overwhelming obtained with polarisation analysis arrangements it might well miss to detect a very exciting but small nuclear-magnetic correlation. We shall see that this results in a substantial rotation of the initial polarisation vector, therefore a transverse component of scattered polarisation. The LPA measurement hardly prove that the nuclear–magnetic interference terms are zero as it is merely insensitive to this. It is only if the 2 amplitudes are comparable that the polarisation vector will be amply rotated, showing up as a reduced longitudinal component of polarisation. As soon as the 2 amplitudes are unbalanced (small nuclear in large magnetic or small magnetism in large nuclear) they can only be easily detected in 2 neutron scattering effects: the polarisation dependence in the cross section when they are in phase, the transverse component of final polarisation when they are in quadrature. This is where polarised neutron techniques are really sensitive and should be pushed.

35

5.3 Experimental

5.3.1 The zero field chamber approach

For a long time, the theory of General Polarisation Analysis [9] had established that the measurement of all three components of the final polarisation were interesting, being sometimes the only means to decide in between two magnetic configurations. [13]
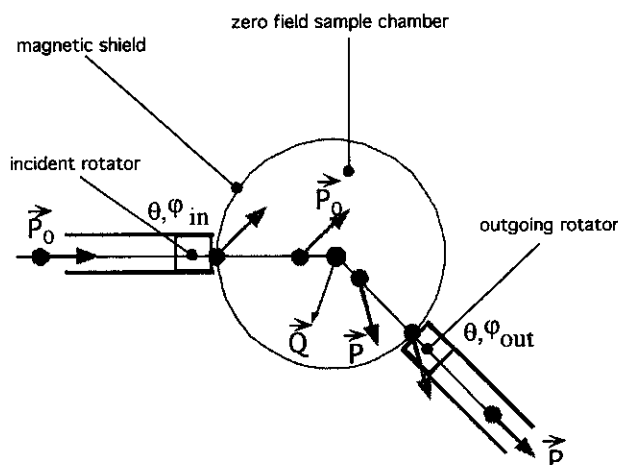

Fig. 25 : Principle of neutron polarimetry in zero field

5.3.2 Cryopad

Such a measurement is a difficult experimental task knowing the strong influence of any magnetic field on neutron polarisation. In fact it requires to connect two different guide-field directions onto a Zero-field sample chamber. We have been able to solve it successfully in our neutron polarimeter CRYOPAD by building the sample chamber with superconducting Meissner screens [3]

Cryopad is a unique facility which is able to achieve full vectorial control of neutron polarisation as it appears necessary in the theory shown in section 5.2 [9]. Being fed with a polarized monochromatic beam out of a primary spectrometer, CRYOPAD orients the polarisation vector in any specific direction and then delivers it to the sample chamber. The sample chamber is maintained in a zero field state, there is no parasitic precession and the change in polarisation, therefore, results only from the interactions present in the scattering process. When the final polarisation exits from the sample chamber, CRYOPAD acts on it in order to measure one by one each 3 components in turn. More details on the design of this polarimeter and the technique of generalized polarisation analysis can be found in [3], [11],[14]

(a) *The host spectrometer.* CRYOPAD can be used as an option to IN20 triple-axis machine which has Heusler polarizing crystals on both the first and last axes or on D3 polarised hot neutron diffractometer with a polarised 3He filter in front of the detector.

A description of IN20 and D3 can be found in the ILL web page (www.ill.fr). On IN20 the Heusler-crystals arrangements are of the vertically focusing type (120 mm high for the monochromator and 85mm for the analyzer) in Bragg reflection geometry, the applied magnetic field being horizontal in the mirror plane and with a

gap of 75mm [15]. Both instruments will be improved in the coming years as they are part of the Millennium programme of the ILL (see Web page)

(b) *The data acquisition system.* On IN20, Cryopad is driven by a special version of the inelastic software. This provides some facilities to set the incoming polarisation in an arbitrary direction and to measure the scattered polarisation in any different direction. Proper currents are automatically introduced in the coils taking into account the different energy in the 2 arms of the spectrometer. On D3, Cryopad is driven by a special version of the crystallographic MAD data acquisition software incorporating special polarisation commands.
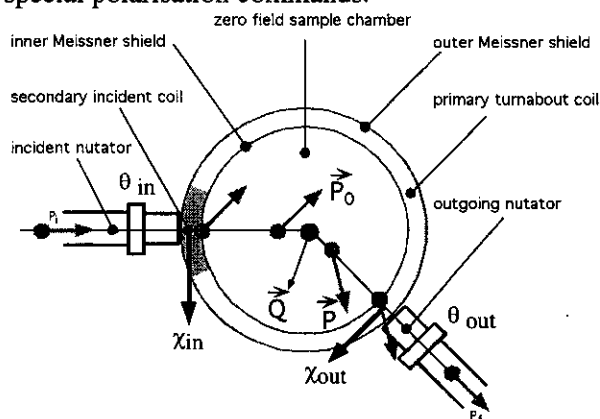
Fig 26 Schematic of the various magnetic regions in CRYOPAD :

5.3.3 LPA in a magnetic Guide-Field

The first systematic polarisation analysis method was developed at Oak-Ridge by Moon Riste and Koehler {MRK} [12]. It was developed at the HFIR using a 3-axes instrument which was providing the proper control of the polarisation direction z at the sample axis with a strong magnetic guide-field.
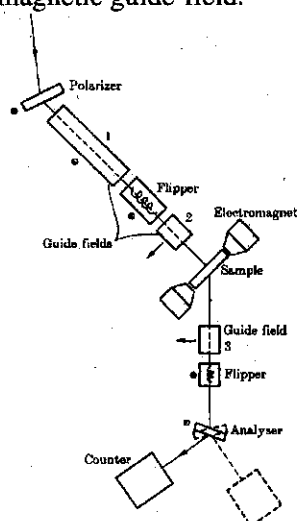
Fig. 27: The schematic representation of a 3 axis spectrometer equipped for polarisation analysis. (after [12])

37

Because only the z longitudinal component of the scattered polarisation (parallel to the field and to the incident polarisation) is measured, the other components being deliberately lost in the measurement (as can be seen in the next picture) and therefore neglected in the analysis, we catalog this method 1D-polarisation analysis. It is generally known as "Polarisation Analysis", and sometimes quoted as "Full polarisation analysis". In view of the preceding discussion and the present existence of SNP we would prefer to call it "Longitudinal Polarisation Analysis" (LPA).

Longitudinal Polarisation Analysis

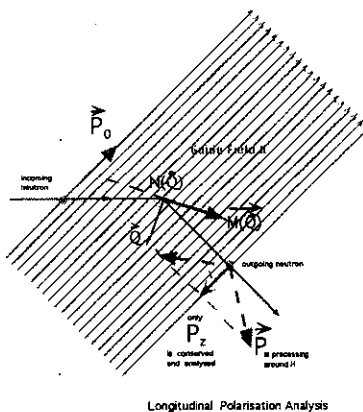*Fig. 28 : LPA: The effect of a magnetic guide-field on the scattered polarisation.*

6. Spherical Neutron Polarimetry at work:

6.1- The use of spherical neutron polarimetry in magnetic structure determination [16]

The determination of magnetic structure is fundamentally different from conventional crystal structure determination whereas in the latter the problem is to determine atomic positions; for magnetic structures the sites of the magnetic atoms are normally known, but both the magnitude and direction of the magnetic moments have to be determined. At the same time the magnetic structure factor differ from the conventional structure factor by being a complex vector, rather than a complex scalar quantity.

Since in a classical diffraction experiment only the intensity of the Bragg reflections can be measured, the phase problem is aggravated in the magnetic case, because six quantities, the amplitudes and phases of the three components of the structure factor, have to be deduced from a single measured intensity. Actually, because of the form of the dipole interaction between the neutron and the magnetic induction in the crystal, only those components of the magnetic structure factor perpendicular to the scattering vector contribute to the scattered intensity and it is this property which may allow the moment directions to be determined. However, in complex, and particularly in noncollinear structures, measurements of the magnetic intensity alone may not be sufficient to determine the magnetic structure uniquely. It is in this context that neutron polarimetry may prove extremely useful, the change in direction of the neutron polarisation vector in the scattering process being rather directly related to the orientation of the magnetic interaction vector (see table below for a graphical summary).

6.1.1- Graphical approach of SNP [10]

$$\sigma_t = \sigma_n + \sigma_m + \sigma_c + \sigma_i \qquad (5.5)$$

$$\vec{P}\sigma_t = \overrightarrow{(P\sigma)}_n + \overrightarrow{(P\sigma)}_m + \overrightarrow{(P\sigma)}_c + \overrightarrow{(P\sigma)}_i \qquad (5.6)$$

(index) /mode	elastic contribution	polarimetric graph
(n) nuclear	$\sigma_n = N\,N^*$ $\overrightarrow{(P\sigma)}_n = \vec{P}_0\,\sigma_n$	
(m) magnetic normal part	$\sigma_m = \vec{M}.\vec{M}^*$ $\overrightarrow{(P\sigma)}_m = -\vec{P}_0\,\sigma_m\left\{1-2(\hat{P}_0\cdot\hat{M})\hat{M}\right\}$	
(c) magnetic chiral part	$\sigma_c = i\left(\vec{M}^* \times \vec{M}\right)\cdot\vec{P}_0$ $\overrightarrow{(P\sigma)}_c = -i\left(\vec{M}^* \times \vec{M}\right)$	M = a + ib (case a=b)
(i)nuclear-mag. interference	$\sigma_i = \left(N\vec{M}^* + N\vec{M}\right).\vec{P}_0$ $\overrightarrow{(P\sigma)}_i = N\vec{M}^* + N^*\vec{M}$ $+ i\left[\left(N\vec{M}^* - N^*\vec{M}\right)\times\vec{P}_0\right]$	

Table 12: The 4 main parts in Elastic Polarimetric Neutron Scattering (a graphical view). Note that the case a=b for the magnetic chiral part (c) should not be considered as a restriction: what remains from the longer component is just acting as a normal magnetic interaction vector (m).

6.1.2- Depolarization due to antiferromagnetic domains

The equations which relate the scattered polarisation vector to the incident one and the physics of the scattering process have been worked out by Blume[9]. For Bragg scattering his formula for the polarisation $\vec{P}$ scattered by a reflection with scattering vector $\vec{Q}$ may be written in terms of its magnetic interaction vector $\vec{M}(\vec{Q})$ as in equations (). The squared modulus of the right hand side of eq. (5.2)

$$\vec{P}\sigma_t = \vec{P}_0 N N^* + \vec{M} N^* + \vec{M}^* N - i(\vec{P}_0 \times \vec{M} N^* - \vec{P}_0 \times \vec{M}^* N)$$

$$+ \vec{M}(\vec{P}_0 . \vec{M}^*) + \vec{M}^*(\vec{P}_0 . \vec{M}) - \vec{P}_0(\vec{M} . \vec{M}^*) - i(\vec{M}^* \times \vec{M})$$

is always greater than or equal to $\quad |\vec{P}_0|^2 \sigma_t^2$ which means that the amplitude of the polarisation is either increased or unchanged by scattering from any pure state, although in general its direction will be altered. Real depolarization of the scattered beam is an indication that a mixed state consisting of more than one type of magnetic domains is present. The ability to distinguish depolarization from rotation of the polarisation vector away from its initial direction is one of the features which makes this technique (SNP) more powerful than conventional longitudinal polarisation analysis (LPA).

6.1.3.- Domain classification

It is worthwhile to rehearse the different types of magnetic domain which may occur in antiferromagnetic structures. They may be classified into:
- configuration domains (K domains),
- 180° domains, (i.e. Magneto-Electric domains)
- orientation domains, (S domains)
- chirality domains.(LR domains)

The type and number of domains that can occur depends on the relative symmetries of the paramagnetic phase and the ordered magnetic phase. In general, if the order of the paramagnetic space group is p and that of the magnetic space group m, the number of different domains is p/m.

6.1.3.1-Configuration domains (K domains)

As was said in section 1 configuration domains exist whenever the propagation vector $\vec{k}$ describing the magnetic structure is not transformed either into itself, or itself plus a reciprocal vector, by all the symmetry operators of the paramagnetic group. When this is the case the operation of the paramagnetic symmetry on $\vec{k}$ generates a set of inequivalent vectors which form the *star of* $\vec{k}$. Each vector in the star generates a different configuration domain, and each configuration domain gives rise to a completely separate set of magnetic reflections.

6.1.3.2- 180º domains

180° domains correspond to regions of crystal in which all the moment directions in one domains are reversed with respect to the corresponding ones in the other. In a structure with a non-zero propagation vector such domains cannot be distinguished except by the defects associated with domain walls. A translation $\vec{\tau}$ such as $\vec{\tau} \cdot \vec{k} = n$, transforms one domain into the other as illustrated into fig. . When the propagation vector is zero, magnetic and nuclear scattering occur in the same reflections and the difference in phase between the magnetic and nuclear scattering differs by π between

a pair of 180° domains. Two simple types of antiferromagnetic structures with zero $\bar{k}$ can be distinguished. In the first the nuclear and magnetic scattering differ in phase by zero or π. These are centrosymmetric structures in which spins related by the centre of symmetry are parallel to one another. An example is Fe2O3, a projection of which, illustrating the 2 domains is shown in fig. 2. For such structures the cross-section

$$\sigma_t = \sigma_n + \sigma_m + \sigma_c + \sigma_i, \qquad \text{eq. (5.5),}$$

is polarisation dependent due to the contribution of the nuclear-mag interference term $\sigma_i = \left(N\vec{M}^* + N\vec{M}\right).\vec{P}_0$, eq. (5.13), and this term has opposite signs for the two domains. The polarisation of the scattered beam is rotated in the plane of the incident polarisation $\vec{P}_0$ and $\vec{M}(\vec{Q})$ due to the terms $\left(-\vec{P}_0(\vec{M}.\vec{M}^*) + \vec{M}(\vec{P}_0.\vec{M}^*) + \vec{M}^*(\vec{P}_0.\vec{M})\right) + \left(N\vec{M}^* + N^*\vec{M}\right)$ in eq. (5.4)

For the second class of structures the nuclear and magnetic scattering differ in phase by $\pm\dfrac{\pi}{2}$ which occurs when moments related by a centre of symmetry are antiparallel.

The cross-section is not polarisation dependent in this case, since due to the phase quadrature, the polarisation dependent term () is zero. However the term of eq(1), which turns the polarisation towards the direction perpendicular to both $\vec{P}_0$ and $\vec{M}(\vec{Q})$ becomes nonzero. The sense of the rotation is determined by the relative phases of the nuclear and magnetic scattering and is opposite for the two types of 180° domains. This overall situation is illustrated in fig. , and exemplified by the antiferromagnetic structures of αFe_2O_3 (hematite) and Cr_2O_3 as shown in figure below.

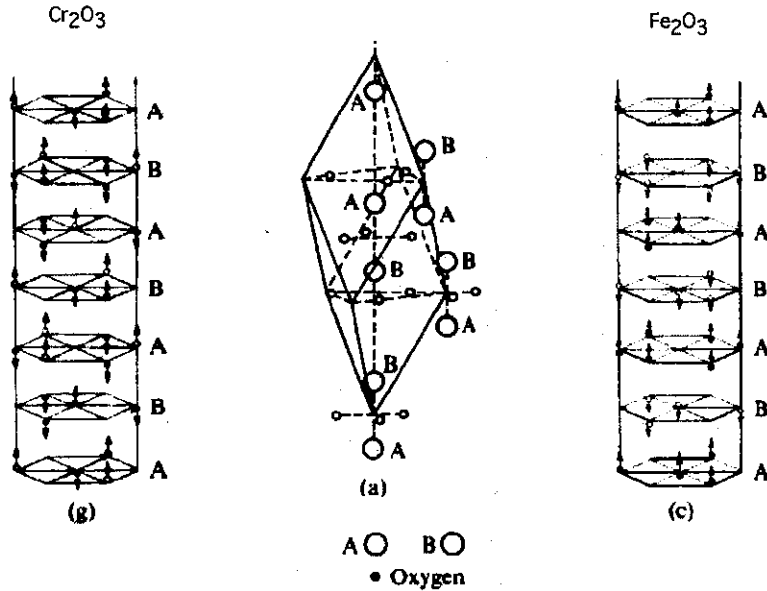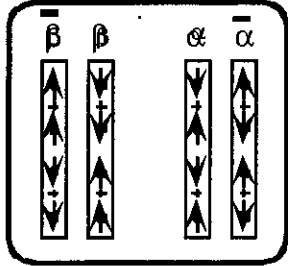Fig. 29: The antiferromagnetic structures of αFe_2O_3 (hematite) and Cr_2O_3 as shown in figure below

Fig. 30 : Magnetic interactions are odd in $\alpha(Cr2O3)$, even in β (Fe2O3) resulting in different rotations for the polarisation. It is possible to imagine what sort of polarisation would result from a mixture of the two.

6.1.3.3- Orientation domains

Orientation domains occur whenever a magnetic structure cannot be described by a magnetic space group which is congruent with that describing the configurational symmetry. For instance, if the configurational symmetry possesses a symmetry axis of order higher than 2, then either the moments lie parallel to this axis, or the structure is noncollinear, or the symmetry axis is not in the magnetic space group. Similarly, in a collinear structure, moments must always lie parallel or perpendicular to mirror planes and diad axes.

In general the magnetic space group $\mathcal{M}$ is congruent with a sub-group S of the configurational symmetry $\mathcal{G}$ and $\mathcal{G}=\mathcal{M}\otimes S$. The sub group S is made up of operators contained in $\mathcal{G}$ which are not in the magnetic group. If the group S is of order s then there are s possible orientation domains which are related to one another by the elements of S. in this case the magnetic interaction vectors for reflections related by the elements of S will be different:

$$\vec{M}(\vec{Q}) \neq \vec{M}(R_s\vec{Q}) \text{ but } \vec{M}_s(\vec{Q}) = \vec{M}(R_s\vec{Q}) \tag{6.1}$$

where R_s is an operator in S and $\vec{M}_s$ is the interaction vector for the domain generated by R_s. For collinear structures the magnetic structure factors of reflections related by the elements of S are equal:

42

$$R_s \vec{F}_M(\vec{Q}) = \vec{F}_M(R_s\vec{Q}) \tag{6.2}$$

but this is not true in the general case

The polarisation scattered by a purely magnetic reflection with magnetic interaction vector $\vec{M} // \vec{M}^*$ is given by

This corresponds to precession of the incident polarisation direction around the direction of $\vec{M}$ by 180° without change in its magnitude [17]. If more than one orientation domain is present in the crystal, the final polarisation vector is the sum of the polarisation vectors scattered by each domain weighted by the intensity scattered by that domain (equal to $\alpha_i \vec{M}_i \vec{M}_i^*$ where α_i is the population of the ith domain). Consider the case illustrated in figure x where the incident polarisation is perpendicular to the scattering vector and in one of the planes or along one of the axes which generate a pair of orientation domains. The magnetic interaction vectors $\vec{M}_1$ and $\vec{M}_2$ of the 2 domains are related by the symmetry axis (Y in Fig x) and rotate the scattered polarisation into the directions indicated by $\vec{P}_1$ and $\vec{P}_2$ respectively. If the domain populations are equal the final polarisation vector is in the same direction as the incident one, but reversed if ϕ is greater than 45°. The same type of behavior occurs if the incident polarisation is perpendicular to the symmetry axis, as shown in Fig. 31

(a)   (b)
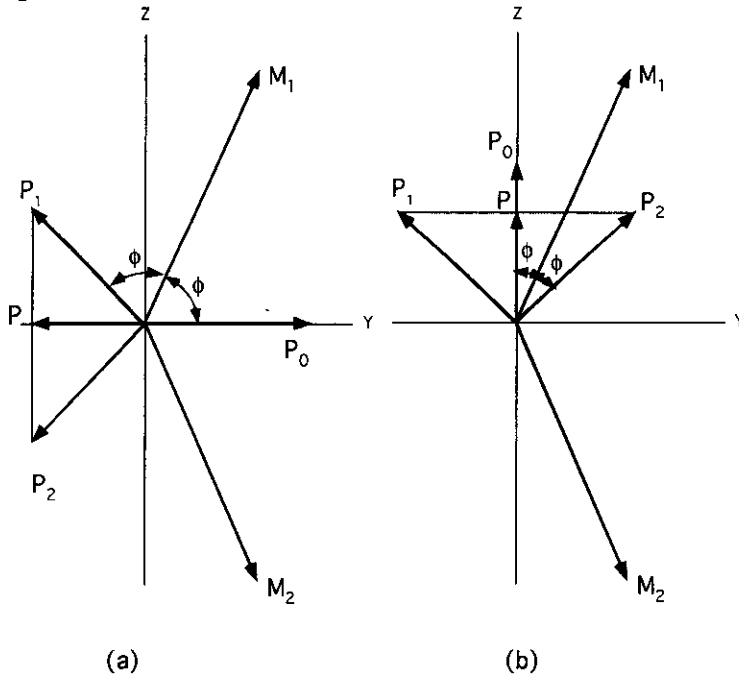
Fig. 31: Diagram showing the rotation of the polarisation direction by scattering from two symmetrically related domains with magnetic interaction vectors $\vec{M}_1$ and $\vec{M}_2$. The incident polarisation $\vec{P}_0$ is rotated to $\vec{P}_1$ by $\vec{M}_1$ and to $\vec{P}_2$ by $\vec{M}_2$. The resultant polarisation is the weighted sum of the two vectors. As we suppose that the 2 domains are in equal proportion the resultant polarisation P is $P_0\cos2\phi$ where ϕ is the angle between $\vec{P}_0$ and $\vec{M}$. (a) The incident polarisation is perpendicular to the

scattering vector and parallel to the symmetry axis relating $\vec{M}_1$ and $\vec{M}_2$. (b) as in (a) but the incident polarisation is perpendicular to the symmetry axis.

6.1.3.4- Chirality domains

Chirality domains occur whenever the paramagnetic space-group is centrosymmetric but the ordered magnetic structure is not. The center of symmetry may be lost because magnetic moments on atoms at positions related by the centre are neither parallel nor anti-parallel to one another. Alternatively it may correspond to a special class of configuration domain: one in which $2\vec{\kappa}$ is not a reciprocal lattice vector ($\vec{\kappa} \neq \vec{\tau} - \vec{\kappa}$), so that the centre of symmetry is not in the configurational group. In the latter case the two chirality domains correspond to positive and negative $\vec{\kappa}$; they both give magnetic reflections at $\vec{g} \pm \vec{\kappa}$ with

$$\vec{M}_\kappa (\vec{\tau} + \vec{\kappa}) = -\vec{M}_\kappa^* (\vec{\tau} - \vec{\kappa}) = -\vec{M}_{-\kappa}^* (\vec{\tau} + \vec{\kappa}). \tag{6.3}$$

For both these types of spin arrangement $\vec{M}$ will not in general be parallel to $\vec{M}^*$ so the terms in eqs x and x respectively are non zero. The first of these terms gives a polarisation dependent cross-section for such structures, and the second results in a rotation of the scattered polarisation towards the scattering vector. Both terms have opposite signs for pairs of chirality domains and therefore cancel each other if the two domains are equally populated, although if the domain population are unequal the polarisation may be reduced
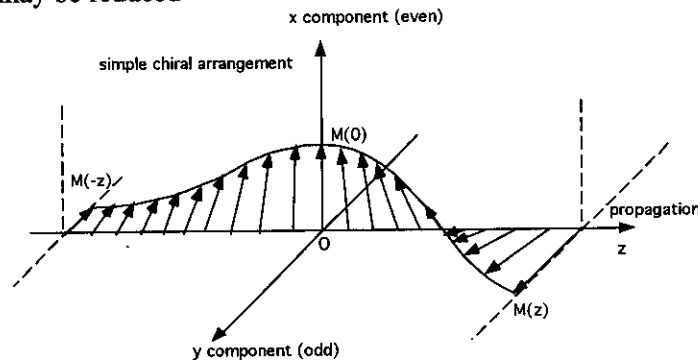
Fig. 32: A tentative 3d representation for an helicoïdal structure showing that the x component of the magnetic moment is an even function of z contrary to the y component which is an odd function. The Fourier transform of an even function being real and that of an odd function imaginary, it results that the real and imaginary part of the magnetic interaction vector are automatically pointing in orthogonal directions: $\vec{M} = a\,\hat{x} + i\,b\,\hat{y}$. As a consequence $\vec{M} \times \vec{M}^* \neq 0$.

Fig. 33: Due to the nature of the dipole interaction the neutron sees only the projection of the helix on a plane perpendicular to its momentum transfer. Depending on the observed reflection a perfectly regular helix can be seen as an elliptic one or even as a sinusoidal modulation (when $\vec{Q} = \vec{\tau} + \vec{k}$ is contained in the "plane of the helix"). As it much influenced by the relative length of the two components in the magnetic interaction vector, the measurement of the final polarisation for 2 orthogonal of the mome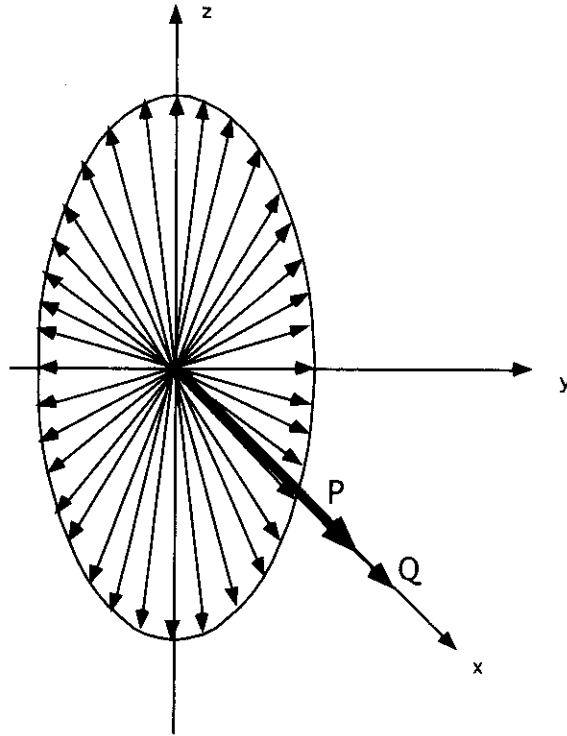ntum transfer, when possible, is a very sensitive tool to distinguish an helix from a collinear sinusoidal arrangement, orient its main axis and measure the ellipticity. (see for example [2, 18])

6.2-Antiferro-magnetic form factor & magnetic density determination [19].

The form factors of magnetic ions in ferromagnetic and paramagnetic materials have been extensively studied using classical polarised neutron flipping ratio measurements and in favorable case the measurements can be very precise[20]. Such form factors are much more difficult to measure in antiferromagnetic structures because in antiferromagnets the neutron scattering cross-section is not often polarisation dependent; the classical method is then not applicable. As a consequence, very few measurements of antiferromagnetic form factors have been made. In the few cases where such measurements have been undertaken they have given very interesting results. The antiferromagnetic form factors are more sensitive that ferromagnetic or paramagnetic ones to the effects of covalency. This because the overlap of positive and negative transferred spin on the ligand ions leads to an actual loss of moment rather than to its redistribution . Up to now no precise measurements of the form factor have been made in antiferromagnetic structures in which the periodicity of the magnetic and nuclear structures are the same and in which magnetic atoms of

45

opposite spin are related by a centre of symmetry. in such structures the magnetic and nuclear scattering are superimposed, making their separation difficult. Additionally the magnetic and nuclear structure factors are in phase quadrature so that there is no interference between them to give a polarisation dependent cross-section. The newly developed technique of spherical neutron polarimetry [14], allows a precise measurement of the magnetic scattering in such structures, and this can be exploited to determine the antiferromagnetic form factor.

The technique of neutron polarimetry which we have developed using Cryopad consists in choosing a direction for the incident neutron polarisation and determining the direction of polarisation of the beam scattered by the sample with a chosen momentum and energy transfer. In the present experiment we are looking at elastic, Bragg, scattering so that the energy transfer is zero.

Cr_2O_3 provides a well known example of an antiferromagnet for which magnetic and nuclear scattering appear in the same Bragg reflections and are in phase quadrature.

$P_{xx} = \beta$	$P_{xy} = 0$	$P_{xz} = \xi$
$P_{yx} = 0$	$P_{yy} = 1$	$P_{yz} = 0$
$P_{zx} = -\xi$	$P_{zy} = 0$	$P_{zz} = \beta$

Table 13: The components of scattered polarisation in Cr_2O_3

It is convenient to choose three orthogonal directions (x, y, z) for the incident polarisation: z perpendicular to the scattering plane, x parallel to the momentum transfer vector, and y completing a right handed Cartesian set. The components of the scattered polarisation parallel to the same three directions can be designated P_{ux}, P_{uy}, P_{uz} where the subscript u indicates the direction of incident polarisation (x, y, z).

$\beta = (1-\gamma^2)/(1+\gamma^2)$ and $\xi = 2m_\gamma\gamma/(1+\gamma^2)$ (6.4)[21]

where γ is the ratio between the magnetic and nuclear structure factors, and m_γ the projection of the magnetic moment direction on the plane perpendicular to the momentum transfer. There are two possible 180 domains for which m_γ is of equal magnitude but opposite in sign. If the volumes of crystal belonging to the two domains are v^+ and v^-, the domain ratio is defined as

$\eta = (v^+ - v^-)/(v^+ + v^-)$ (6.5)

and the non-zero off-diagonal terms in the polarisation matrix become

$P_{xz} = \eta\xi$ and $P_{zx} = -\eta\xi$.   (6.6)

We have already measured the ratios of all reflections of the form $h\,0\,.\,\ell$ with $\sin\theta/\lambda \langle 0.5\,Å^{-1}$ using Cryopad II on IN20 [21]. These measurements, which were made on two crystals of different sizes in three different degrees of domain imbalance, gave amazingly consistent results which enabled the lower angle part of the $Cr3+$ form factor shown in figure1 to be determined with high precision. It is not

however possible to extend these measurements to higher $\sin\theta/\lambda$ using IN20 since the highest useable incident wave-vector is $4.1\,\AA^{-1}$.

We have recently however been able to extend our measurements to higher momentum transfer by installing Cryopad on the hot-source polarised neutron diffractometer D3 and using the newly available 3He neutron spin filter to allow polarisation analysis of the diffracted beam. The experimental arrangement is shown in figure2. At the higher $\sin\theta/\lambda$ values the magnetic scattering becomes very weak and it is impractical to carry out the full polarisation analysis. However, if the domain ratio is high and is determined using the lower angle reflections, then it is sufficient to measure just P_{zz} and P_{zx} components of scattered polarisation. These are linearly rather than quadratically dependent on and may be corrected for deficiencies in the transmitted polarisation using the P_{yy} component. Using this method we are able to deduce the magnetic structure factors of 14 $h\,0\,.\,\ell$ reflections with $\sin\theta/\lambda$ between 0.5 and 0.75 $\AA^{-1}$. Their contributions to the Cr^{2+} form factor are shown in figure 1 and are magnified in the inset.

We were able to fit the low angle data to the Cr^{3+} free atom form factor by assuming a chromium moment of 2.5 μ_B. The rather low value suggests that there is significant covalent transfer to the oxygen ligands. These lower angle data fit rather well onto a smooth curve. The higher angle data are scattered above and below the curve corresponding to a spherical distribution of moment, this scatter contains information about the deviations from spherical symmetry and can be used to determine the distribution of unpaired electrons amongst the different 3d orbitals.
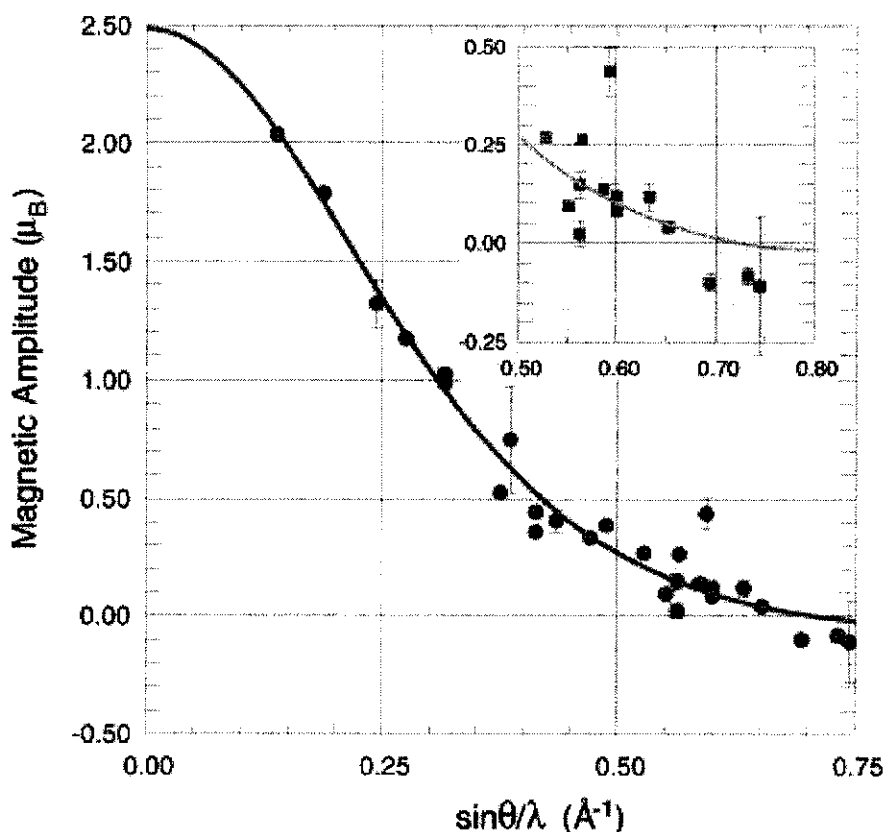
Fig. 34: the experimental values of the magnetic form factor measured at the $h\,0\,.\,\ell$ Bragg reflections of Cr_2O_3. The smooth curve is the spin-only free ion form factor for Cr^{3+} normalized to 2.5 μ_B.

6.3 Theory of Nuclear-magnetic interference in the inelastic scattering of polarised neutrons

Very recently, Maleyev revisited this theoretical issue in details. We give here the abstract of his paper followed by a table of the master formulae where we reconcile his notations with ours. Here is the abstract of his paper [22]

The problem of the inelastic nuclear-magnetic interference (INMI) at the scattering of the polarized neutrons is considered theoretically. General expressions for this interference are derived and discussed. It is shown that the INMI appears at the presence of some interaction, which connects nuclear and magnetic variables and contributes to both nuclear and magnetic parts of the scattering. However at $\vec{H} = 0$, where H is the applied magnetic field or the sample magnetization, the INMI takes place if the spin-lattice interaction is characterized by an axial vector. An example of the Dzialoshinskii-Moriya interaction is considered. It is shown that in this case the

48

INMI is connected to the three spin non-diagonal susceptibility with non-local chiral spin operator. Application of the theory to the spin-Peierls compound $CuGeO_3$ is discussed on the basis of preliminary experimental findings.

The notation used in the table are adapted from Maleyev :

At a position Q in reciprocal space, the neutron scattering amplitude is

$$F_Q = N_Q + \vec{M}_Q \cdot \vec{\sigma} \tag{6.7}$$

$$\text{with } N_Q = -N^{-\frac{1}{2}} \sum_n b_n e^{i\vec{Q}.\vec{r}_n} \text{ and } \vec{M}_Q = p\vec{F}_{M\perp}(\vec{Q}), \tag{6.8}$$

$$p = 0.269510^{-12}[cm/\mu_B] \text{ and } F_{M\perp}(\vec{Q}) = -N^{-\frac{1}{2}} \sum_m f_m(\vec{Q}) e^{i\vec{Q}.\vec{r}_m} \left[\vec{m}_m - (\hat{Q}.\vec{m}_m)\hat{Q} \right]. \tag{6.9}$$

b_n the nuclear scattering length for the atom localized in $\vec{r}_n$, $\vec{m}_m$ the local magnetic moment in μ_B of the magnetic atom m in position $\vec{r}_m$ and $f_m(\vec{Q})$ its local magnetic form factor normalized to 1 at Q=0.

In the inelastic case, the retarded generalized susceptibility is used $\langle A, B \rangle_\omega = i \int_{-\infty}^{+\infty} dt\, e^{i\omega t} \langle [A(t), B(0)] \rangle$ (6.10)

It is splitted in a dispersive (') and a absorptive (") part

$$\langle A, B \rangle_\omega = \langle A, B \rangle'_\omega + i\langle A, B \rangle''_\omega \tag{6.11}$$

The absorptive part is then used to define the various Van Hove correlation function in eq. VH which are contained in the inelastic equations:

$$S_{AB}(\omega) = \chi_\pi \left[1 - e^{\left(-\frac{\omega}{T}\right)} \right]^{-1} \langle A, B \rangle''_\omega . \tag{6.12}$$

The 2 master formulae are sliced into 4 parts given in the table according to

$$\sigma_t = \sigma_n + \sigma_m + \sigma_c + \sigma_i \qquad (6.13)$$

$$\vec{P}\sigma_t = \overrightarrow{(P\sigma)}_n + \overrightarrow{(P\sigma)}_m + \overrightarrow{(P\sigma)}_c + \overrightarrow{(P\sigma)}_i \qquad (6.14)$$

(index) /mode	Elastic:(Blume 1963)[9]	Inelastic : (Maleyev 1998)[22]
	See section 5.2 for notations	Van Hove Correlation Function: $$VHCF : S_{AB}(\omega) = \mathcal{V}_\pi \left[1 - e^{\left(-\frac{\omega}{T}\right)} \right]^{-1} \langle A, B \rangle''_\omega \quad)$$ (6.15)
(n) nuclear part	$\sigma_n = N\,N^* \qquad (5.7)$ $\overrightarrow{(P\sigma)}_n = \vec{P}_0\,\sigma_n \qquad (5.8)$	$\sigma_n = (k_f/k_i)S_n \qquad (6.16)$ $\overrightarrow{(P\sigma)}_n = \vec{P}_0\sigma_n \qquad (6.17)$ $S_n \text{ is } VHCF \text{ for } \langle N_{-Q}, N_Q \rangle''_\omega \qquad (6.18)$
	$\sigma_m = \vec{M}.\vec{M}^* \qquad (5.9)$ $\overrightarrow{(P\sigma)}_m = -\vec{P}_0\,\sigma_m \{1-2(\hat{P}_0 \cdot \hat{M})\hat{M}\} \qquad (5.10)$	$\sigma_m = (k_f/k_i)S_{\alpha\beta}\delta_{\alpha\beta} \qquad (6.19)$ $\overrightarrow{(P_\alpha\sigma)}_m = \left(\frac{k_f}{k_i}\right) P_{0\beta}\left[\left(S_{\alpha\beta}+S_{\beta\alpha}\right) - \delta_{\alpha\beta}S_{\alpha\beta}\right]$ (6.20) $S_{\alpha\beta} \text{ is } VHCF \text{ for } \langle M^\alpha_{-Q}, M^\beta_Q \rangle''_\omega \qquad (6.21)$
(c) magnetic chiral part	$\sigma_c = i\left(\vec{M}^* \times \vec{M}\right) \cdot \vec{P}_0 \quad (5.11)$ $\overrightarrow{(P\sigma)}_c = -i\left(\vec{M}^* \times \vec{M}\right) \qquad (5.12)$	$\sigma_c = (k_f/k_i)\,i\,S_{\alpha\beta}\,\varepsilon_{\alpha\beta\gamma}\,P_{0\gamma} \qquad (6.22)$ $\overrightarrow{(P_\alpha\sigma)}_c = -(k_f/k_i)\,i\,\varepsilon_{\alpha\beta\gamma}\,S_{\beta\gamma} \qquad (6.23)$ $S_{\alpha\beta} \text{ is } VHCF \text{ for } \langle M^\alpha_{-Q}, M^\beta_Q \rangle''_\omega \qquad (6.24)$
(i) nuclear-mag. interference	$\sigma_i = \left(N\vec{M}^* + N\vec{M}\right) \cdot \vec{P}_0 \qquad (5.13)$ $\overrightarrow{(P\sigma)}_i = N\,\vec{M}^* + N^*\,\vec{M} + i\left[\left(N\,\vec{M}^* - N^*\,\vec{M}\right) \times \vec{P}_0\right] \qquad (5.14)$	$\sigma_i = (k_f/k_i)\,i\,\vec{S}_+ \cdot \vec{P}_0 \qquad (6.25)$ $\overrightarrow{(P\sigma)}_i = (k_f/k_i)\left\{\vec{S}_+ + i\left[\vec{S}_- \times \vec{P}_o\right]\right\}$ (6.26) $S_\pm \text{ is } VHCF \text{ for }$ $\langle N_{-Q}, \vec{M}_Q \rangle''_{\omega \pm} = \langle N_{-Q}, \vec{M}_Q \rangle''_\omega \pm \langle \vec{M}_{-Q}, N_Q \rangle''_\omega$ (6.27)

Table 14: A parallel in between elastic and inelastic SNP formulae (note that in the original table [4] an error exists in formulae 4.20 which has been corrected here. We thank B. Roessli for raising our attention to this point.)

Conclusion

Magnetic neutron scattering remains a first class tool for the study of magnetic order and interactions. Powder scattering has made progress with the introduction of large position sensitive detectors. Unpolarised single crystals studies are being revolutionised with the introduction of a new quasi-Laue method using image plate detectors. Unpolarised neutrons show geometrical features of the cross-section and give the modulus of the magnetic interaction vector $\bar{M}$ at many points in reciprocal space. Based on the dipolar anisotropy of its magnetic interaction the neutron can tell us what are the direction of the magnetic moments from observed extinction and relative intensities systematically measured at many different momentum transfer $\bar{Q}$ in reciprocal space.

At one particular $\bar{Q}$, the application of Spherical Neutron Polarimetry (SNP), can check, often directly, what is the direction of the magnetic interaction vector $\bar{M}$ in its plane. This has been a powerful direct method for detecting the limitations of the classical measurement of cross-sections in the numerous cases where the integrated intensities are not sensitive enough to the details of the magnetic structure. (Essentially due to domains superposition there are many possible models for a given, limited, set of intensities). Moreover, in such difficult situations, SNP lead to an unambiguous understanding of what neutron can tell of a complicated antiferromagnetic structures like triangular and helicoïdal arrangements.

What is most spectacular with neutron scattering is the exploitation of the nuclear-magnetic interference term which gives a great sensitivity for the measurement of very small magnetic amplitude. It has been extensively used for the complete determination of the magnetic form factor and anisotropy in it, telling us about the exact shape and spatial density of magnetic ions. It has now been demonstrated that SNP can do that in favorable antiferromagnetic arrangements like for magneto electric compounds.

But the most promising feature is in the field of inelastic neutron scattering where, triggered by SNP experiments, recent theoretical analysis has shown that the measurement of the transverse component of scattered polarisation is a way to measure mixed nuclear-magnetic pair correlation functions. Such measurements are being done and may well have a serious impact on the future understanding of microscopic physics at low dimensional, spin driven phase transitions.

Annexes: [23]

A1. The polarized neutron beam

A.1.1. Quantum aspects...

Because the neutron carries a spin 1/2, (an internal degree of freedom...) the complete quantum mechanical description for it's dynamical state $|\psi\rangle$ has two components (+, -). In term of real space wave-functions we have

$$\psi_+(\vec{r}) = \langle \vec{r},+|\psi \rangle \quad \text{and} \quad \psi_-(\vec{r}) = \langle \vec{r},-|\psi \rangle \tag{A 1}$$

which are generally grouped in a two component spinor:

$$[\psi(\vec{r})] = \begin{pmatrix} \psi_+(\vec{r}) \\ \psi_-(\vec{r}) \end{pmatrix} \tag{A 2}$$

These two functions of space variables may be completely distinct if the Hamiltonian comprises important coupling terms in between orbital $(\vec{r})$ and spin (+,-) coordinates.

An example of historical importance is the Stern-Gerlach experiment. A static magnetic field with a large gradient produces two possible deviations for silver neutral atoms depending on which spin state they go into at the entrance in the magnetic field. Such an experiment could not be made directly on an electron beam because of the dominant Lorentz force which couples strongly the orbit $\vec{v}$ to the field $\vec{B}$ for a charged particle q.

For the neutron q=0, the Lorentz force disappears and we can use the Stern-Gerlach experiment in order to demonstrate the quantification of the 1/2 angular momentum. Nevertheless we shall see later that slowly varying fields are used very often on neutron beams without any mention of Stern-Gerlach orbital effects. This is because the magnetic moment of the neutron is 3 orders of magnitude smaller than the electron's one:

$$\mu_{neut.} = g_n \mu_0 = -1.913 \frac{m_e}{M_p} \mu_B \tag{A 3}$$

$$\mu_B = 9.2741 \quad 10^{-24} JT^{-1}(SI)$$

$$\mu_{neut.} = 9.6622 \quad 10^{-27} JT^{-1}(SI) \tag{A 4}$$

Because the orbital deviation is generally so small we often write the neutron spinor as the product of a single wave function times a spin 1/2 state vector:

$$[\psi(\vec{r})] = \varphi(\vec{r}) \cdot [\chi] \tag{A 5}$$

In all the experimental aspects which are discussed in section 1 what happens to the magnetic field is at a length scale which is orders of magnitude larger than the neutron wavelength, therefore the position of the neutron can be considered as a classical point variable [24] and the neutron magnetic moment will sense only the magnetic field at this point. Time and space being then simply coupled through the classical speed of the neutron, inhomogeneous magnetic fields along the neutron trajectory will appear in spin space as simple, time dependent quantities.

The spin 1/2 state vector evolution

$$|\chi\rangle = e^{-i\varphi/2}\cos\tfrac{\theta}{2}|+\rangle + e^{i\varphi/2}\sin\tfrac{\theta}{2}|-\rangle \tag{A 6}$$

will be governed by the usual time dependent Schrödinger equation and θ and φ will appear to be functions of time (As usual they give the polar angles for the proper spin quantization direction i. e. the direction relative to which the spin component S_z is $+\tfrac{1}{2}$, that is also the direction of the corresponding classical angular momentum vector)

The 3 components of the angular momentum vector operator $\vec{S}$ are simply expressed in the $|+\rangle, |-\rangle$ basis with the 3 Pauli Matrices:

$$\sigma_x = \begin{bmatrix} 0 & 1 \\ 1 & 0 \end{bmatrix}, \quad \sigma_y = \begin{bmatrix} 0 & -i \\ i & 0 \end{bmatrix}, \quad \sigma_z = \begin{bmatrix} 1 & 0 \\ 0 & -1 \end{bmatrix} \tag{A 7}$$

$$S_\alpha = \tfrac{\hbar}{2}\langle \chi | \sigma_\alpha | \chi \rangle. \tag{A 8}$$

$$\langle S_x \rangle = \tfrac{\hbar}{2}\sin\theta\cos\varphi, \quad \langle S_y \rangle = \tfrac{\hbar}{2}\sin\theta\sin\varphi, \quad \langle S_z \rangle = \tfrac{\hbar}{2}\cos\theta \tag{A 9}$$

Note that any Hermitian operator can also be expressed on this basis as a linear combination of the identity matrix and the 3 Pauli matrices.

A.1.2 Statistical average

Because the beam contains many neutrons which are not necessarily in the same spin state we shall call polarisation for a beam of neutron the ensemble average of the angular momentum (see Annex 1)

$$\vec{P} = \langle \chi | \hat{\sigma} | \chi \rangle \tag{A 10}$$

An interesting quantum mechanical derivation is the time evolution of the beam polarisation vector $\vec{P}$ in an homogeneous magnetic field $\vec{H}$. (see Annex 2)

Let us start from the dynamical equation for mean quantum values:

$$\frac{\partial \vec{P}}{\partial t} = \frac{\partial \langle \hat{\sigma} \rangle}{\partial t} = \tfrac{1}{\hbar}\langle [\hat{\sigma}, H_s] \rangle \tag{A 11}$$

With the appropriate Zeeman energy term:

$$H_s = -\hat{\mu} \cdot \vec{H} = -\gamma \tfrac{\hbar}{2}(\hat{\sigma} \cdot \vec{H}) \tag{A 12}$$

we find:

$$\frac{\partial \vec{P}}{\partial t} = -\tfrac{\gamma}{2}\langle [\hat{\sigma}, (\hat{\sigma} \cdot \vec{H})] \rangle = \tfrac{1}{2}i\gamma\langle (\vec{H} \wedge (\hat{\sigma} \wedge \hat{\sigma})) \rangle \tag{1.13}$$

Using the commutation relation :

$$\sigma_x\sigma_y - \sigma_y\sigma_x = 2i\sigma_z \tag{A 14}$$

we have:

$$\frac{\partial \vec{P}}{\partial t} = -\gamma\langle (\vec{H} \wedge \langle \hat{\sigma} \rangle) \rangle \tag{A 16}$$

and finally

$$\frac{\partial \vec{P}}{\partial t} = -\gamma \left\langle \left(\vec{H} \wedge \vec{P} \right) \right\rangle \tag{A 17}$$

$$\text{with } \gamma = -18324.61 \, s^{-1} Gauss^{-1} \tag{A 18}$$

A.1.3....and classical behavior.

At this stage it is interesting to establish the classical equation of motion for a magnetic moment m in interaction with a magnetic field. We have to consider two torques:

$$\Gamma_1 = \vec{m} \wedge \vec{H} \tag{A 19}$$

and the inertia of angular momentum:

$$\vec{\Gamma}_2 = -\frac{d\vec{j}}{dt} = -\gamma^{-1} \frac{d\vec{m}}{dt} \tag{A 20}$$

At equilibrium these two torques must cancel out:

$$\frac{\partial \vec{m}}{\partial t} = -\gamma \left(\vec{H} \wedge \vec{m} \right) \tag{A 21}$$

We note that this classical derivation let us exactly with the quantum equation of motion ($\vec{P}$ and $\vec{m}$ are obviously proportional vectors). When dealing with "gentle" magnetic fields not only we can separate the spin and the orbit , but in addition we find that the spin polarisation behaves classically.
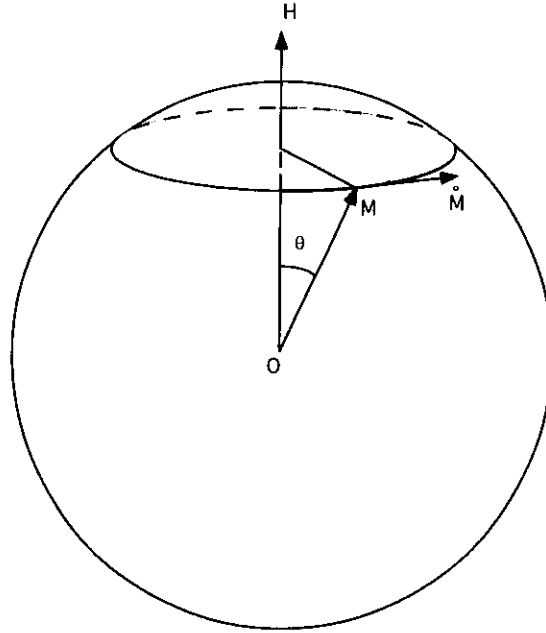
A.1.4. Larmor precession...

From the preceding equation of motion we can now easily extract the main characteristics of the solution in a constant magnetic field:

$$\frac{\partial \vec{m}^2}{\partial t} = 2\vec{m} \frac{\partial \vec{m}}{\partial t} = 2\gamma \vec{m} \left(\vec{H} \wedge \vec{m} \right) = 0 \tag{A 22}$$

i. e. $\vec{m}^2 = const.$, the modulus of the polarisation remains constant:

$$\vec{H} \cdot \frac{\partial \vec{m}}{\partial t} = -\gamma \cdot \vec{H} \cdot \left(\vec{H} \wedge \vec{m} \right) = 0 \tag{A 23}$$

i.e. $\vec{H} \cdot \vec{m} = Const.$, the projection of the polarisation on the applied field remains constant as shown in Figure 1.

FigA- 1 Larmor precession of the neutron magnetic moment in a constant magnetic field

Finally

$$\left|\omega_L\right| = \frac{1}{m_\perp}\left|\frac{d\vec{m}}{dt}\right| = \frac{\gamma \vec{m} \wedge \vec{H}}{\dfrac{\left|\vec{m} \wedge \vec{H}\right|}{\left|\vec{H}\right|}} = \gamma H$$

$$\omega_L = \frac{-1.913\,e}{M_p} \cdot B\,(SI) \qquad\qquad (A\ 25)$$

$$\left|\omega_L\right|[rad\,/\,\sec] = 18325 \cdot H[Gauss] \qquad\qquad (A\ 26)$$

and for the moving neutron

$$\frac{\Delta\varphi}{\Delta x}[deg/\ cm] = 2.65\,\lambda\left[\mathring{A}\right]H[Gauss]$$

$$\qquad\qquad (A\ 27)$$

A neutron with a 2.4 Å wavelength will precess by 60° in a 10 Gauss.cm field integral.

A.1.5 Rotation of the neutron quantization axis in a "guide-field" and the adiabaticity parameter:

We shall see later that it is often desirable to change the direction of the neutron polarisation along the traveling beam in order to adapt it to the various requirements at different points on the instrument. This is generally achieved by introducing appropriate helicoïdal guide-field sections on the neutron trajectory. The field amplitude remains roughly constant as in *Fig. A 2:*.
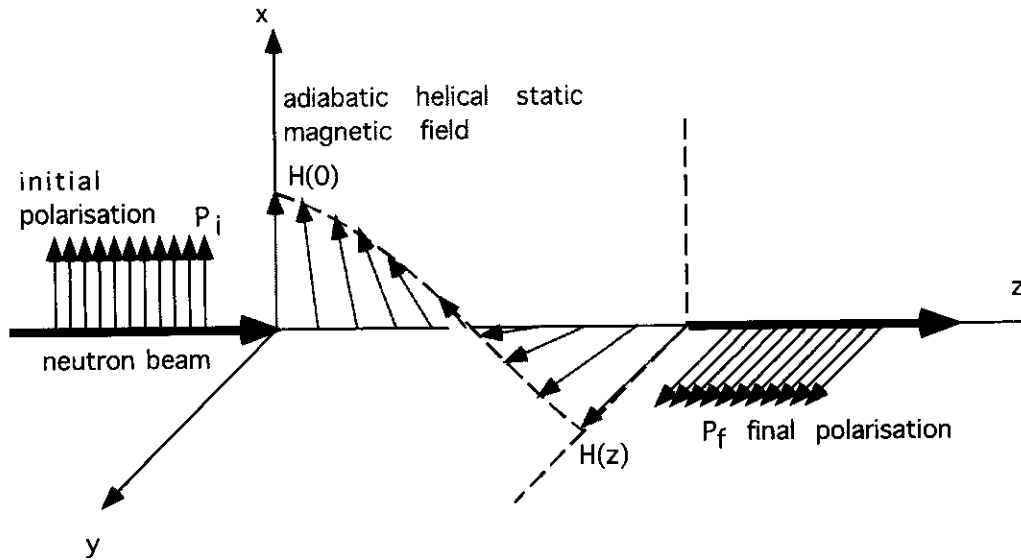
Fig. A 2: Propagation of the neutron polarisation vector in an helicoïdal field which rotates by $\frac{\pi}{2}$ at constant modulus. We suppose here that the component of polarisation parallel to the field follows adiabatically the field direction (the longitudinal component is adiabatically conserved. see text).

By solving the time dependent Schrödinger equation or the equivalent "classical" equation of motion the final polarisation after a π field rotation [25] and in the general case [26] have been deduced. It appears that , apart from Berry phase which is not our problem here, the dynamical behavior is controlled by a single "adiabaticity parameter E", a pure number which is the ratio of the neutron Larmor precession versus the angle of rotation for the guide-field (both being expressed in deg/cm.).

$$E = \frac{\omega_L}{\omega_H}$$

(A 28)

We give in the figure the 3 final components of polarisation for the important practical case of a full initial polarisation entering a field rotation of $\pi/2$

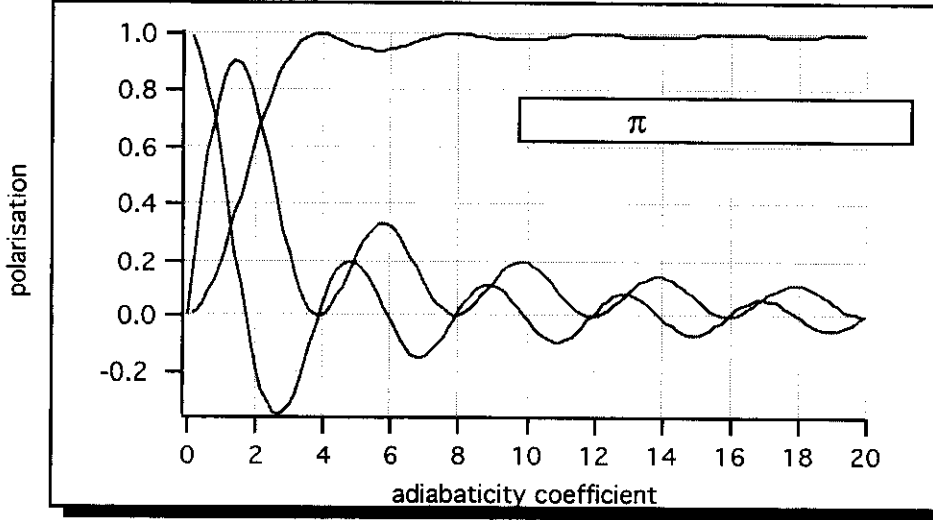## Components of P as a function of the adiabaticity parameter

Fig. A3: The 3 final components of polarisation as a function of the adiabaticity parameter
At the extreme left of the adiabaticity scale, E is very small, the field reorients itself quickly (in much less than a Larmor precession period) : the neutron spin remains in its initial direction. This means that the field direction which was parallel to the spin at the entrance in the system is orthogonal to it at the exit (The Zeeman energy is changed and therefore the process is non-adiabatic for the neutron). At the extreme right of the scale the field reorientation is slow (i.e. the neutron has made several Larmor precessions during the time spent in the helical field region). We see that two components of the neutron spin have been interchanged in such a way that the spin remains fully aligned with the applied field. (The Zeeman energy is unchanged, the field has "guided" the neutron spin component which was parallel to it and the process is fully adiabatic for the neutron).

For completeness we give here the expressions for the component parallel to the final direction of the field assuming it was fully polarized along x at the entrance:

For a $\Pi/2$ field rotation:

$$P_y^{\pi/2} = 1 - \frac{2}{1+E^2} Sin^2\left(\frac{\pi}{4}\sqrt{1+E^2} \right),$$

(A 29)

with $E = 0.03\,H[Gauss] \cdot S[cm] \cdot \lambda[\mathring{A}]$

(A 30)

and for a Π field rotation:

$$P_x^{\pi} = -1 + \frac{2}{1+E^2} Sin^2\left(\frac{\pi}{2}\sqrt{1+E^2} \right),$$

(A 31)

with $E = 0.015\,H[Gauss] \cdot S[cm] \cdot \lambda[\mathring{A}]$

(A 32)

The polarisation transmission along the guide-field direction becomes better than 95% for values of E greater than 3; 98% for values greater than 8; and 99.5% for values greater than 15. Still we have to be careful, when they matter, with orthogonal components which decay slowly and are still of the order of 10% at E=20.

Let us finish this discussion by looking at the expression for the time derivative of the Zeeman term.

$$\frac{d\vec{H}.\vec{P}}{dt} = \vec{H}\cdot\frac{d\vec{P}}{dt} + \vec{P}\frac{d\vec{H}}{dt} = -\gamma\vec{H}\cdot\left(\vec{H}\wedge\vec{P}\right) + \vec{P}\frac{d\vec{H}}{dt} \tag{A 33}$$

The mixed product on the right term is always zero, it appears clearly that only a change in the field can change the energy. If the modulus of the guide field remains constant $\frac{d\vec{H}}{dt}$ is orthogonal to $\vec{H}$ and therefore only couples with the components of $\vec{P}$ which are oscillating at Larmor Frequency. The product will zero out to the first order. Only second order terms may change energy. This is the mechanical origin of the guide field adiabaticity.

A.1.6. Non-adiabatic passage through a magnetic field discontinuity:

In some other instrumental aspects in neutron polarimetry, one is dealing with the extreme left of the dynamical scale. We shall see for example that in the measurement of the spin dependent cross-section we must be able to reverse at will (flip) the direction of the incident polarisation in order to measure the "flipping ratio".

Amongst several techniques which have been used to accomplish such a flipping is the Dabbs-foil system. The neutron goes through a transverse current sheet in a very short time compared with the Larmor period. The idealized problem looks simple and could be viewed as a peculiar E=0 point on the preceding field-rotation curves when calculated for a π field rotation. In practice, the problem deserve a separate discussion because the magnetic field has no constant modulus. It goes instead through a node at the center of the sheet.

What happens at that point of zero-field depends critically on the presence of small orthogonal components coming from any stray-field. This problem has been discussed carefully many years ago in the context of successive Stern-Gerlach measurement where the same experimental difficulty happened [27].

From Majorana equations we can calculate the atomic beam polarisation after the field reversal:
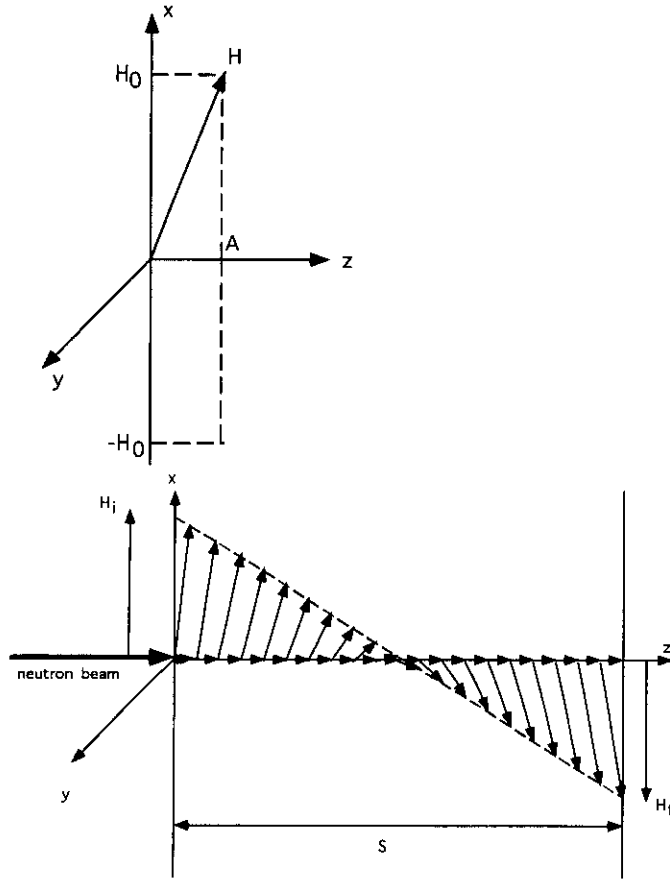
Fig A-4 The magnetic field components used in the Majorana calculation of the non adiabatic crossing through a field node

With the stray-field $H_z = A$; $H_y = 0$; $H_x = -Ct$ and $P_f = P_x$ we find

$$\frac{P_f^x}{P_0^x} = 1 - 2\exp(-k\frac{\pi}{2}) \quad \text{with} \quad k = \frac{g\mu_N A^2}{\hbar C} \tag{A 34}$$

For thermal neutrons and then keeping only first order in the exponential we find the following:

$$\frac{P_x^f}{P_x^0} \cong -1 + \frac{0.036 A^2 [Gauss^2] \lambda [\mathring{A}]}{\frac{dH}{dx}[Gauss/cm]} \tag{A 35}$$

The amount by which the process will depart in first approximation from the ideal reversal depend linearly on the inverse gradient of the main field but quadratically in the stray field amplitude By looking at Fig. 5 were we have reported the variation of the ratio $\frac{P_f}{P_0}$ for various realistic values of stray-field A and main-field gradient for thermal neutron wavelength, we conclude that for cold neutrons and standard current sheets conditions such departure from pure non-adiabaticity may become important.
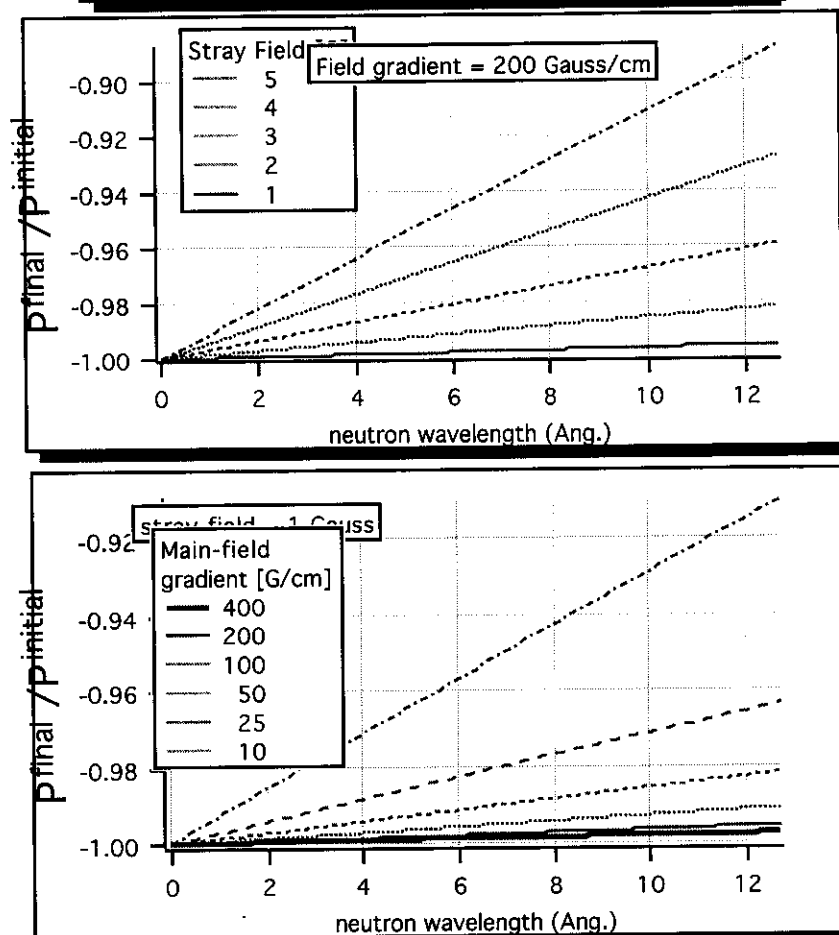
Fig.A 5 Lambda dependence of the polarisation reversal when crossing a Dabbs foil
for various values of the parasitic component A and of the principal field gradient.

A2. The Neutron Spin Filter

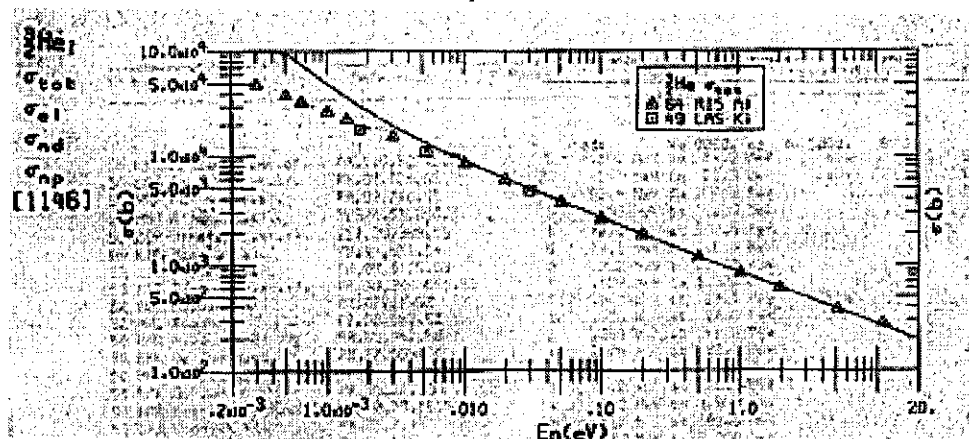### A 2.1. More polarized neutrons: the polarized 3He filter.

Fig A 6 Total neutron absorption cross section for the 3He

(a) Decoupling the optics from the polarisation with the transmission filter.

The production of hot neutron beams with polarisation greater than 95% and energies up to 500 meV (lambda = 0.4 Å.) has only been possible until now by using selected Bragg reflections from certain magnetic crystals. The polarisation results from the fact that magnetic and nuclear scattering amplitudes cancel each other for one of the two spin states of the neutron. Unfortunately, with existing crystals, polarizing reflections arise at relatively low Bragg angle and have small structure factors for reasons which are inherent to the cancellation process [28]. This generally results in low reflectivity and poor resolution conditions for polarized neutron measurements at high energy and large momentum transfer.

Spin selective absorption in highly polarized nuclei also leads to the polarisation of the neutron beam . It has the obvious advantage that it completely decouples the energy selection from the polarisation selection in both the incident and scattered beams thus giving freedom to optimize the resolution conditions.

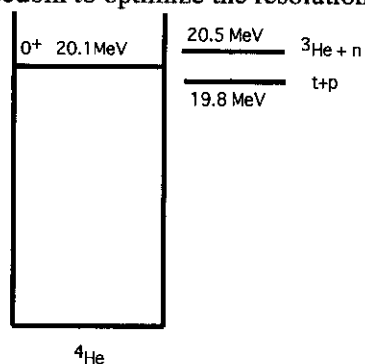_Fig. A 7_   The level of 4He corresponding to the resonance responsible for the strength and spin dependence of the 3He(n,p)t reaction

(b) Highly spin selective absorption in ^3He. ^{3}He might seems at first sight a strange candidate for a device dedicated to the transmission of thermal neutrons since it

absorbs them so effectively in many neutron detectors. Indeed the cross-section for neutron capture is huge and falls off inversely with neutron velocity (Fig A 9).

In fact this capture cross section for the reaction $^3He + n \rightarrow t + p$ has been shown to be strongly spin dependent [29]. It is associated with a broad resonance (270 keV), near threshold resonance for ^{3}He+n, corresponding to a J=O$^+$ energy level in ^{4}He (FigA 10). With a fully polarized ^{3}He absorber, only those neutrons with spins anti parallel to the ^{3}He polarization may be absorbed via the resonance. Practically, with a 80% ^{3}He polarisation and an appropriate thickness (opacity), it is possible to produce a spin filter with high neutron polarization (95%) and small attenuation of the desired spin (Fig. A 11) [30-32].

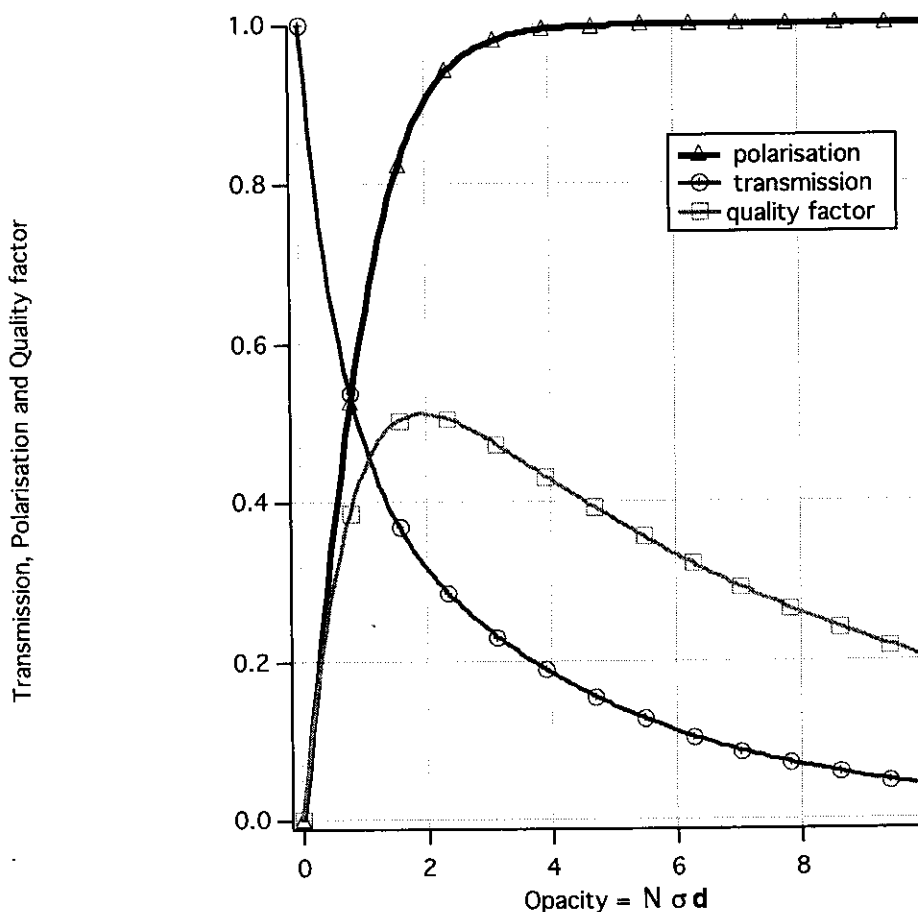

Fig. A8 Expected Transmission, T, polarisation P and quality factor $PT^{1/2}$ for the neutrons versus "opacity" Nσd of the Neutron Spin Filter for 75 % polarized ^{3}He nuclei. It can be shown that the optimum is reach for Nσd=2.2 (N atomic density, σ absorption cross section, d thickness of the filter)

Bibliography

1.   Shull, C.G. and J.S. Smart, MnO. Phys. Rev., 1949. 76: p. 1256.

2.   Brown, P.J. and T. Chattopadhyay, The helimagnetic structure of Eu(As0.2P0.8)3 determined by zero-field neutron polarimetry.
Journal of Physics: Condensed Matter, 1997. 9: p. 9167-9173.

3.   Tasset, F., Zero field neutron polarimetry.
Physica B, 1989. 156-157: p. 627-630.

4.   Tasset, F., et al., Spherical neutron polarimetry with Cryopad-II.
Physica B, 1999. 267-268: p. 69-74.

5.   Regnault, L.P., et al., Polarized neutron inelastic scattering on the spin-Peierls system CuGeO3: "three-directional" versus "three-dimensional polarization analysis". Physica B, 1999. 267-268: p. 227-235.

6.   Nathans, R., et al., The use of polarized neutrons in determining the magnetic scattering by Iron and Nickel.
J. Phys. Chem. Solids, 1959. 10: p. 138-146.

7.   Brown, P.J. and J.C. Matthewman,
The Cambridge Crystallographic Subroutine Library-MK3, . 1987.

8.   Schweizer, J., Hercules 1991, Lecture Notes:A .3 Magnetism; Form factors and magnetization densities, MDN/SPh-DRF, CEN Grenoble.

9.   Blume, M., Polarization Effects in the magnetic Elastic Scattering of Slow Neutrons. Phys. Rev., 1963. 130: p. 1670-1676.

10.   Nunez, V., et al., Zero field neutron polarimetry.
Physica B, 1991. 174: p. 60-65.

11.   Brown, P.J., et al., Determination of the magnetic structure of Mn3Sn using generalized neutron polarization analysis.
J. Phys. : Cond. Mat., 1990. 2: p. 9409-9422.

12.   Moon, R.M., T. Riste, and W. Koehler, Polarization Analysis of Thermal-Neutron Scattering. Phys. Rev., 1969. 181: p. 920-931.

13.   Alperin, H. Rotation of the polarization of neutrons scattered from Cr2O3. in Int. Conf. Magnetism. 1973. Moscow: Proc. ICM-73.

14.   Brown, P.J., J.B. Forsyth, and F. Tasset, Neutron polarimetry.
Proc. R. Soc. Lond. A, 1993. 442: p. 147-160.

15.   Freund, A.K., Cross-Sections of Materials used as neutron Monochromators and Filters.
Nuclear Instruments and Methods,1983. 213: p. 495-501.

16.   Brown, P.J., Magnetic Structure studied with Zero Field Polarimetry.
Physica B, 1993. 192(1&2): p. 14-24.

17.   Izyumov, Y.A. and S.V. Maleev, Scattering of polarised neutrons by ferromagnets and antiferromagnets. Sov. Phys. JETP, 1962. 14(5): p. 1168-1171.

18.   Brown, P.J., et al., Antiferromagnetism in CuO studied by neutron polarimetry. J. Phys.: Condens. Matter, 1991. 3: p. 4281-4287.

19.   Brown, P.J., et al., Determination of the antiferromagnetic form-factor of Cr3+, ILL Annual Report. 1999, Grenoble.

20.   Mook, H.A., Magnetic moment distribution of Nickel Metal.
Phys. Rev., 1966. 148(2): p. 495.

21.   Brown, P.J., J.B. Forsyth, and F. Tasset, Precision measurement of antiferromagnetic form factors.
Physica B, 1999. **267-268**: p. 215-220.

22.   Maleyev, S.V., Nuclear-Magnetic interference at the inelastic scattering of the polarized neutrons.
Physica B, 1999. **267-268**: p. 236-242.

23.   Tasset, F., Hercules 1999 -A8 Lecture notes -Neutron Polarimetry, ILL Grenoble.

24.   Halpern, O. and T. Holstein, On the Passage of Neutrons Through Ferromagnets.
Phys. Rev., 1941. **59**: p. 960-981.

25.   Güttinger, P., Das Verhalten von Atomen im Magnetischen Drehfeld. Z. Phys., 1932. **73**: p. 169.

26.   Newton, R.R. and C. Kittel, On a Proposal for Determining the Thickness of the Transition Layer between Ferromagnetic Domains by a Neutron Polarization Experiment.
Phys. Rev., 1948. **74(11)**: p. 1604-1605.

27.   Majorana, E., Atomi orientati in campo magnetico variabile.
Nuovo Cimento, 1932. **9**: p. 43.

28.   Tasset, F., Report on Allevard discussion for polarisation techniques, . 1989, ILL.

29.   Passel, L. and R.I. Schermer, Measurement of the spin dependence of the 3He(n,p)T Reaction and of the nuclear susceptibility of adsorbed 3He.
Phys. Rev., 1966. **150**: p. 146.

30.   Tasset, F., Towards Helium-3 neutron polarisers.
Physica B, 1994. **213&214**: p. 935-938.

31.   Tasset, F. and E. Ressouche, Optimum Transmission for an 3He Neutron Polariser. NIM, A., 1995. **359**: p. 537-541.

32.   Becker, J., et al., Development of a dense polarized 3He spin filter based on compression of optically pumped gas.
Journal of Neutron Research, 1996. **5(1-2)**: p. 1-10.

Polarimetric Neutron Scattering
Annexes

Annexe 1:

General properties of the density matrix

Ter Haar, D., *Theory and applications of the density matrix.*

Rep. Prog. Phys., 1961. 24: p. 304-362.

Page 312: In this section, we shall discuss the general properties of the density matrix. We shall introduce the density matrix first of all through the statistical approach and prove some of its properties. After that we shall introduce it through the quantum-mechanical approach and show that the two density matrices are, indeed, the same. We may refer to the following papers and books to supplement the discussion in this section: Kemble 1937[1], Tolman 1938[2], Husimi 1940[3], ter Haar 1954[4], Fano 1957[5], and Hagedorn 1958[6].

In the statistical approach to the density matrix we are concerned with the description of a physical system by an ensemble. This ensemble will often be a grand ensemble, that is, the number of particle in the different constituent systems will not necessarily be the same for all systems. We shall, however, in this section not emphasize this aspect, but it will be important in the discussion in §4. Let there be N systems in the ensemble and let these systems be described by normalized wave functions $\psi^k (k = 1,...., N)$. It is convenient to introduce a complete orthonormal set φ_n in terms of which the ψ^k can be expanded. To simplify our discussion in the present section we shall neglect complications introduced by spin, that is, we assume the ψ^k and φ_n to be scalars. It is easy enough to take spin into account, and we shall do this, for instance, in § 8. In terms of the φ_n we have

$$\psi^k = \sum_n c_n^k \varphi_{n,} (k = 1,..., N) \qquad .....(2.1)$$

Originally we had defined our ensemble by the wave functions ψ^k. In the new representation it is defined by the coefficients c_n^k.

Let A be a physical quantity, the value of which we wish to determine for the system which is represented by our ensemble. This quantity will correspond quantum mechanically to an operator $\hat{A}$ (all operators will be denoted by ^) and its average value for the kth system will be given by the equation

$$A_k = \int \psi^{k*} \hat{A} \psi^k d\tau , \qquad ....(2.2)$$

where indicates integration over all arguments of ψ^k. Taking the average over the ensemble, which we shall denote by $\langle...\rangle$, we obtain the expectation value of $\hat{A}$ for the system under consideration, and we get

$$A_k = N^{-1} \sum_{k=1}^{N} \int \psi^{k*} \hat{A} \psi^k d\tau \qquad (2.3)$$

or using Eqn (2.1),

$$A_k = N^{-1} \sum_k \sum_{m,n} c_m^k * c_n^k A_{mn},$$ .....(2.4)

where A_{mn} is the matrix element of $\hat{A}$ in the φ_n-representation:

$$A_{mn} = \int \varphi_m^* \hat{A} \varphi_n d\tau$$ ....(2.3)

Introducing the density matrix $\hat{\rho}$ by its matrix elements in the φ_n-representation,

$$\rho_{mn} = N^{-1} \sum_k c_n^k * c_m^k,$$ .....(2.6)

we can write Eqn (2.4) in the form

$$\langle \hat{A} \rangle = \sum_{m,n} A_{m,n} \rho_{nm} = Tr(\hat{\rho}\hat{A}),$$ .....(2.7)

where Tr indicates the trace, that is, the sum of the diagonal elements.

A few remarks should be made here about Eqns (2.3), (2.6) and (2.7). First of all we notice that $\langle \hat{A} \rangle$ is a double average: one average is the quantum-mechanical average given by Eqn(2.2), and the other is the statistical average over the ensemble. This means that two different kind of probability considerations enter into our discussion; this point was specially discussed by London and Bauer (1939)[7]. The quantum-mechanical probability considerations enter even if we have as complete a knowledge about the physical system as is possible in quantum mechanics, that is, if we know the wave function of the system; they are a feature inherent in quantum mechanics and are not related to any lack of (possible)knowledge. The statistical probability considerations, on the other hand, are closely connected to our lack of knowledge-as they are in classical statistics-and were introduced exactly because our knowledge is incomplete. Secondly, we note that the density matrix, or statistical operator as it is sometimes called, is defined by its matrix elements in the particular representation in which we are working. We shall see presently that if we change to another representation the density matrix will change according to the usual rules of quantum mechanical transformation theory. Finally, we note the intimate connection between the density matrix elements and the average values of physical quantities. This connection is used by the operational approach to define the density matrix in term of averages. There are cases where the density matrix is a finite matrix- for instance, when we are dealing with polarization experiments- and if it is a matrix of rank M it is determined by $M^2 - 1$ independent parameters (vide infra). If we can find the average values of $M^2 - 1$ physical quantities A_j these will suffice to determine the density matrix. In the case of the polarization of light, for instance, M will be 2, and the three components of the polarization vector will just be sufficient to determine the density matrix completely, as we shall see in §8.

From the definition (2.6) we see that $\hat{\rho}$ is Hermitian,

$$\rho_{mn} = \rho_{nm} *.$$ ......(2.8)

3

Applying Eqn(2.7) to the unit operator $\left(\hat{A}=\hat{1}\right)$ we find that $\hat{\rho}$ is normalized (to unity),

$$1 = \left\langle\hat{1}\right\rangle = Tr\hat{\rho}.\hat{1} = Tr\hat{\rho}. \qquad\qquad.....(2.9)$$

This result could also have been obtained directly from Eqn (2.6) and the fact that the ψ^k are normalized

$$Tr\hat{\rho} = N^{-1}\sum_k\sum_n a_n^k * a_n^k = N^{-1}\sum_k 1 = 1. \qquad\qquad.....(2.10)$$

From Eqn(2.8) it follows that the diagonal elements of the density matrix, ρ_{nm}, are real, and from Eqn(2.10) it follows that they must satisfy the relations

$$\sum_n \rho_{nn} = 1, \ 0 \leq \rho_{nn} \leq 1. \qquad\qquad.....(2.11)$$

The physical meaning of the ρ_{nn} is clear from Eqn(2.6) and (2.1): it is the (normalized) probability that φ_n is realized in the ensemble.

Let us now consider a change from the φ_n-representation to another representation, say, the χ_p-representation. Instead of Eqn(2.1) we have now

$$\psi^k = \sum_n c_n^k \varphi_n = \sum_p d_p^k \chi_p. \qquad\qquad......(2.12)$$

The transformation from the φ_n- to the χ_p-representation will be characterized by a unitary transformation matrix S_{np} such that

$$\chi_p = \sum_n \varphi_n S_{np}, \qquad\qquad.....(2.13)$$

while $\qquad\qquad S_{np}* = \left(S^{-1}\right)_{pn}, \qquad\qquad.....(2.14)$

so that $\qquad\qquad \sum_n S_{np}* S_{nq} = \delta_{pq}, \qquad\qquad....(2.15)$

where δ_{pq} is the Kronecker delta function.

From Eqns(2.12) and (2.13) it follows that

$$c_n^k = \sum_q S_{nq} d_q^k, \qquad\qquad.....(2.16)$$

and using Eqn (2.15) we get from this equation

$$d_q^k = \sum_n c_n^k S_{np}*. \qquad\qquad....(2.17)$$

If we denote the transformed density matrix by a prime, we have instead of Eqn (2.6) the equation

$$\rho_{pq}' = N^{-1}\sum_k d_q^k * d_p^k, \qquad\qquad.....(2.18)$$

and from Eqns (2.17) and 2.14) we get

$$\rho_{pq}' = N^{-1}\sum_{k,m,n} c_n^k * S_{nq} c_m^k S_{mp}* = \sum_{m,n}\left(S^{-1}\right)_{pm}\rho_{mn}S_{nq} \qquad\qquad....(2.19)$$

or, in matrix notation,

$$\hat{\rho}' = S^{-1}\hat{\rho}S, \qquad\qquad.....(2.20)$$

which is the normal equation for the transformation of an operator.

We notice, by the way, that the averages $\left\langle\hat{A}\right\rangle$ will be unaffected by the transformation since

$$\left\langle\hat{A}\right\rangle' = Tr\hat{\rho}'\hat{A}' = TrS^{-1}\hat{\rho}SS^{-1}\hat{A}S = TrS^{-1}\hat{\rho}\hat{A}S = TrSS^{-1}\hat{\rho}\hat{A} = Tr\hat{\rho}\hat{A} = \left\langle\hat{A}\right\rangle, \qquad....(2.21)$$

where we have used the property of the trace

$$Tr\hat{A}\hat{B}\hat{C} = Tr\hat{B}\hat{C}\hat{A}, \qquad\qquad .....(2.22)$$

and the fact that $SS^{-1} = 1$.

Let now assume that we have made a transformation to a representation in which $\hat{\rho}$ is diagonal,

$$\rho_{mn} = \rho_m \delta_{mn} \qquad\qquad .....(2.23)$$

Consider now $Tr\hat{\rho}^2 (=\langle\hat{\rho}\rangle)$. We have

$$Tr\hat{\rho}^2 = \sum_m \rho_m^2 \le \left(\sum_m \rho_m\right)^2 = \left(Tr\hat{\rho}\right)^2 = 1 \qquad\qquad ....(2.24)$$

where we have used Eqn(2.9) and the fact that the ρ_m are non-negative. As the trace is invariant under a unitary transformation, we can write Eqn(2.24) in the form

$$Tr\hat{\rho}^2 \le 1, \text{ or, } \sum_{n,\,m} \rho_{mn}\rho_{nm} = \sum_{n,\,m} |\rho_{mn}|^2 \le 1 \qquad\qquad .....(2.25)$$

where we have used Eqn(2.8). Inequality (2.25) imposes a limitation upon all elements of the density matrix, that is, upon both the diagonal and the off-diagonal elements.

If we are dealing with a finite matrix, say of rank M, there are altogether M^2 complex matrix elements ρ_{mn}, that is, $2M^2$ parameters. This number is reduced by a factor 2 because of Eqn (2.8) and reduced by unity because of the normalization condition (2.9) so that there are M^2-1 independent parameters. From the operational point of view this means that one needs M^2-1 independently measured quantity to fix the density matrix.

In the preceding section we have discussed the difference between a pure state and a mixture. We now wish to establish the condition that the density matrix corresponds to a pure state. A pure state corresponds to the case where we have the maximum information available about the physical system, that is, where all systems in the ensemble possess the same wave function, ψ_0 say. In that case there is only one averaging process involved in obtaining $\langle\hat{A}\rangle$, namely, the quantum mechanical one.

The pure state is characterized by the existence of what Fano (1957)[5] calls a 'complete' experiment; this is an experiment which gives a result predictable with certainty when performed on this state and gives this particular result only for this particular state. The possibility of such an experiment is apparent if we bear in mind that it is possible to find a Hermitian operator, corresponding to a physical observable, which possesses this particular state as a (non degenerate) eigenstate. This complete experiment can be used as a filter. It should be an experiment designed to measure the observable, of which ψ_0 is an eigenfunction. We may mention a Nicol prism as a possible apparatus which could serve as a filter when we are dealing with density matrices describing the polarization of light (compare §8).

We shall now prove that the necessary and sufficient condition that $\hat{\rho}$ describe a pure state is

5

$$\hat{\rho}^2 = \hat{\rho},$$ ....(2.26)

that is, $\hat{\rho}$ should be idempotent. That Eqn (2.26) is a necessary condition follows easily from the fact that Eqn (2.6) now leads to

$$\rho_{mn} = c_n^{(0)} * c_m^{(0)},$$ ....(2.27)

as the c_n^k are independent of k and are all equal to the expansion coefficients $c_n^{(0)}$ of ψ_0 where ψ_0 is the wave function of all systems in the ensemble. As ψ_0 is normalized we get immediately

$$\rho(\rho^2)_{mn} = \sum_l c_m^{(0)} c_l^{(0)} * c_l^{(0)} c_n^{(0)} * = c_m^{(0)} c_n^{(0)} * = \rho_{mn}$$ .....(2.28)

To prove that Eqn (2.26) is a sufficient condition we consider again a representation for which $\hat{\rho}$ is diagonal. In that case $\hat{\rho}^2$ is also diagonal, and Eqn (2.26) is now equivalent to

$$\rho_n^2 = \rho_n \text{ for all values of n,}$$ .....(2.29)

or: either $\rho_n = 0$ or $\rho_n = 1$. ....(2.30)

From the normalization condition (2.9) and Eqn (2.30) it follows that one of the ρ_n, say ρ_0 is equal to unity while the other ρ_n vanish:

$$\rho_0 = 1; \rho_n = 0, n \neq 0.$$ ......(2.31)

From Eqn (2.6) we then get

$$\rho_0 = N^{-1} \sum_k |c_0^k|^2 = 1,$$ ....(2.32)

and as all $|c_n^k|^2$ must be not greater than 1, Eqn(2,32) can only be satisfied by putting

$$|c_0^k| = 1, \quad k = 1, \dots, N,$$ ....(2.33)

or $$\psi^k = \exp(i\alpha_k)\varphi_0, \quad \alpha_k \, real,$$ ....(2.34)

which means that, apart from an irrelevant phase factor $\exp(i\alpha_k)$, all ψ^k correspond to the same wave function.

We shall derive the equation of motion for the density matrix. We have assumed that the systems in the ensemble are describable by a wave function and we shall assume that the wave function satisfies the Schrödinger equation

$$\hat{H}\psi^k = i\hbar\dot{\psi}^k,$$ .....(2.35)

where, as usual, the dot indicates differentiation with respect to time. The operator $\hat{H}$ is the Hamiltonian of the system. It is convenient to use Eqn (2.1) to obtain the transformed Schrödinger equation

$$i\hbar\dot{c}_n^k = \sum_l H_{nl}c_l^k,$$ .....(2.36)

and from Eqns(2.36) and (2.6) and the fact that $\hat{H}$ is Hermitian it follows straightforwardly that

$$i\hbar\dot{\rho}_{mn} = \left[\hat{H},\hat{\rho}\right]_{-mn}, \text{ or } i\hbar\dot{\hat{\rho}} = \left[\hat{H},\hat{\rho}\right]_-,$$ .....(2.37)

where $[\, , \,]_-$ indicates the commutator. We shall defer a discussion of Eqn (2.37) until after we have considered the quantum mechanical approach to the density matrix, but there are one or two remarks we wish to make at this juncture.

We have so far been working in the Schrödinger representation, that is, the operators are assumed to be time-independent and the time dependence is contained in the wave function (compare Eqn (2.35)). In the Heisenberg representation, on the other hand, the time dependence is in the operators. Instead of a wave (or Schrödinger) equation one has equations of motion for the operators. These are of the same form as the equation of motion (2.37) for $\hat{\rho}$ but with the opposite sign. If we were to change to the Heisenberg representation we would find that $\hat{\rho}$ would be a constant operator (see, for instance, Hagedorn 1958).

The time dependence of $\langle\hat{A}\rangle$ is, in the Schrödinger picture, invested in $\hat{\rho}$ and in the Heisenberg picture in $\hat{A}$. For $\langle\hat{A}\rangle$ we find from Eqns (2.7) and (2.37), using the fact that $\hat{A}$ is time-independent in the Schrödinger picture

$$i\hbar\langle\dot{\hat{A}}\rangle = i\hbar\overline{Tr\dot{\hat{\rho}}\hat{A}} = i\hbar Tr\dot{\hat{\rho}}\hat{A} = Tr[\hat{H},\hat{\rho}]_{-}\hat{A} = Tr(\hat{H}\hat{\rho}\hat{A} - \hat{\rho}\hat{H}\hat{A})$$

or,
$$i\hbar\langle\dot{\hat{A}}\rangle = \langle[\hat{A},\hat{H}]_{-}\rangle, \qquad\qquad ......(2.38)$$

with the sign corresponding to the Heisenberg picture! Eqn (2.38) is, of course, true in all representations.

7

Annexe 2:

Polarization experiments

Ter Haar, D., *Theory and applications of the density matrix.*

Rep. Prog. Phys., 1961. 24: p. 304-362.

page 341: We mentioned in the introduction that often one can use an operational approach to the density matrix. This is especially the case when one discusses polarization or scattering experiments, as one is in that case interested in only a few of the many parameters which specify the system and one can use a density matrix which refers to only those degrees of freedom which are studied experimentally. The simplest example is the polarization of a beam of electrons which we shall discuss in some detail. A related problem is that of the polarization of light which we shall also consider here, without going into a very detailed discussion. Our final discussion will be of scattering and angular correlation experiments. For a consideration of such experiments elaborate matrix techniques have been developed, some of which are based upon the density matrix, but we must refer to the literature for a discussion of such techniques (see, for instance, Tolhoek and de Groot 1951 b, c[8], Cox and Tolhoek 1953[9], Tolhoek and Cox 1953[10], Hartogh, Tolhoek and de Groot 1954[11], de Groot and Tolhoek 1955[12], Huby 1958[13]).We can only touch upon some aspects of density matrix techniques; for more details of those techniques as applied to polarization, scattering, and angular correlation experiments in nuclear physics we may refer, for instance, to the papers by Tolhoek and de Groot (1951 a)[8], Lipps and Tolhoek (1954 a, b)[14], Kotani (1955)[15], Tolhoek (1956)[16], Fano (1957)[5], Hagedorn (1958)[6] and Zaidi (1959). We may also mention some unpublished lectures delivered by L. Rosenfeld to Nordita in Copenhagen which have been of great use in writing this section. The use of density matrices in discussing the polarization of electromagnetic radiation is based upon the fundamental ideas of Stokes(1852). Recently Fano (1949, 1957)[5, 17] and Wolf and Roman (see , for instance, Wolf 1954, 1959 a, b, 1960, Roman 1959[18], Parrent andRoman 1960)[19] have discussed this problem in great detail, but we can refer here only to those papers which are relevant to our discussion of density matrix techniques. In the present section we shall consider the polarization of particles with spin 1/2; the case of larger spin values will be mentioned only briefly.

Let us consider a beam of particles with spin 1/2, for instance, a beam of electrons. If we are only interested in the polarization or spin-orientation properties of this beam, we have a system of particles with two degrees of freedom, as long as we neglect negative energy states as we shall do here. The system should thus be

describable by a 2 by 2 density matrix, and we need only 3 independent parameters to determine fully the density matrix,(Compare the discussion in §2). The physical situation is completely defined, if we know the polarization vector $\mathbf{P}$, that is, the average value of the spin vector in the system,

$$\mathbf{P} = \langle \hat{\sigma} \rangle, \qquad \qquad ....(8.1)$$

where $\hat{\sigma}$ is the vector the components of which are the Pauli matrices,

$$\hat{\sigma}_x = \begin{Vmatrix} 0 & 1 \\ 1 & 0 \end{Vmatrix}, \qquad \hat{\sigma}_y = \begin{Vmatrix} 0 & -i \\ i & 0 \end{Vmatrix}, \qquad \hat{\sigma}_z = \begin{Vmatrix} 1 & 0 \\ 0 & -1 \end{Vmatrix} \qquad ....(8.2)$$

We note that these matrices satisfy the following relations

$$Tr\ \sigma_x = Tr\ \sigma_y = Tr\ \sigma_z = 0 \qquad .....(8.3a)$$

$$\hat{\sigma}_x\hat{\sigma}_y = -\hat{\sigma}_y\hat{\sigma}_x = i\hat{\sigma}_z, \quad \hat{\sigma}_y\hat{\sigma}_z = -\hat{\sigma}_z\hat{\sigma}_y = i\hat{\sigma}_x, \quad \hat{\sigma}_z\hat{\sigma}_x = -\hat{\sigma}_x\hat{\sigma}_z = i\hat{\sigma}_y;$$

$$\hat{\sigma}_x^{\ 2} = \hat{\sigma}_y^{\ 2} = \hat{\sigma}_z^{\ 2} = \hat{1}; \qquad .....(8.3b)$$

$$Tr\ \hat{\sigma}_x\hat{\sigma}_y = Tr\ \hat{\sigma}_y\hat{\sigma}_z = Tr\ \hat{\sigma}_z\hat{\sigma}_x = 0, \quad Tr\ \hat{\sigma}_x^{\ 2} = Tr\ \hat{\sigma}_y^{\ 2} = Tr\ \hat{\sigma}_z^{\ 2} = 2 \qquad ....(8.3c)$$

As $\mathbf{P}$ has three components we can use these as the three independent parameters to determine the density matrix $\hat{\rho}$. As $\hat{\rho}$ is a 2 by 2 matrix, we can express it in terms of the unit matrix $\hat{1}$ and the Pauli matrices,

$$\hat{\rho} = a.\hat{1} + (\mathbf{a}.\hat{\sigma}). \qquad ....(8.4)$$

From the normalisation condition (2.9) and Eqn (8.3a) we get

$$Tr\ \hat{\rho} = 1 = 2a, \quad \text{or,} \quad a = \frac{1}{2} \qquad .....(8.5)$$

while Eqn (8.1) leads with the aid of Eqns (8.3a) and (8.3c) to

$$\mathbf{P} = \langle \hat{\sigma} \rangle = Tr\ \hat{\rho}\hat{\sigma} = Tr[a\hat{\sigma} + \hat{\sigma}(\mathbf{a}.\hat{\sigma})] = 2\mathbf{a} \qquad .....(8.6)$$

Combining Eqns (8.4) to (8.6) we get

$$\hat{\rho} = \frac{1}{2}[\hat{1} + (\mathbf{P}.\hat{\sigma})] = \frac{1}{2}\begin{Vmatrix} 1 + P_z & P_x - iP_y \\ P_x + iP_y & 1 - P_z \end{Vmatrix}. \qquad ....(8.7)$$

This equation shows that, indeed, $\hat{\rho}$ is determined, once $\mathbf{P}$ is known.

Let us now consider the case where this beam passes through a magnetic field, and ask what will happen to the polarization of the beam. We could use Eqn (2.37) for the rate of change of the density matrix and as $\hat{\rho}$ contains $\mathbf{P}$ obtain in that way the equation of motion for $\mathbf{P}$. The drawback of this procedure is that one cannot apply it with the same ease to the case of particles with spin greater than $\frac{1}{2}$. We shall instead use Eqn (2.38) for the rate of change of average values. From this equation and Eqn (8.11) we get

$$\frac{\partial \mathbf{P}}{\partial t} = \frac{\partial \langle \hat{\sigma} \rangle}{\partial t} = -\frac{i}{\hbar} \langle [\hat{\sigma}, \hat{H}_s] \rangle \qquad ......(8.8)$$

where $\hat{H}_s$ is the Hamiltonian referring to the spin coordinate (the *spin Hamiltonian*) which is given by the equation

$$\hat{H}_s = -(\hat{\mu}.\mathbf{H}) = -\frac{1}{2}\gamma\hbar(\hat{\sigma}.\mathbf{H}),\qquad\qquad .....(8.9)$$

where **H** is the magnetic field, $\hat{\mu}$ the magnetic moment of the electron $\hat{\mu} = e\hbar\hat{\sigma}/2mc$ with e, electronic charge; m, electronic mass; c, velocity of light), and γ the magnetogyric ratio $(\gamma = e/mc)$. If we write Eqns (8.3 b) in the symbolical form

$$[\hat{\sigma}\wedge\hat{\sigma}] = 2i\hat{\sigma}\qquad\qquad .....(8.10)$$

we find from Eqns (8.8) and (8.9)

$$\frac{\partial\mathbf{P}}{\partial t} = \frac{1}{2}i\gamma\langle[\hat{\sigma},(\hat{\sigma}.\mathbf{H})]_-\rangle$$

$$= \frac{1}{2}i\gamma\langle[\mathbf{H}\wedge(\hat{\sigma}\wedge\hat{\sigma})]\rangle = -\gamma\langle[\mathbf{H}\wedge\langle\hat{\sigma}\rangle]\rangle$$

or,

$$\frac{\partial\mathbf{P}}{\partial t} = -\gamma\langle[\mathbf{H}\wedge\mathbf{P}]\rangle,$$

which is just the classical equation of motion for the polarization vector. One could prove Eqn (8.11) starting from the Schrödinger equation, but the proof is cumbersome. The ease with which we could prove Eqn (8.11) is an example of the advantages of the density matrix. Eqn (8.11) itself is a consequence of the generalized Ehrenfest theorem (Ehrenfest 1927[20], Kramers 1957[21], § 30) which states that any quantum-mechanical average will obey the corresponding classical equation of motion.

We can easily generalize the discussion leading to Eqn (8.11) to the case of larger spin values. Let j(>1/2) be the largest possible value of the angular momentum of the particle. The density matrix will now be a 2j+1 by 2j+1 matrix, and apart from the components of the polarization vector **P** we need other quantities to determine $\hat{\rho}$ completely. The vector **P** can be called the dipole polarization vector, and the other quantities which can be used to determine $\hat{\rho}$ are the quadrupole polarisation tensor (5 components; its components and the 3 components of **P** are the 8 parameters which are sufficient to determine $\hat{\rho}$ if j=1), the octupole polarization tensor (7 components; it comes into play if j>1), ..., in general the 2^l-polarization tensor (with 2l+1 components; for a given j, all multipoles with l≤2j will be involved). We do not have the space here to go into a detailed discussion of the determination of the density matrix for this general case and refer to Fano's review article (1957) where further references can be found. The polarization vector **P** is now defined by the equation

$$\mathbf{P} = \langle\hat{\mathbf{J}}\rangle/j\hbar,\qquad\qquad .....(8.12)$$

where $\hat{\mathbf{J}}$ is the angular momentum. It satisfies the commutation relation which can be expressed by a formal equation similar to Eqn (8.10),

$$[\hat{\mathbf{J}}\wedge\hat{\mathbf{J}}] = i\hbar\hat{\mathbf{J}}.\qquad\qquad .....(8.13)$$

The spin Hamiltonian is given by the equation

10

$$\hat{H}_s = -\gamma \left(\hat{J}.\mathbf{H} \right), \qquad\qquad .....(8.14)$$

and from Eqns (8.12), (8.13), (8.14) and (2.38) we find that Eqn (8.11) holds also for the general case.

Annexe 3

Magnetic Scattering of Neutrons:

A Technique with a Real Future [22]

J. Schweizer

,DRFMC/MDN/CEA-Grenoble, 1996,

The scattering by one atom, in a well defined quantum state, transforms a neutron spin state $|\chi\rangle$ in another spin state $|\chi'\rangle$ by the action of an S matrix:

$$|\chi'\rangle = S|\chi\rangle$$

with

$$|\chi\rangle = a|+\rangle + b|-\rangle$$

and

$$|\chi'\rangle = a'|+\rangle + b'|-\rangle$$

One can write

$$\begin{vmatrix} a' \\ b' \end{vmatrix} = \begin{pmatrix} a_{11} & a_{12} \\ a_{21} & a_{22} \end{pmatrix} \begin{vmatrix} a \\ b \end{vmatrix} \tag{S9}$$

The S matrix is expressed as

$$\begin{pmatrix} a_{11} & a_{12} \\ a_{21} & a_{22} \end{pmatrix} = \begin{pmatrix} \dfrac{a_{11} + a_{22}}{2} & 0 \\ 0 & \dfrac{a_{11} + a_{22}}{2} \end{pmatrix} + \begin{pmatrix} \dfrac{a_{11} - a_{22}}{2} & 0 \\ 0 & \dfrac{-(a_{11} - a_{22})}{2} \end{pmatrix}$$

$$\begin{pmatrix} a_{11} & a_{12} \\ a_{21} & a_{22} \end{pmatrix} = \begin{pmatrix} \beta & 0 \\ 0 & \beta \end{pmatrix} + \begin{pmatrix} A_z & A_x - iA_y \\ A_x + iA_y & -A_z \end{pmatrix} \tag{S10}$$

which means that formally, the S matrix can be written:

$$S = \beta I + \vec{A}.\vec{\sigma} \tag{S11}$$

where I is the unit matrix, β is a scalar and $\vec{A}$ is a vector.

The polarisation dependant neutron cross section

In order to express the cross section of a scattering process in which the scattering system changes from $|\lambda\rangle$ to $|\lambda'\rangle$, and the neutron state changes from $|k,\chi\rangle$, to $|k,\chi'\rangle$,

12

k being the wave vector of the neutron, one uses the master "Fermi Golden rule" formula:

$$\frac{d^2\sigma}{d\Omega dE'} = \frac{k'}{k}\left(\frac{m}{2\pi h^2}\right)^2 \sum_{\lambda\lambda'} p_\lambda |\langle \lambda'k'\chi'|V|\lambda k\chi\rangle|^2 \delta\left(E_\lambda - E_{\lambda'} + h\omega\right)$$

(12)

where p_λ is the probability of finding the system in the quantum state $|\lambda\rangle$, and $V(\vec{r})$ is the interaction potential between the neutron and the atoms.

The spatial part of the matrix element can be written

$$\langle \lambda'k'|V|\lambda k\rangle = \int \psi_\lambda^* e^{-i\vec{k}\cdot\vec{r}} V(\vec{r}) e^{i\vec{k}\cdot\vec{r}} \psi_\lambda \cdot d^3r = V(\vec{q})$$

(S13)

which is the Fourier transform of the potential, with $\vec{q} = \vec{k}' - \vec{k}$.

We are left with the matrix element of $V(\vec{q})$ between two spin states:

$$\langle\chi'|V(q)|\chi\rangle$$

with:

$$|\chi\rangle = a|+\rangle + b|-\rangle$$

$$|\chi'\rangle = a'|+\rangle + b'|-\rangle$$

$$|\chi'\rangle = V(q)|\chi\rangle$$

and the following relation:

$$\begin{vmatrix} a' \\ b' \end{vmatrix} = \begin{pmatrix} \beta(\vec{q}) + A_z(\vec{q}) & A_x(\vec{q}) - iA_y(\vec{q}) \\ A_x(\vec{q}) + iA_y(\vec{q}) & \beta(\vec{q}) - A_z(\vec{q}) \end{pmatrix} \begin{vmatrix} a \\ b \end{vmatrix}$$

(S14)

The partial scattering amplitudes

Starting with a spin state $|\chi\rangle = |+\rangle$

$$\begin{vmatrix} a' \\ b' \end{vmatrix} = \begin{pmatrix} \beta(\vec{q}) + A_z(\vec{q}) & A_x(\vec{q}) - iA_y(\vec{q}) \\ A_x(\vec{q}) + iA_y(\vec{q}) & \beta(\vec{q}) - A_z(\vec{q}) \end{pmatrix} \begin{vmatrix} 1 \\ 0 \end{vmatrix} = \begin{vmatrix} \beta(\vec{q}) + A_z(\vec{q}) \\ A_x(\vec{q}) + iA_y(\vec{q}) \end{vmatrix}$$

(S15)

$a' = \beta(\vec{q}) + A_z(\vec{q})$ is the non spin flip amplitude U^{++}

$b' = A_x(\vec{q}) + iA_y(\vec{q})$ is the spin flip amplitude U^{+-}

Starting with a spin state $|\chi\rangle = |-\rangle$

$$\begin{vmatrix} a' \\ b' \end{vmatrix} = \begin{pmatrix} \beta(\vec{q}) + A_z(\vec{q}) & A_x(\vec{q}) - iA_y(\vec{q}) \\ A_x(\vec{q}) + iA_y(\vec{q}) & \beta(\vec{q}) - A_z(\vec{q}) \end{pmatrix} \begin{vmatrix} 0 \\ 1 \end{vmatrix} = \begin{vmatrix} A_x(\vec{q}) - iA_y(\vec{q}) \\ \beta(\vec{q}) - A_z(\vec{q}) \end{vmatrix}$$

(S16)

$a' = A_x(\vec{q}) - iA_y(\vec{q})$ is the spin flip amplitude U^{-+}

13

$b' = \beta(\vec{q}) - A_z(\vec{q})$ is the non spin flip amplitude U^-

These partial scattering amplitudes may be written in the contracted form:

$$U^{\pm\pm} = \beta(\vec{q}) \pm A_z(\vec{q}) \tag{S17}$$

$$U^{\pm\mp} = A_x(\vec{q}) \pm iA_y(\vec{q}) \tag{S18}$$

The scattering cross section can be written:

$$\frac{d^2\sigma}{d\Omega dE'} = \frac{k'}{k}\left(\frac{m}{2\pi\hbar^2}\right)^2 \sum_{\lambda\lambda} p_\lambda \delta\left(E_\lambda - E_{\lambda'} + \hbar\omega\right)\langle\chi'|\chi'\rangle \tag{S23}$$

If the system is in a well defined quqntum state λ before the scattering process, and a well defined state λ' after, there is one function $|\chi'\rangle$ only and:

$$\frac{d^2\sigma}{d\Omega dE'} = \frac{k'}{k}\left(\frac{m}{2\pi\hbar^2}\right)^2 \delta\left(E_\lambda - E_{\lambda'} + \hbar\omega\right)\langle\chi'|\chi'\rangle \tag{S24}$$

Starting first with a perfect polarization along Oz

$$|\chi\rangle = |+\rangle$$

$$|\chi'\rangle = V|\chi\rangle = (\beta + A_z)|+\rangle + \left(A_x + iA_y\right)|-\rangle$$

$$\langle\chi'|\chi'\rangle = |\beta + A_z|^2 + |A_x + iA_y|^2 \tag{S25}$$

Starting then from a perfect polarization antiparallel to Oz, one gets:

$$\langle\chi'|\chi'\rangle = |\beta - A_z|^2 + |A_x - iA_y|^2 \tag{S26}$$

For a beam of neutrons, with a non perfect polarization $\vec{P}$, one chooses the Oz direction parallel to $\vec{P}$, and average expressions (S25) and (S26) for

$$n^+ = \frac{1+P}{2} \text{ neutrons polarized along Oz}$$

$$n^+ = \frac{1-P}{2} \text{ neutrons polarized along -Oz}$$

This results in the general formula for the cross section:

$$\frac{d^2\sigma}{d\Omega dE'} = \frac{k'}{k}\left(\frac{m}{2\pi\hbar^2}\right)^2 \delta\left(E_\lambda - E_{\lambda'} + \hbar\omega\right)\left[\beta^*\beta + \vec{A}^*\vec{A} + \vec{P}\left(\beta^*\vec{A} + \vec{A}^*\beta\right) + i\vec{P}\left(\vec{A}^* \wedge \vec{A}\right)\right]$$

(S27)

14

The final polarisation

In the same conditions, when the states λ and λ' of the system are well defined, the polarization $\vec{P}'$ of the scattered beam is the average value of the vector operator $\vec{\sigma}$

$$\vec{P}' = \frac{\langle\chi'|\vec{\sigma}|\chi'\rangle}{\langle\chi'|\chi'\rangle}$$

(S28)

Starting first with a perfect polarization along Oz

$$|\chi\rangle = |+\rangle$$

$$|\chi'\rangle = (\beta + A_z)|+\rangle + (A_x + A_y)|-\rangle$$

one gets

$$\langle\chi'|\chi'\rangle\vec{P}' = \left[\langle+|(\beta^* + A_z^*) + \langle-|(A_x^* - iA_y^*)\right]\vec{\sigma}\left[(\beta + A_z)|+\rangle + (A_x + iA_y)|-\rangle\right]$$

(S29)

which corresponds for the 3 components of $\vec{P}'$ to the 3 equations

$$\langle\chi'|\chi'\rangle P_x' = \left[\langle+|(\beta^* + A_z^*) + \langle-|(A_x^* - iA_y^*)\right]\begin{pmatrix} 0 & 1 \\ 1 & 0 \end{pmatrix}\left[(\beta + A_z)|+\rangle + (A_x + iA_y)|-\rangle\right]$$

(S30)

$$\langle\chi'|\chi'\rangle P_y' = \left[\langle+|(\beta^* + A_z^*) + \langle-|(A_x^* - iA_y^*)\right]\begin{pmatrix} 0 & -i \\ i & 0 \end{pmatrix}\left[(\beta + A_z)|+\rangle + (A_x + iA_y)|-\rangle\right]$$

(S31)

$$\langle\chi'|\chi'\rangle P_z' = \left[\langle+|(\beta^* + A_z^*) + \langle-|(A_x^* - iA_y^*)\right]\begin{pmatrix} 1 & 0 \\ 0 & -1 \end{pmatrix}\left[(\beta + A_z)|+\rangle + (A_x + iA_y)|-\rangle\right]$$

(S32)

Starting then from a perfect incident polarization antiparallel to Oz, one calculates:

$$\langle\chi'|\chi'\rangle P' = \langle\chi'|\vec{\sigma}|\chi'\rangle$$

with $$|\chi'\rangle = (A_x - iA_y)|+\rangle + (\beta - A_z)|-\rangle$$

For a beam partly polarised, after choosing the Oz direction parallel to $\vec{P}'$ and averaging over n^+ neutrons polarised along Oz and n^- neutrons polarised along -Oz, one gets:

$$\frac{d^2\sigma}{d\Omega dE'}\vec{P}' = \frac{k'}{k}\left(\frac{m}{2\pi\hbar^2}\right)^2 \delta(E_\lambda - E_{\lambda'} + \hbar\omega)$$

$$\left\{\beta^*\vec{A} + \vec{A}^*\beta - i\vec{A}^* \wedge \vec{A} + \beta^*\beta\vec{P} + (\vec{A}^*\cdot\vec{P})\vec{A} + \vec{A}^*(\vec{P}\vec{A}) - \vec{P}(\vec{A}^*\vec{A}) + i\left[\beta^*(\vec{A} \wedge \vec{P}) + (\vec{P} \wedge \vec{A})\beta\right]\right\}$$

(S33)

The cross section, which has been formulated

$$\frac{d^2\sigma}{d\Omega dE'} \propto \langle\chi'|\chi'\rangle = \beta^*\beta + \vec{A}^*\vec{A} + \vec{P}(\beta^*\vec{A} + \vec{A}^*\beta) + i\vec{P}(\vec{A}^* \wedge \vec{A})$$

15

can be expressed as a sum of two terms:

$$\frac{d^2\sigma}{d\Omega\,dE'} = a + \vec{P}.\vec{V}$$

where a is a scalar

$$a = \beta^{*}\beta + \vec{A}^{*}\vec{A}$$

and $\vec{V}$ is a vector $\vec{V} = \beta^{*}\vec{A} + \vec{A}^{*}\beta + i\vec{A}^{*} \wedge \vec{A}$

By varying the incident polarisation $\vec{V}$, the measurement of the cross section gives access to 4 quantities: the scalar a and the 3 components Vx, Vy, and Vz of the vector $\vec{V}$

In the same way, when formulating the polarisation of the scattered beam as:

$$\langle\chi'|\chi'\rangle\vec{P}' = \beta^{*}\vec{A} + \vec{A}^{*}\beta - i\vec{A}^{*} \wedge \vec{A} + \beta^{*}\beta\vec{P} + \left(\vec{A}^{*}\vec{P}\right)\vec{A} + \vec{A}^{*}\left(\vec{P}\vec{A}\right) - \vec{P}\left(\vec{A}^{*}\vec{A}\right) + i\left[\beta^{*}\left(\vec{A} \wedge \vec{P}\right) + \left(\vec{P} \wedge \vec{A}\right)\beta\right]$$

this expression is equivalent to $\vec{P}' = \vec{V}' + \bar{\bar{T}}\vec{P}$

where $\vec{V}'$ is the vector $\beta^{*}\vec{A} + \vec{A}^{*}\beta - i\vec{A}^{*} \wedge \vec{A}$ and where $\bar{\bar{T}}$ is a tensor.

Annexe 4

Cross-section and polarisation of scattered beam

Marshall, W. and S. Lovesey,

Theory of thermal neutron scattering. 1971, Oxford: Oxford University Press.

page 327

The partial differential cross-section derived in Chapter 1 is given by

$$\frac{d^2\sigma}{d\Omega dE} = \left(\frac{m}{2\pi\hbar^2}\right)^2 \frac{k'}{k} \sum_{\lambda,\sigma} p_\lambda p_\sigma \sum_{\lambda',\sigma'} \langle \lambda,\sigma | \hat{V}^+(\kappa) | \lambda',\sigma' \rangle \times$$

$$\times \langle \lambda',\sigma' | \hat{V}(\kappa) | \lambda,\sigma \rangle \delta\left(\hbar\omega + E_\lambda - E_{\lambda'}\right) \qquad \ldots (10.20)$$

In (10.20), $\hat{V}(\kappa)$ is the Fourier transform of the interaction potential between the incident neutron and the target system.

For purely nuclear scattering from an array of rigid nuclei,

$$\hat{V}_N(\kappa) = \frac{2\pi\hbar^2}{m} \sum_{l,d} \exp\left(i\kappa.\mathbf{R}_{ld}\right) \hat{b}_{ld}. \qquad (10.21)$$

Here $\hat{b}_{ld}$ is the scattering amplitude operator (cf. (1.26))

$$\hat{b}_{ld} = A_{ld} + \frac{1}{2} B_{ld} \hat{\sigma} \cdot \hat{\mathbf{i}}_{ld} \qquad (10.22)$$

where $\hat{\mathbf{i}}_{ld}$ is the angular momentum operator for the nucleus at lattice site

$$\mathbf{R}_{ld} = \mathbf{l} + \mathbf{d}.$$

For purely magnetic scattering (cf. (5.10))

$$\hat{V}_M(\kappa) = \left(\frac{2\pi\hbar^2}{m}\right)\left(\frac{\gamma e^2}{m_e c^2}\right) \hat{\sigma} \cdot \sum_i \exp\left(i\kappa.\mathbf{r}_i\right)\left\{ \tilde{\kappa} \times \left(\hat{\mathbf{s}}_i \times \tilde{\kappa}\right) - \frac{i}{\hbar|\kappa|} \tilde{\kappa} \times \hat{\mathbf{p}}_i \right\} \qquad (10.23)$$

In a later section of this chapter we calculate the cross section for the scattering of neutrons by the electric field produced by the nuclei and atomic electrons in solid. The interaction potential for the process is there shown to be

$$\hat{V}_E(\kappa) = \left(\frac{2\pi\hbar^2}{m}\right)\left(\frac{m_e}{2m}\right)\left(\frac{\gamma e^2}{m_e c^2}\right)\left\{ i\cot(\frac{1}{2}\theta)\tilde{\mathbf{n}} \cdot \hat{\sigma} - 1 \right\} \times$$

$$\times \left\{ \sum_{l,d} \exp\left(i\kappa.\mathbf{R}_{ld}\right) Z_d - \sum_i \exp\left(i\kappa.\mathbf{r}_i\right) \right\} \qquad (10.24)$$

where
$$\mathbf{k}' \times \mathbf{k} = k^2 \sin\theta \tilde{\mathbf{n}} \qquad (10.25)$$

defines the unit vector and eZ_d is the charge associated with the nucleus of site **d** within the unit cell.

An examination of the three types of interaction potential given above shows that they all have the form

17

$$\hat{v} = \hat{\beta} + \hat{\alpha}.\hat{\sigma} \tag{10.26}$$

where the operators $\hat{\beta}$ and $\hat{\alpha}$ refer to the target system. It is therefore sufficient in studying the modification to the cross section due to polarisation, to consider just the general form of interaction potential (10.26).

Let us also, for the moment, consider that part of the cross-section (10.20) that depends on the neutron spin, namely,

$$\sum_{\sigma,\sigma'} p_\sigma \langle \sigma | \hat{v}^+ | \sigma' \rangle \langle \sigma' | \hat{v} | \sigma \rangle \tag{10.27}$$

The sum over σ' in (10.27) can be done by closure, to give

$$\sum_\sigma p_\sigma \langle \sigma | \hat{v}^+ \hat{v} | \sigma \rangle \tag{10.28}$$

This is valid only if there is no phase correlation between the states labeled with the quantum number σ, i.e. only if with respect to these states σ the density matrix is diagonal. But in this case the probability p_σ is just the diagonal element $\langle \sigma | \hat{\rho} | \sigma \rangle$, so (10,28) can be rewritten

$$\sum_\sigma \langle \sigma | \hat{\rho} | \sigma \rangle \langle \sigma | \hat{v}^+ \hat{v} | \sigma \rangle \tag{10.29}$$

Furthermore, if $\hat{\rho}$ is diagonal,

$$\langle \sigma' | \hat{\rho} | \sigma \rangle = \delta_{\sigma,\sigma'} \langle \sigma | \hat{\rho} | \sigma \rangle$$

so that (10.29) becomes

$$\sum_{\sigma,\sigma'} \langle \sigma | \hat{v}^+ \hat{v} | \sigma \rangle \langle \sigma | \hat{\rho} | \sigma \rangle$$

and the sum over σ' can be done by closure to give for (10.27)

$$\sum_{\sigma,\sigma'} p_\sigma \langle \sigma | \hat{v}^+ | \sigma' \rangle \langle \sigma' | \hat{v} | \sigma \rangle = \sum_\sigma \langle \sigma | \hat{v}^+ \hat{v} \hat{\rho} | \sigma \rangle \equiv Tr\, \hat{v}^+ \hat{v} \hat{\rho} \equiv Tr\, \hat{\rho} \hat{v}^+ \hat{v} \tag{10.30}$$

This final form is independent of the representation that is chosen to label the states and hence for this last form it does not matter whether or not $\hat{\rho}$ is diagonal. We conclude therefore that a formula which is much more general than (10.20) is

$$\frac{d^2\sigma}{d\Omega dE'} = \left(\frac{m}{2\pi\hbar^2} \right)^2 \frac{k'}{k} \sum_{\lambda,\lambda'} p_\lambda\, Tr\, \hat{\rho} \langle \lambda | \hat{V}^+(\kappa) | \lambda' \rangle \langle \lambda' | \hat{V}(\kappa) | \lambda \rangle \delta(\hbar\omega + E_\lambda - E_{\lambda'}) \tag{10.31}$$

where it is understood that the trace is to be taken with respect only to the neutron spin coordinates. Before we examine the structure of the spin-dependent part of this cross-section we derive an expression for the polarization of the scattered beam, P'. The formula for P' must represent the transformation of the spin state of the incident neutron beam, defined by P, due to the interaction with the target system; we must average the initial spin state of the beam over all possible scattering processes and sum over all possible final states. Thus

$$\mathbf{P}' \propto Tr\, \hat{\rho} \hat{v}^+ \hat{\sigma} \hat{v}.$$

The constant of proportionality is determined by normalisation; viz.

$$\mathbf{P}' = Tr\, \hat{\rho} \hat{v}^+ \hat{\sigma} \hat{v} / Tr\, \hat{\rho} \hat{v}^+ \hat{v} \tag{10.32}$$

18

In full we have

$$\mathbf{P}'\frac{d^2\sigma}{d\Omega dE} = \left(\frac{m}{2\pi\hbar^2}\right)^2 \frac{k'}{k}\sum_{\lambda,\lambda'} p_\lambda \, Tr\hat{\rho}\langle\lambda|\hat{V}^+(\kappa)|\lambda'\rangle\hat{\sigma}\times$$

$$\times\langle\lambda'|\hat{V}(\kappa)|\lambda\rangle\delta(\hbar\omega + E_\lambda - E_{\lambda'})$$

(10.33)

Let us examine the structure of eqns (10.30) and (10.32) with the general form of $\hat{v}$ given by eqn (10,26). For the cross-section we need to evaluate (10.30),

$$Tr\hat{\rho}\hat{v}^+\hat{v} = \frac{1}{2}Tr\left(I+\mathbf{P}.\hat{\sigma}\right)\left(\hat{\beta}^+ + \hat{\alpha}^+.\hat{\sigma}\right)\left(\hat{\beta} + \hat{\alpha}.\hat{\sigma}\right)$$

$$= \frac{1}{2}Tr\left(I+\mathbf{P}.\hat{\sigma}\right)\left(\hat{\beta}^+\hat{\beta} + \hat{\beta}^+\hat{\alpha}.\hat{\sigma} + \hat{\alpha}^+.\hat{\sigma}\hat{\beta} + \hat{\alpha}^+.\hat{\sigma}\hat{\alpha}.\hat{\sigma}\right)$$

(10.34)

The evaluation of the trace of products of Pauli operators is facilitated by making use of the identity

$$\hat{\sigma}_\alpha\hat{\sigma}_\beta = \delta_{\alpha,\beta}I + i\sum_\gamma \varepsilon_{\alpha\beta\gamma}\hat{\sigma}_\gamma$$

(10.35)

where $\varepsilon_{\alpha\beta\gamma}$ is the completely antisymmetrical tensor with three indices,

i.e. $\qquad \varepsilon_{\alpha\beta\gamma} = +1$ if α, β, γ are in cyclic order,

$\qquad\qquad = -1$ if α, β, γ are not in cyclic order,

$\qquad\qquad = 0$ otherwise.

This identity is derived by using the commutation relation for angular momentum operator,

$$\left[\hat{L}_\alpha, \hat{L}_\beta\right] = i\sum_\gamma \varepsilon_{\alpha\beta\gamma}\hat{L}_\gamma$$

and the fact that Pauli operators anticommute,

$$\hat{\sigma}_\alpha\hat{\sigma}_\beta + \hat{\sigma}_\beta\hat{\sigma}_\alpha = 2\delta_{\alpha,\beta}I$$

Because $Tr\hat{\sigma}_\gamma$ is zero, we obtain from (10.35)

$$Tr\hat{\sigma}_\alpha\hat{\sigma}_\beta = 2\delta_{\alpha,\beta}$$

Also with the aid of this result,

$$Tr\hat{\sigma}_\alpha\hat{\sigma}_\beta\hat{\sigma}_\gamma = i\sum_{\gamma'}\varepsilon_{\alpha\beta\gamma'}Tr\sigma_{\gamma'}\sigma_\gamma = 2i\varepsilon_{\alpha\beta\gamma} .$$

(10.36)

With the aid of these formulae we find for (10.34) the result,

$$Tr\hat{\rho}\hat{v}^+\hat{v} = \hat{\alpha}^+.\hat{\alpha} + \hat{\beta}^+\hat{\beta} + \hat{\beta}^+\left(\hat{\alpha}.\mathbf{P}\right) + \left(\hat{\alpha}^+.\mathbf{P}\right)\hat{\beta} + i\mathbf{P}.\left(\hat{\alpha}^+ \times \hat{\alpha}\right).$$

(10.37)

When it is adequate to consider only nuclear and magnetic scattering, an examination of the corresponding interaction potentials, (10.21) and (10.23), shows that $\hat{\beta}$ contains only nuclear terms and $\hat{\alpha}$ both nuclear and magnetic scattering. This interference has been utilized to perform very accurate measurements of magnetic structure factors. Bearing in mind that the cross-section must be averaged over the orientations of the nuclei, it can be seen that for randomly oriented nuclei the last term on the right-hand side of (10.37) is purely magnetic.

In order to evaluate

$$Tr\hat{\rho}\hat{v}^+\hat{\sigma}\hat{v}$$

(10.38)

as required in the formula for $\mathbf{P}'$, eqn (10.32), we need, in addition to (10.12) and (10.36) the identity

$$Tr\,\hat{\sigma}_\alpha\hat{\sigma}_\beta\hat{\sigma}_\gamma\hat{\sigma}_\delta = 2\left(\delta_{\alpha,\beta}\delta_{\gamma,\delta} - \delta_{\alpha,\gamma}\delta_{\beta,\delta} + \delta_{\alpha,\delta}\delta_{\beta,\gamma}\right) \tag{10.39}$$

which can be derived from (10.35). Also note that, if $\mathbf{A}$ and $\mathbf{B}$ are arbitrary vectors

$$(\mathbf{A}\times\mathbf{B})_\alpha = \sum_{\beta,\gamma}\varepsilon_{\alpha\beta\gamma}A_\beta A\gamma\ ; \tag{10.40}$$

With these results,

$$Tr\,\hat{\rho}\hat{v}^+\hat{\sigma}\,\hat{v} = \hat{\beta}^+\hat{\alpha} + \hat{\alpha}^+\hat{\beta} + \hat{\beta}^+\hat{\beta}\,\mathbf{P} + \hat{\alpha}^+\left(\hat{\alpha}.\mathbf{P}\right) + \left(\hat{\alpha}^+.\mathbf{P}\right)\hat{\alpha} - $$
$$-\mathbf{P}.\left(\hat{\alpha}^+.\hat{\alpha}\right) - i\hat{\alpha}^+\times\hat{\alpha} + i\hat{\beta}^+\left(\hat{\alpha}\times\mathbf{P}\right) + i\left(\mathbf{P}\times\hat{\alpha}^+\right)\hat{\beta} \tag{10.41}$$

If we again consider just nuclear and magnetic scattering, we see that in the limit of an unpolarized incident beam of neutrons there is a creation of polarization by a purely magnetic term (for randomly oriented nuclei), $-i\hat{\alpha}^+\times\hat{\alpha}$.

To sum up, we use (10.37) in conjunction with (10.31) to give the cross sections and we use (10.41) in conjunction with (10.33) to give the polarization $\mathbf{P}'$ of the scattered neutrons.

References

1. Kemble, E.C., Fundamental Principles of Quantum Mechanics. 1937, New York: McGraw-Hill.
2. Tolman, R.C., The principles of Statistical Mechanics. Vol. (1,2,4,10). 1938, Oxford: University Press.
3. Husimi, K., Proc. Phys. Math. Soc., Japan, 1940. **22**: p. 264.
4. Ter Haar, D., Elements of Statistical Mechanics. 1954, New York: Rinehart.
5. Fano, U., Review of modern Physics, 1957. **29**: p. 74.
6. Hagedorn, R., . 1958, CERN.
7. London, F. and E. Bauer, La Théorie de l'Observation en Mécanique Quantique. 1939, Paris: Hermann.
8. Tolhoek, H.A. and S.R. de Groot, Physica, 1951. **17**: p. 17.
9. Cox, J.A.M. and H.A. Tolhoek, Physica, 1953. **19**: p. 673.
10. Tolhoek, H.A. and J.A.M. Cox, Physica, 1953. **19**: p. 101.
11. Hartogh, C.D., H.A. Tolhoek, and S.R. de Groot, Physica, 1954. **20**: p. 1310.
12. de Groot, S.R. and H.A. Tolhoek, Beta- and Gamma-Ray Spectroscopy p.613. 1955, Amsterdam: North-Holland.
13. Huby, R., Proc. Phys. Soc., 1958. **72**: p. 97.
14. Lipps, F.W. and H.A. Tolhoek, Physica, 1954. **20**: p. 85.
15. Kotani, T., Prog. Theor. Phys., Japan, 1955. **14**: p. 379.
16. Tolhoek, H.A., Rev. Mod. Phys., 1956. **28**: p. 277.
17. Fano, U., J. Opt. Soc. Amer., 1949. **39**: p. 859.
18. Roman, P., Nuovo Cim., 1959. **13**: p. 974.
19. Parrent, G.B. and P. Roman, Nuovo Cim., 1960. **15**: p. 370.
20. Ehrenfest, P., Z. Phys., 1927. **45**: p. 455.
21. Kramers, H.A., Quantum Mechanics. 1957, Amsterdam: North-Holland.
22. Schweizer, J., Magnetic Scattering of Neutrons: A Technique with a Real Future, . 1996, DRFMC/MDN/CEA-Grenoble.